Short Title

A GDT Study of the Current Element and Rectangular Plate

(56 characters)

Christopher W. Trueman Electrical Engineering

A GDT METHOD STUDY OF THE CURRENT ELEMENT AND RECTANGULAR PLATE

by

Christopher W. Trueman, B. Eng. (McGill)

Department of Electrical Engineering

McGill University,

Montreal, Canada.

March, 1975

A GDT METHOD STUDY OF THE CURRENT ELEMENT ANTENNA AND RECTANGULAR PLATE

by

Christopher W. Trueman, B. Eng. (McGill University)

A thesis submitted to the

Faculty of Graduate Studies and Research
in partial fulfillment of the requirements
for the degree of Master of Engineering

Department of Electrical Engineering

McGill University

Montreal, Quebec

March, 1975

ABSTRACT

In this thesis, the H-plane pattern of a current element antenna centered in front of a rectangular conducting plate, parallel to a "vertical" edge, is studied by the Geometrical Diffraction Theory method of analysis. An extensive exploitation of the two-dimensional plate program reveals a systematic behavior of the radiation pattern which is quite striking. This behavior can be extracted from the large number of computed patterns for discrete values of width and separation, and expressed as a simple, continuous graphical synopsis. These "synoptic graphs" not only allow the reconstruction of the original finite number of patterns, but also the plotting of patterns for a continuum of widths and separations within the range examined, without further computation. The three-dimensional plate model's H-plane pattern is studied as a function of plate height, and computed results are compared with published data and also measurements obtained in an anechoic room facility.

The conclusions suggest that the synoptic graphs are a representation of a multidimensional function which generates the radiation pattern in terms of the physical dimensions of the antenna, or "Pattern Generator Function".

The concept of a Pattern Generator Function transcends the computational, analytic or experimental method used to obtain it, and may be a useful tool for design purposes.

RESUME

Dans cette thèse, nous avons étudié par la méthode de Diffraction Geométrique, la configuration du champ H d'une antenne élémentaire, centrée au devant d'une plaque conductrice rectangulaire, et parallèle à un côté "vertical" de la plaque.

Une utilisation intensive du programme élaboré pour la plaque a trois dimensions, révèle d'une manière éclatante, le comportement systématique du champ de radiation. Le comportement peut alors être connu à partir d'un nombre considérable de configurations, calculées pour des valeurs discrètes de largeur et de séparation, et il peut être representé par une méthode graphique très simple, les courbes "synoptiques" permettant non seulement de reconstruire les configurations initiales, mais aussi de connaître les configurations pour des valeurs continues de largeurs et de séparations, et cela sans avoir recours à de nouveaux calculs.

La configuration tridimensionelle du champ H est étudiée en fonction de la hauteur de la plaque, et nous avons comparé les resultats obtenus avec ceux qui ont été publiés, ainsi qu'avec des mesures faites dans une chambre anechoide specialement aménagée.

En conclusion, il apparait que les courbes "synoptiques" constituent un "générateur multidimensionel de champ de radiation" en fonction des dimensions physiques de l'antenne. Ce concept de "générateur de fonctions" est plus général et en quelque sorte transcende les méthodes de calcul analytique ou experimental généralement utilisés. Aussi peut-il constituer un outil utile pour le développement de nouveux systèmes.

ACKNOWLEDGEMENTS

The author wishes to express his sincere gratitude to Dr. T.J.F. Pavlasek, his research director, for his encouragement, guidance, and criticism throughout the work leading to this thesis.

The author would also like to sincerely thank Dr. S.J. Kubina, for suggesting the method of analysis used in this thesis, and for his guidance in matters both experimental and computational. Special thanks are due to Mr. A. Skalina for his advice on a wide range of topics, and to Mr. R.C. Murphy for practical guidance in the production of the artwork for this thesis.

Thanks are due to Mrs. Charlotte Cooper for her excellent typing of the manuscript.

The author wishes to express his gratitude to the National Research Courcil of Canada for providing support for this work.

TABLE OF CONTENTS

ACKNOWLEDGEMENTS TABLE OF CONTENTS CHAPTER I INTRODUCTION 1.1 Statement of the Problem Survey of the Methods of Analysis 1.2 The Present Work 1.3 CHAPTER II GEOMETRICAL OPTICS AND GEOMETRICAL DIFFRACTION 2.1 Ray Theory and the Geometrical Theory of Optics 2-1 The Current Element Antenna 2.2 2-2 2.3 The Reflected Field 2-4 2.4 Smooth Bodies and Bodies With Edges 2-9 2.5 Geometrical Diffraction Theory 2-10 CHAPTER III THE INFINITE WEDGE CANONICAL PROBLEM 3.1 The Infinite Wedge Canonical Problem 3-1 3.2 The Law of Edge Diffraction 3-2 3.3 The Simple Diffraction Coefficient 3-4 3.4 The Edge-Related Coordinates 3-7 3.5 The Transition Diffraction Coefficient 3-10 Evaluation of the Field Diffracted From a Straight Edge 3-13 CHAPTER IV THE FLAT PLATE PROBLEM Y 4.1 The Flat Plate Problem 4-1 4.2 The Two-Dimensional Plate 4-1 4.3 The GTO Solution to the Flat Plate Problem 4-3 4.4 The GDT Model of the 2-d Plate 4-8 4.5 Computing the Radiation Pattern 4-10 4.6 The Geometrical Diffraction Fields 4-16

CHAPTER V SUMMARY AND CONCLUSIONS

4.8

4.9

4.10

4.11

4.12

4.13

4.14

4.15

Narrow Plate Patterns

Moment Method Comparison

The 3-d Plate Patterns

Comparison with Burnside

Pattern Amplitude Parameters

The Three Dimensional Plate

Radiation Pattern Measurements

Comparison With Measured Patterns

Minima Location Angles for Any Plate Width

Parametric Graphs, P	'arametric Families, and	Synoptic Graphs	
Parametric Graphs an	d a Synoptic Graph for	the Flat Plate Pro	blem .
Vertex Diffractions		,	
The GDT Method	· ·	•	•

4-18

4-19

4-24

4-25

4-28

4-30

4-32

4-37

4-38

ABSTRACT RESUME

CHAPTER 1

INTRODUCTION

1.1 Statement of the Problem

When an antenna is mounted near a conducting body, there is an interaction between the body and the antenna which results in a radiation pattern which is considerably different from that of the original antenna. It has been possible to determine the resulting radiation pattern by various numerical methods, using a digital computer, for a variety of structures such as cylinders (8,13), rectangular plates (11,14), a small aircraft (3), and a small helicopter (12), among others. Once the radiation pattern has been determined, the problem is generally considered solved. However, Bayou (8), in analyzing the H-plane pattern of a dipole antenna parallel to the axis of a nearby cylinder, notes that the pattern exhibits a systematic behavior with changing cylinder diameter and cylinder to dipole spacing. Based on a large number of patterns generated by this computer program, Bayou draws up a rudimentary set of "parametric curves" which describe this functional relationship. Further consideration of the "parametric curve" idea and a detailed investigation of a different geometrical configuration, using other analytic methods, as described in this thesis, leads to a conclusion of potential utility to the antenna designer. The conclusion is that, for any complex antenna system, it may be possible to determine a simple direct functional relationship, defined here as the "pattern generator function", which provides significant far field pattern information, for a particular antenna geometry, in terms of the dimensional parameters of the radiating system.

In this thesis, an antenna near a conducting body problem is analyzed and the resulting program for the computation of the radiation pattern is exploited to determine a representation of the pattern generator function. A current

element source antenna (16) radiates in the presence of a flat rectangular conducting surface or "plate": The source is centered in front of the plate, separated from it, and parallel to one of its edges. The effect of the plate on the current element's H-plane pattern is studied by the "Geometrical Diffraction Theory" (GDT) (6,16). The chief advantage of this method is that it allows the components of field which have the most significant effect in each region of space to be identified with particular features on the scattering body and hence the effect of any part of the body on the pattern is readily apparent. The GDT is exploited to reveal new information about the shape of the H-plane pattern, as the size of the plate and the distance to the source change. A large number of computed patterns are reduced to a brief set of "synoptic graphs" which allow the pattern to be reconstructed for any plate width and source separation distance over the range covered. Thus, the "synoptic graphs" are a representation of the pattern generator function for this radiating system.

1.2 Survey of the Methods of Analysis

The numerical analysis of a radiating system can proceed by a "finite elements" method, which seeks the current distribution on the body and hence the secondar's radiation fields, or by "Geometrical Diffraction Theory" (GDT), which relies upon ray optics. The "radiating system" usually consists of a source antenna such as a dipole or current

element, and a "body" which may be solid such as an aircraft, or composed of thin rods, such as the truss-like tail section of a Bell 47G-4A helicopter or the passive elements in a Yagi array, or it may be an infinitely thin conducting surface such as the plate.

The finite elements method has two chief sub-classes, the surface element modelling, and the wire-grid modelling.

The surface element modelling divides the surface of the body into "patches" and assumes a functional form for the current flowing on each patch by representing it as a linear combination of "hasis functions", often chosen as piecewise linear, polynomial or trigonometric functions. The unknown coefficients are found by solving an integral equation by a projective method. In order to simplify the integrals encountered, and reduce the running time of the computer program, the current is often represented as having constant value over the patch (pulse basis) and the current complex amplitudes found by Dirac delta function projection, or "point-matching". Thus Bavou (8) solves the dipole anténna near a conducting cylinder problem by assuming a z-directed surface [current, which is found by this "surface patch" method. If the body has sharp edges, they tend to carry large currents which have a high rate of change with distance from the edge. In order to represent such a current adequately, a large number of small patches would be needed, which requires large matrix equations and hence long computing times. Thus the surface patch technique is poorly suited to the flat plate problem.

A heuristic approach, making use of a physical assumption about the current, allows the surface element technique to be used to

solve the plate problem. The current on the plate is assumed to flow only in the longitudinal direction. In the equivalent two-dimensional problem, the conducting strip, this longitudinal current is only a function of crosswise position on the strip. Then a one dimensional current representation is all that is necessary, and Shafai and El-Moazzen (11) have solved this problem by using a truncated Fourier series (trigonometric basis) and point-matching. Their solution is valid only for narrow plates, however, as the current representation is inadequate when the width is large. The fully three dimensional plate problem can also be solved in this way, by assuming zero current in the crosswise direction and by accounting for the Variation in the longitudinally directed current in both the longitudinal and the crosswise sense. Nan Wang (18) solves the plate problem in this way, with piecewise ° sinusoidal functions in the crosswise direction and pulse basis in the longitudinal sense. The crosswise directed component of current could also be accounted for, but at the cost of doubling the number of unknowns and hence the matrix size.

The wire-grid modelling method uses current's constrained to flow along lines or "wires" to represent the body, and also relies on the projective solution of an integral equation to find unknown current amplitudes. Wire antennas and arrays are easily modelled, as well as truss-like structures such as towers, or the tail of the small helicopter (12). Because all functions are one-dimensional, general basis and projection functions may be used, rather than pulse basis and point matching.

Generalized problem solving computer programs, using straight wire elements,

are available (15). An edge on a body which carries a high current along its length is well represented by a line current flowing in wire elements oriented along the edge, and the remainder of the body can be modelled with wires in sufficient density to resemble a surface current. The plate as a scatterer has been dealt with by Richmond (14), using constant currents on short wire elements, and point matching. Richmond estimates that about 100 such elements are needed per square wavelength of surface to adequately represent the current. This severely limits the size of plate that can be handled.

A body on which the edge currents dominate is much more naturally modelled by Geometrical Diffraction Theory. The GDT is based on ray optics, and assumes that energy travels outward from the source along lines called "rays", and that the field at any point in space is the complex vector sum of the fields associated with all the rays through the point. Rays may be reflected from conducting surfaces, but more important, a ray incident on an edge or vertex, or tangentially incident on a curved surface, will set up diffracted rays. A body is readily modelled by identifying its reflecting surfaces and its diffracting features, and tracing rays from the source to the field point.

The chief advantage of the GDT is the direct correspondence between the features on the body and components of field at the field point. The effect of any of the body's features on the field is thus readily assessed, by examining its component of field. Hence an enormous insight is gained into the behavior of the radiating system. Other advantages of the GDT include the ease of analysis of a problem by simple ray tracing, and

that it is not necessary to formulate large matrix equations, nor to solve them, and so a great saving in computer time is realized.

A more subtle advantage of the GDT lies in the fact that a model of a radiating system can be built in stages, each including new classes of rays, and so the program can be debugged one part at a time. Thus if a crude model generates promising patterns, it can be refined by adding further diffraction effects to it. In contrast, a finite elements program must be virtually complete and fully debugged before any indication of its success is obtained.

The GDT has been applied to the plate problem by Burnside (3), in order to verify the operation of a GDT program written to solve a more general class of problem. Burnside compares his computations with measurements for the plate, and other configurations; but the plate patterns are not further explored.

1.3 The Present Work

The objective of the present work is to systematically study the H-plane pattern of a current element antenna centered in front of a conducting plate, parallel to an edge. The specific goal is to determine a graphical representation of the pattern generator function.

The Geometrical Diffraction Theory is used to build a model of the current element-plate radiating system each step including a new class of rays, and giving further insight into the behavior of the system. An intensive study of the H-plane pattern via the GDT computer program reveals previously

unknown information about the pattern as a function of plate height and width, and source separation distance.

The radiation field of the current element plate system is computed by summing up the complex vector fields associated with the ray from the source, the ray reflected from the plate's front face, and the diffracted rays emanating from the plate's edges. The diffracted fields are found using Kouvoumjian's Transition Diffraction Coefficient (TDC)

(5) *. The patterns are compared critically with computations and measurements published by Burnside (3), computations published by Shafai and El-Moazzen (11), and experimental patterns obtained especially for this work.

Good agreement is noted.

In Chapter 2 of this thesis, the "Geometrical Theory of Ontics" (GTO) is briefly outlined, and convenient methods of computing current element fields and reflected fields are detailed. Then the effect of edges and vertices on a GTO pattern is discussed, leading to an outline of the "Geometrical Diffraction Theory" method of analysis.

^{*} Kouvoumjian in (1,4,5) uses the term "dyadic diffraction coefficient to refer to his diffraction coefficient function. This function will be called the "Transition Diffraction Coefficient" in this thesis. The term "Dyadic Diffraction Coefficient" will be used to denote the dyadic $\overline{\overline{D}}$ (Sect. 2.5) as opposed to the elements of D which will be called "diffraction coefficients". The TDC is a specific expression for the elements of $\overline{\overline{D}}$.

Chapter 3 details the method used to calculate the diffracted field from an edge. The "Law of Edge Diffraction" is given and its significance in the calculation of a radiation pattern is discussed.

A coordinate transformation called the "edge-related coordinates" which facilitates the calculation of an edge diffracted field is given in detail, and the best available diffraction coefficient, the Transition Diffraction Coefficient, is quoted from the literature. A practical approach to finding the point of diffraction or "flash point" on a straight edge is given, and then the reader is taken step by step through an edge diffracted field calculation.

The fourth chapter is devoted to a study of the flat plate problem. The geometrical optics model of the current element-plate radiating system, which accounts for the direct and reflected ray, is thoroughly analysed and provides an insight into the behavior of the radiation pattern as a function of the plate width and source separation distance which is helpful in later stages of the analysis. A package of computer subroutines which facilitate the calculation of the radiation fields of a class of simple antenna problems by GDT was developed during the work for this thesis and is presented at this point. The two-dimensional (2-d) model of the plate is constructed which adds the diffracted ravs from the edges parallel to the source current element to the GTO fields. The computation of the radiation pattern using the GDT subroutine package is outlined. The radiation nattern of the 2-d model is examined in detail, as a function of the plate width and source separation distance. The accuracy of the two-edge program is established by comparison with data computed by the surface element method, published by Shafai and El-Moazzen (11). The final stage model adds

the diffracted rays from the two other edges of the plate, and so includes the effect of all four of the plate's edges. The pattern is studied as a function of plate height. The radiation patterns computed by the four-edge program are compared with computations and measurements published by Burnside (3), and also with experimental patterns for several values of plate height and width, and source separation, obtained in an anechoic room facility.

The final chapter summarizes the chief results of the study. New information, of considerable practical interest, about the behavior of the H-plane pattern of the current element-rectangular plate radiating system as a function of its physical dimensions, has been generated. It is found that this behavior can be extracted from a large number of patterns computed for discrete values of plate width and source separation distance, and expressed as a simple, continuous graphical synopsis. These "synoptic graphs" allow a continuum of new patterns to be obtained without further computation. Thus the "synoptic graphs" are a representation of the system's Pattern Generator Function. The Pattern Generator Function transcends the computational, analytic or experimental method used to obtain it, and may be a useful tool for design purposes.

CHAPTER 2

GEOMETRICAL OPTICS AND GEOMETRICAL DIFFRACTION

2.1 Ray Theory and the Geometrical Theory of Optics

This chapter outlines the "geometrical optics" method, and details suitable expressions for calculating the fields of a current element source and the reflected field from a smooth surface. The far field pattern of a current element antenna near a body is discussed and the "geometrical diffraction" method is described.

The "ray theory" assumes that electromagnetic radiation travels along straight lines called "rays", which obey Alhazen's Law of Reflection (17) at reflective surfaces, cannot penetrate perfectly conducting objects, and obey Snell's Law at media discontinuities. Ray theory is primarily useful for problems involving incoherent radiation.

Each ray convergent on a point after the first raises the intensity by 3 dB. Simple ray theory is not reffective for problems involving coherent waves, or in situations where diffraction plays a large rôle, and relative phase and polarization must therefore be considered.

The "Geometrical Theory of Optics" is an extension of ray theory and takes into account polarization and phase of the fields. Thus each ray has a field associated with it which is a complex vector quantity. The "net field" or "total field" at any observation point ("field point") is the complex vector sum of the fields associated with all of the rays through the point.

^{*} In the rest of this thesis, when the term "conducting" is used, a perfectly conducting object is meant.

In the following sections, first, the current element antenna is re-examined as a GTO radiator, and suitable expressions for calculating its fields are derived. A conducting body is then introduced near the current element, and its effect on the radiation pattern is examined.

2.2 The Current Element Antenna

Consider a current element source antenna located at source point \overline{R}_c , Fig. 2.1. The source field is thought of as travelling outward from the source point \overline{R}_c in all directions along straight line rays. Given a field point \overline{R}_f with a source ray through it, the complex amplitude and vector direction of the source field is sought. The source carries a current I_s in direction \hat{p} . Let the "source coordinates" be centered at \overline{R}_c with unit vectors \hat{x}_s , \hat{y}_s , and $\hat{z}_s = \hat{p}$. Then in the associated "source spherical coordinates" ($\hat{\mathbf{r}}_s$, $\hat{\boldsymbol{\theta}}_s$, $\hat{\boldsymbol{\phi}}_s$) the current element's field is (10)

$$\overline{E} = \frac{I_s 1}{4\pi} \frac{e^{-jkR_s}}{R_s} j\omega\mu \sin\theta_s \hat{\theta}_s$$
 2.2.1

where $R_s = |\overline{R}_f - \overline{R}_c|$ 2.2.2

and 1 is the length of the current element.

This is simplified by collecting constants,

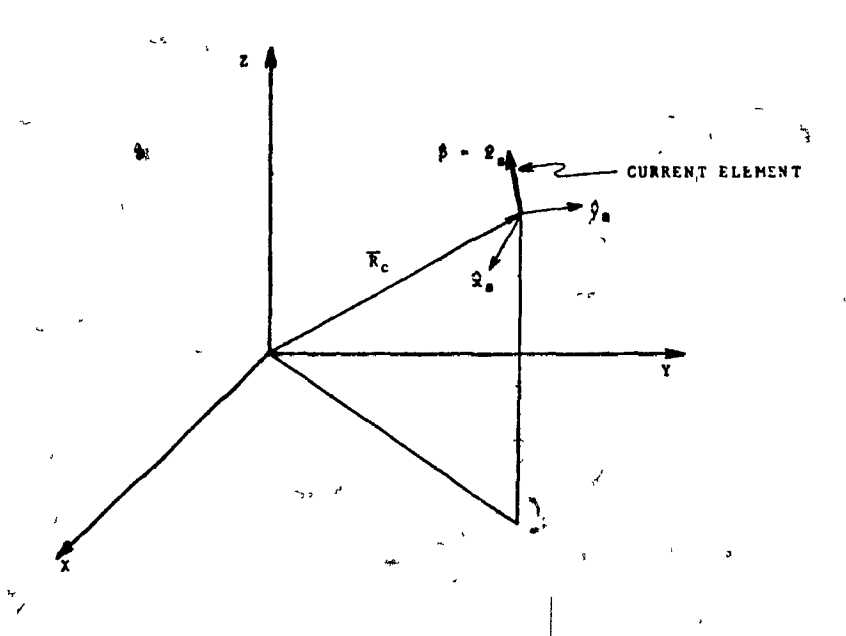


Fig. 2.1 The current element antenna.

$$\overline{E} = E_0 \frac{e^{-jkR}s}{kR_s} = \sin \theta_s \hat{\theta}_s$$
 2.2.3

The current element's field can then be re-written in the base coordinate system in a form convenient for computation by noting that since

$$\hat{\phi} \times \hat{r}_{s} = \sin \theta_{s} \hat{\phi}_{s}$$

$$\hat{\phi}_{s} \times \hat{r}_{s} = \hat{\theta}_{s}$$

and

we may write

$$\sin \theta_{s} \hat{\theta}_{s} = \sin \theta_{s} \hat{\phi}_{s} \times \hat{r}_{s}$$

$$= (\hat{p} \times \hat{r}_{s}) \times \hat{r}_{s}$$

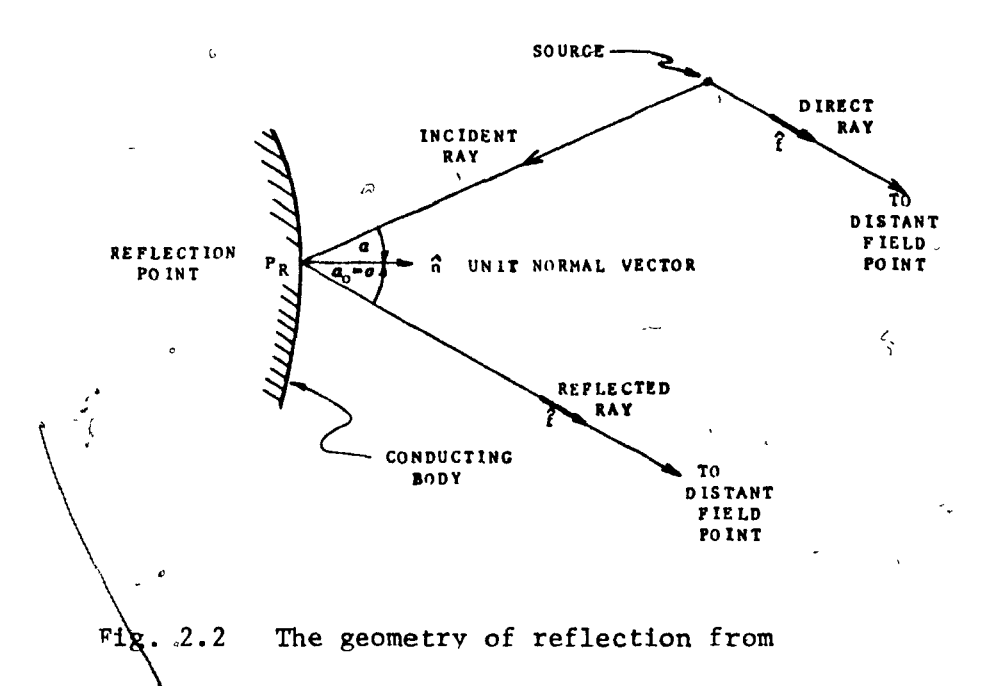
$$= e^{-jkR_{s}} \hat{p} \times \hat{r}_{s} \times \hat{r}_{s}$$

$$= (\hat{p} \times \hat{r}_{s}) \times \hat{r}_{s}$$

hence

where
$$\hat{r}_s = \frac{R_f - R_c}{R_s}$$

2.2.5



Subroutine "SFLD" (Ann.1) was developed for this project to evaluate the source field vector at any field point, and uses these

a smooth conducting surface.

2.3 The Reflected Field

expressions.

Consider a current element antenna radiating in the presence of a conducting body, Fig. 2.2. At any field point, there will be a reflected ray if a point P_R exists on the body which satisfies Alhazen's Law of Reflection . Alhazen's Law states that the reflected ray must lie in the plane of the incident ray and the unit normal vector $\hat{\mathbf{n}}$ to the surface at P_R , and that the angle $\boldsymbol{\alpha}$ between the incident ray and $\hat{\mathbf{n}}$ must equal the angle $\boldsymbol{\alpha}_0$ that the reflected ray makes with $\hat{\mathbf{n}}$.

To calculate the field associated with the reflected ray, we assume that the radius of curvature at P_R is sufficiently large that the surface may be approximated by its tangent plane. Then the method of images is used. The image source is located at \overline{R}_{ci} , the same distance

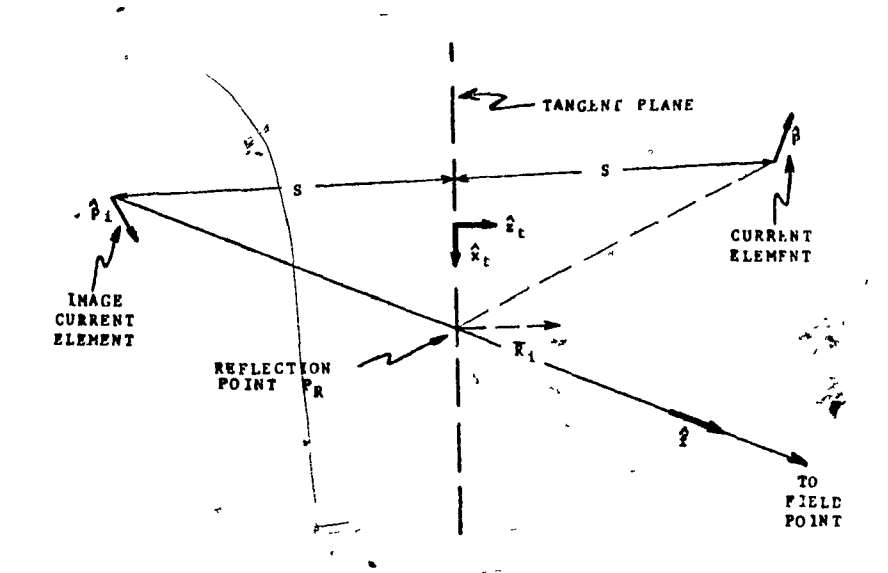


Fig. 2.3 Calculating the reflected field by the Method of Images.

behind the tangent plane as the primary source is in front of it, Fig. 2.3. If $\hat{\mathbf{x}}_t$ and $\hat{\mathbf{v}}_t$ are unit vectors in the tangent plane, and the primary source orientation vector is resolved as

$$\hat{p} = (p_{xt}, n_{yt}, p_n)$$
 2.3.1

the image orientation vector is given by

$$\hat{p}_i = (-p_{xt}, -p_{yt}, p_n)$$

The reflected field is then calculated for the image current element exactly as the primary current element's field was found in Sect. 2.2. If \overline{R}_f is the position vector of the field point,

$$\overline{E}_{r} = E_{o} \frac{e^{-jkR}i}{kR_{i}} \qquad (\hat{p}_{i} \times \hat{f}) \times \hat{f} \qquad 2.3.2$$

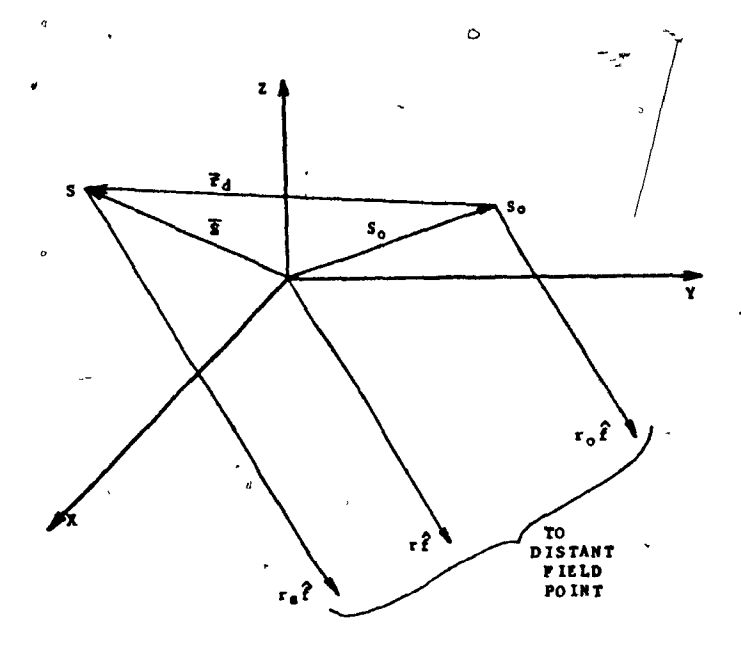


Fig. 2.4 The geometry of phase referencing.

where

$$R_{i} = |\overline{R}_{f} - \overline{R}_{ci}| \qquad 2.3.3$$

is the distance from the image to the field point, and

$$\hat{f} = \frac{\overline{R}_f - \overline{R}_{ci}}{R_i}$$
2.3.4

is a unit vector in the field direction.

All fields must be phase referred to the same point in space. In Fig. 2.4, a source at \overline{s} radiates a wave with phase factor $e^{-jkr}s$, where r_s is the distance from \overline{s} to the field point, which is assumed to be far away. The phase must be referred to point \overline{s}_o . In the f, f_d plane, Fig. 2.5, where f is the field direction,

$$r_{s} = r_{o} + d$$

$$d = \overline{r}_{d} \cdot (-\hat{f}) = -\overline{r}_{d} \cdot \hat{f}$$

$$r_{s} = r_{o} - \overline{r}_{d} \cdot \hat{f}$$

where

hence

2.3.5

+

63

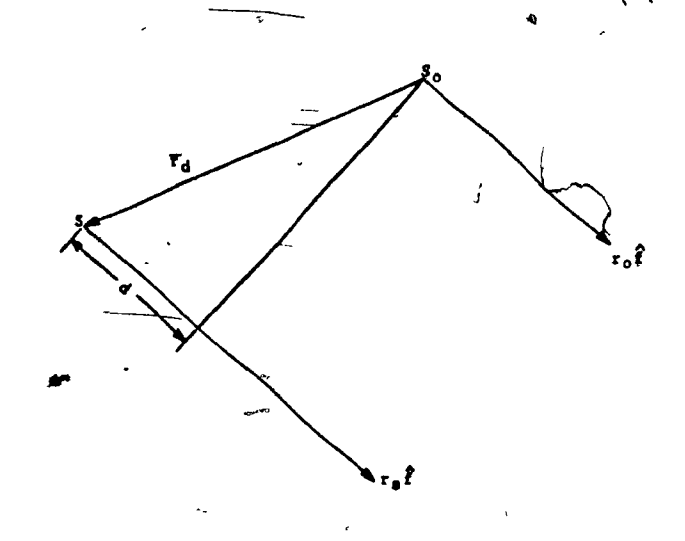


Fig. 2.5 The \hat{f} , \hat{r}_d plane

Thus the phase factor of source \overline{s} , referred to point \overline{s}_0 is

$$e^{-jkr}$$
 e^{jk} r_d f 2.3.6

Thus the reflected field may be re-written phase referred to the position of the primary source, by noting that in Fig. 2.3,

hence
$$R_{\hat{1}} = R_{\hat{s}} + 2s \hat{n} \cdot \hat{f}$$
 2.3.6

thus
$$\overline{E}_r = E_o e^{-jk} \hat{n} \cdot \hat{f} = \frac{e^{-jkR}s}{kR_o} = (\hat{p}_i \times \hat{f}) \times \hat{f}$$
 2.3.7

where R_s replaces R_i in the denominator, since the field point is very far away and for amplitude purposes, $R_s = R_i$.

Consider the special case of a planar reflecting surface perpendicular to the x,y plane, Fig. 2.6, where the source lies in that plane. There will be a reflected ray in the field direction \hat{f} in the x,y plane if there is a point P_R on the plane satisfying Alhazen's Law. But P_R is simply the point where the ray from the image intersects.

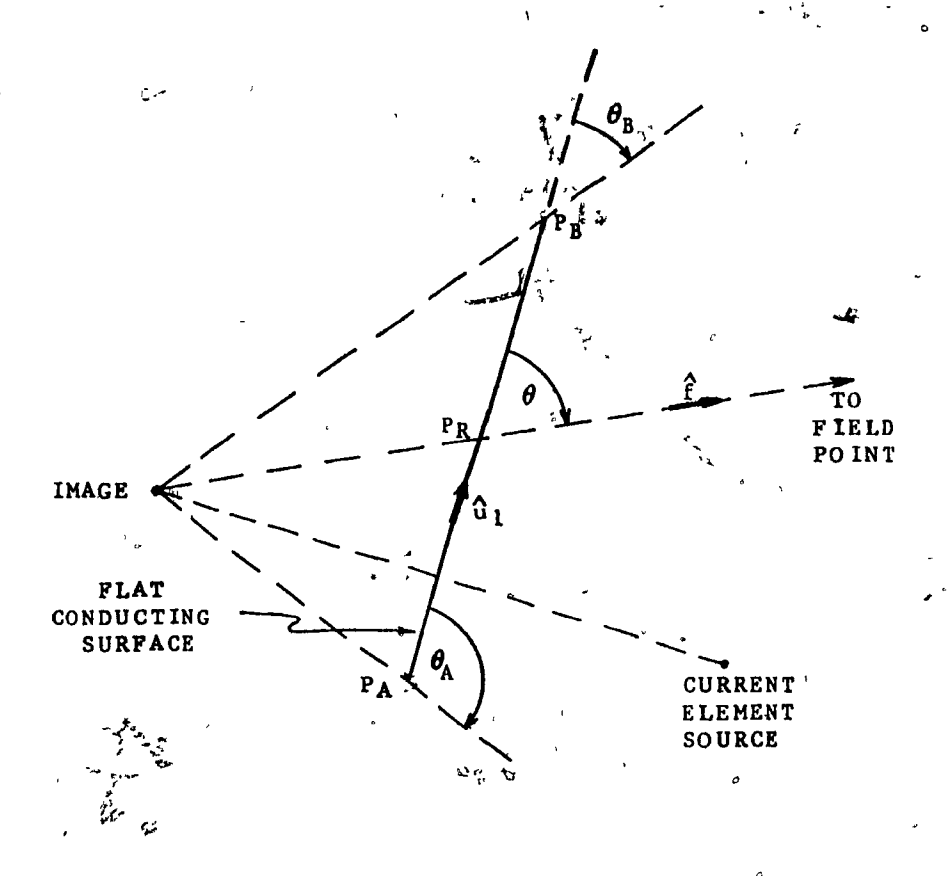


Fig. 2.6. Reflection from a flat conducting surface perpendicular to the horizontal plane.

the reflecting plane. Thus there is a reflected ray in direction \hat{f} if P_R lies between the plane's endpoints P_B and P_B , Fig. 2.6. Thus P_R exists if

$$\theta_{B} < \theta < \theta_{A}$$
or
$$\cos \theta_{B} > \cos \theta > \cos \theta_{A}$$
or
$$\cos \theta_{B} > \hat{f} \cdot \hat{u}_{1} > \cos \theta_{A}$$

2.3.8

where \hat{u}_1 is a unit vector from P_A to P_B . This is a convenient test for the presence of a reflected ray in direction \hat{f} for this special geometry. Subroutine "RER" (App. 2) was developed for this project to compute the reflected field for this problem.

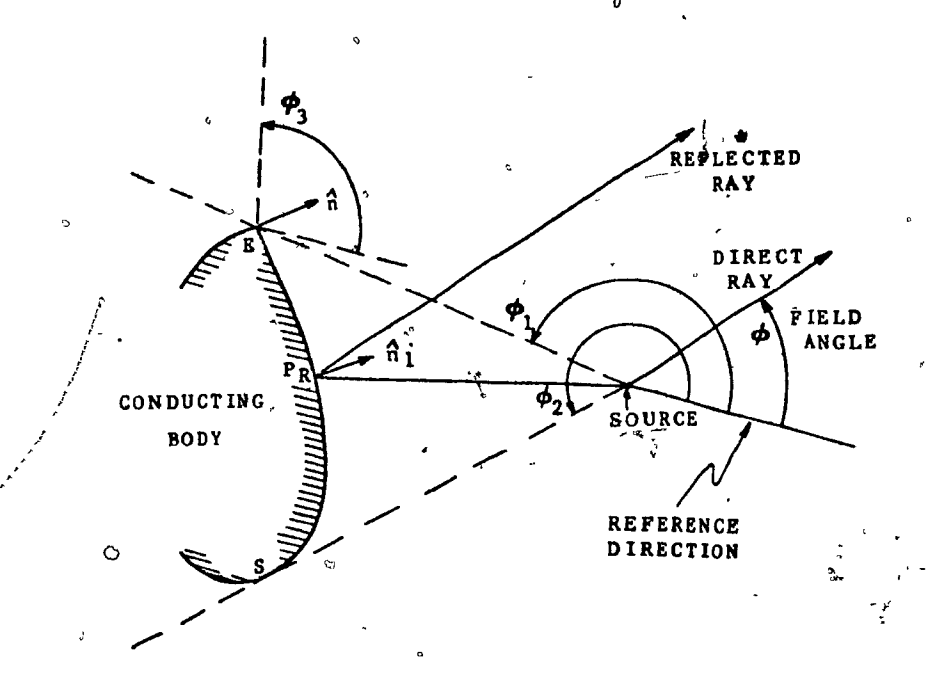


Fig. 2.7 A point source radiating in the presence of a conducting body.

2.4 Smooth Bodies and Bodies with Edges.

A body is smooth at a point on its surface if the unit normal vector is continuous. An edge is a locus of points on the surface where the body is not smooth. By definition, an edge has a continuous tangent vector. A "vertex" is a point where two or more edges meet, or where an edge terminates. Edge-less vertices also exist, such as the vertex of a cone.

A current element radiates in the presence of a body, Fig. 2.7, and the far field in the plane of the paper is sought as a function of the field angle. For $\phi < \phi_1$ there is a direct ray through the distant field point. For $\phi > \phi_1$ the body obstructs the direct ray and there is null GTO field at the field point, which lies in the body's

غر

٨

shadow. Angle ϕ 1 is a "shadow boundary" (SB). The GTO field is discontinuous at an SB, because the direct field vanishes. Angle ϕ 1 is also an SB.

The body of Fig. 2.7 has an edge at E. For $\phi < \phi_3$ the point of reflection on the body lies away from the edge, and there is a reflected ray at the field point. For $\phi + \phi_3$ the reflection point approaches the edge. For $\phi > \phi_3$ there is no point P_R on the body which satisfies Alhazen's Law. Hence at ϕ_3 the reflected field vanishes. Angle ϕ_3 is a "reflection boundary" (RB). The GTO field is discontinuous at an RB.

A point of "grazing incidence" is a point on the body where the ray from the source travelling along the body just touches the body's surface. Points E and S are points of grazing incidence in Fig. 2.7. Note that angle ϕ_2 is also an RB as well as an SB. When the body is smooth at a point of grazing incidence, the RB and the SB coincide.

2.5 Geometrical Diffraction Theory

The "Geometrical Diffraction Theory" (GDT) is an extension of geometrical optics, in which a new class of ravs is introduced, called "diffracted rays". These were first proposed by J.B. Keller in 1953 (16). The GDT field at any point is the sum of the GTO field, and the field associated with all the diffracted rays through the point.

A ray incident upon a point on an edge causes diffracted rays to emanate from that point. A ray illuminating a vertex gives rise to a class of diffracted rays originating at the vertex point. When a ray

has grazing incidence at a point on a body, a "surface diffracted" ray travels out along the body's surface, "shedding" diffracted rays tangentially out from each point on its path (1,4,5).

The GDT models diffracting features by simpler "canonical problems", with the same local geometry as the body has in the neighbourhood of the point of diffraction. It is a fundamental assumption of the GDT that diffraction is a local process so that the diffracted field of the feature is identical to and indistinguishable from the diffracted field of the canonical problem. Each canonical problem has its "Law of Diffraction", which determines the direction in which the diffracted rays will travel out from the point of diffraction, and a "diffraction coefficient" which relates the field on each diffracted ray to the field illuminating the feature. The linearity of Maxwell's Equations dictates that the diffracted field must be proportional to the strength and vector direction of the incident field. Hence we would expect a transformation to exist which maps incident fields into diffracted field

$$\overline{E}_{d} = \overline{E}_{1} \overline{\overline{D}} \rightarrow \cdot$$

2.5.1

The dvadic diffraction coefficient \overline{D} can change the magnitude, phase, and vector direction of the incident field. Its elements are functions of the angles of incidence and diffraction, the distances to the source and field point, and the radii of curvature of the incident wavefront. In solving a canonical problem, the simplest form of $\overline{\overline{D}}$ is sought.

wedge. It is used to find edge diffracted fields by orienting its planes to be tangent to the body's surfaces at the point of diffraction. At present there is no vertex diffraction coefficient available in the

literature (1). Other canonical problems have been tried, such as the diffraction from a small cylinder, used by Burnside (3) to model the wing-mounted engines in the roll plane analysis of the radiation fields of an antenna on a small aircraft. The method of calculating the diffracted fields of an infinite wedge is given in Chapter 3, including the Law of Edge Diffraction, the reduction of $\overline{\overline{D}}$ to its simplest form, and a new expression for the elements of $\overline{\overline{D}}$, Kouvoumian's "Transition Diffraction Coefficient", which is designed to overcome many of the disadvantages of the original Keller coefficient.

CHAPTER 3

THE INFINITE WEDGE CANONICAL PROBLEM

3.1 The Infinite Wedge Canonical Problem

The infinite wedge consists of two conducting half-planes which meet at a straight line to form an edge, Fig. 3.1. The incident ray makes an angle β 0 to the edge, and its projection onto a plane perpendicular to the edge makes an "incident angle" ψ 0 with the wedge's reference plane, Fig. 3.2. Similarly, the out-going diffracted ray makes an angle β 1 to the edge and a "diffraction angle" ψ 1 to the reference plane. The wedge itself has an angle α .

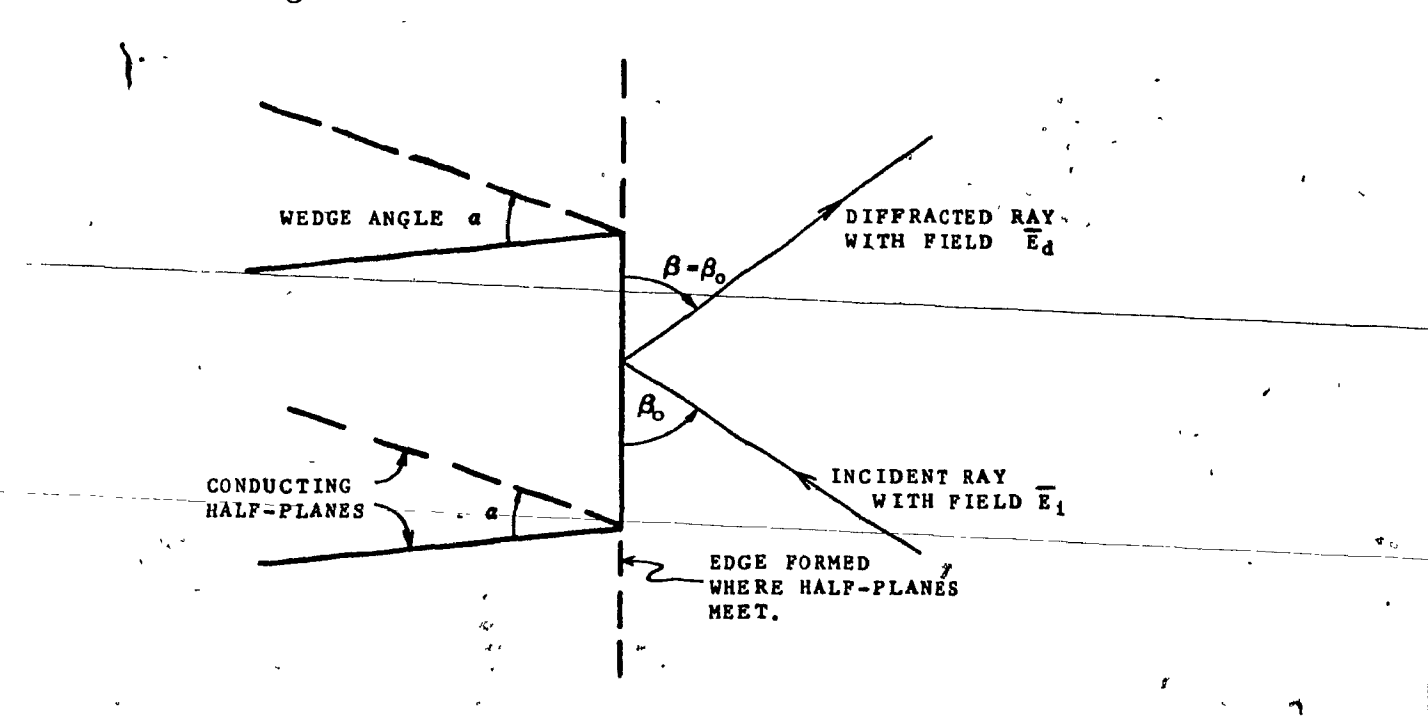


Fig. 3.1 The infinite wedge.

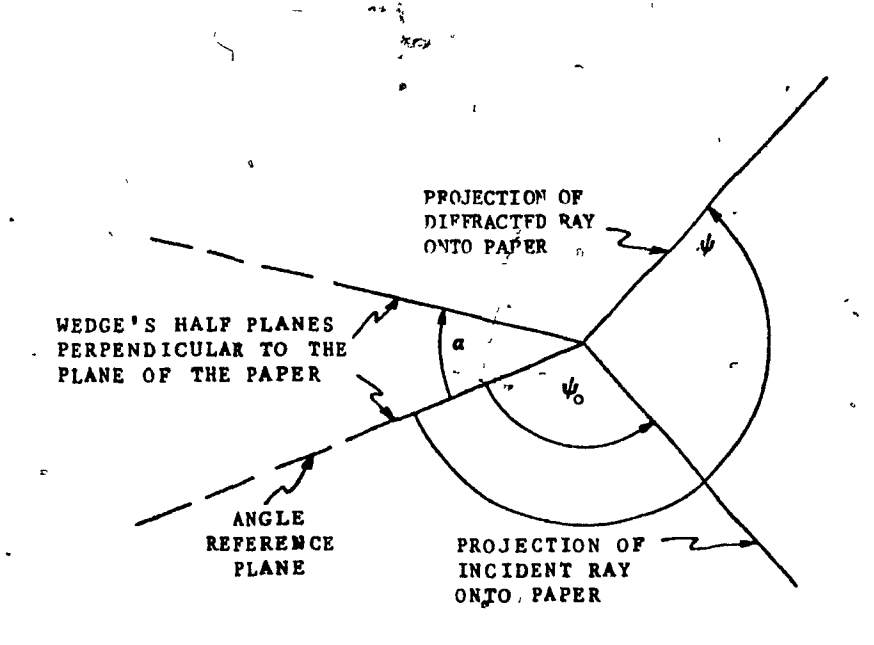


Fig. 3.2 Cross section of the infinite wedge problem

This chapter details the infinite wedge canonical problem, which is used in the next chapter to calculate fields diffracted from edges. The "Law of Diffraction" is given and its consequences discussed. The simplest form of the dyadic diffraction coefficient is developed and expressions for its elements are quoted from the literature. A set of subroutines for computing the diffracted field from a straight edge are given which are useful in the solution of an antenna-scatterer problem in the next chapter.

3.2 The Law of Edge Diffraction

The "Law of Edge Diffraction" (1,4,5) states that the diffracted rays lie on a cone of half angle β equal to the angle of incidence β 0, with the point of diffraction as its vertex, and the tangent to the edge as its axis.

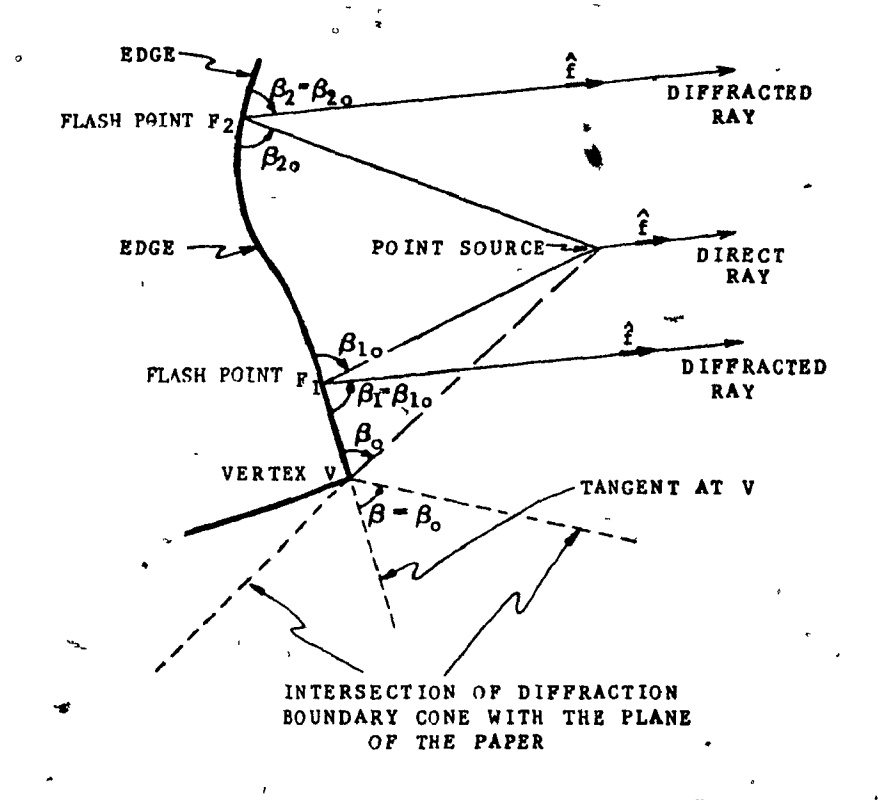


Fig. 3.3 Flash points on an edge, and a diffraction boundary.

In Fig. 3.3, a point source radiates near an edge which lies in the (x,y) plane. It is a direct consequence of the Law of Edge Diffraction that only certain "flash points" on the edge, F_1 and F_2 , can launch a diffracted ray in a given "field direction", designated by direction vector $\hat{\mathbf{f}}$. When an infinite wedge is located at a flash point with planes coincident with the body's tangent planes, the ray from the source to the flash point and the field direction vector $\hat{\mathbf{f}}$ satisfy the Law of Edge Diffraction. Other points on the edge do not have $\beta = \beta o$. The edge diffracted field is then identical to the field diffracted by the infinite wedge, which is readily calculated, as detailed below.

If the body has a vertex, as at V in Fig. 3.3, then the tangent to the edge and the ray from source to vertex define a cone in space according

0

to the Law of Edge Diffraction. On one side of this conical surface, there is a diffracted ray from the edge, but on the other side, there is no point on the edge which satisfies the Law, and hence no diffracted ray. The diffracted field vanishes as the surface of this limiting cone is crossed, and this surface is defined as the "diffraction boundary" (DB).

3.3 The Simple Diffraction Coefficient

The "simple" form of the wedge diffraction coefficient (6) is obtained as follows. Consider a plane wave normally incident on the edge of an infinite wedge, Fig. 3.4. Any general polarization can be resolved into two components, in which the electric field vector is perpendicular to the edge ("hard" boundary condition) or the magnetic field is perpendicular ("soft' case). In either case the field may be then treated as scalar. Keller argues that the diffracted field must be an outgoing cylindrical wave with the edge as its axis,

$$E_{d} = D_{s}^{i} E_{i} \frac{e^{-jkr}}{\sqrt{kr}}$$
3.3.1

where E_1 is the incident field evaluated at the point of diffraction, r is the distance from the edge, and the subscripts are for "soft" or "hard". The reduced diffraction coefficient D' is related to the full coefficient by

$$\frac{e^{-jkr}}{h} = \frac{\sqrt{kr'}}{\sqrt{kr'}}$$

In turn, D must later be related to the elements of the dyadic diffraction h coefficient $\overline{\overline{b}}$ in (2.5.1). Keller compares (3.3.1) with an expression asymp-

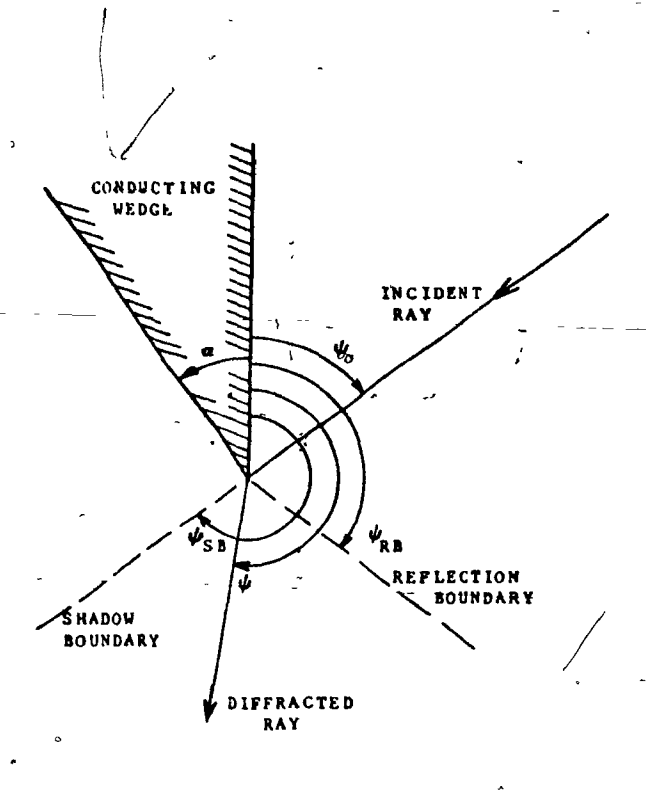


Fig. 3.4 A ray normally incident on a conducting wedge.

and concludes that the reduced coefficient must be

$$\overset{\circ}{\mathbf{h}} = \frac{e^{j\pi/4} \sin \pi/n}{n \sqrt{2\pi} \sin \beta} \left[\frac{\cos \pi}{n} - \cos \frac{\psi - \psi_0}{n} \right]^{-1} \\
+ \left[\cos \frac{\pi}{n} - \cos \frac{\psi + \psi_0}{n} \right]^{-1} \\
3.3.3$$

where n is related to the Wedge angle α by

$$(2-n)\pi = \alpha$$
 3.3.4

For normal incidence β = 90° and $\sin \beta$ = 1. For other than normal incidence, conservation of energy in the cone of diffracted rays gives the 1 / $\sin \beta$ factor. The "-" sign is for the "soft" case, and the "+" for the "hard".

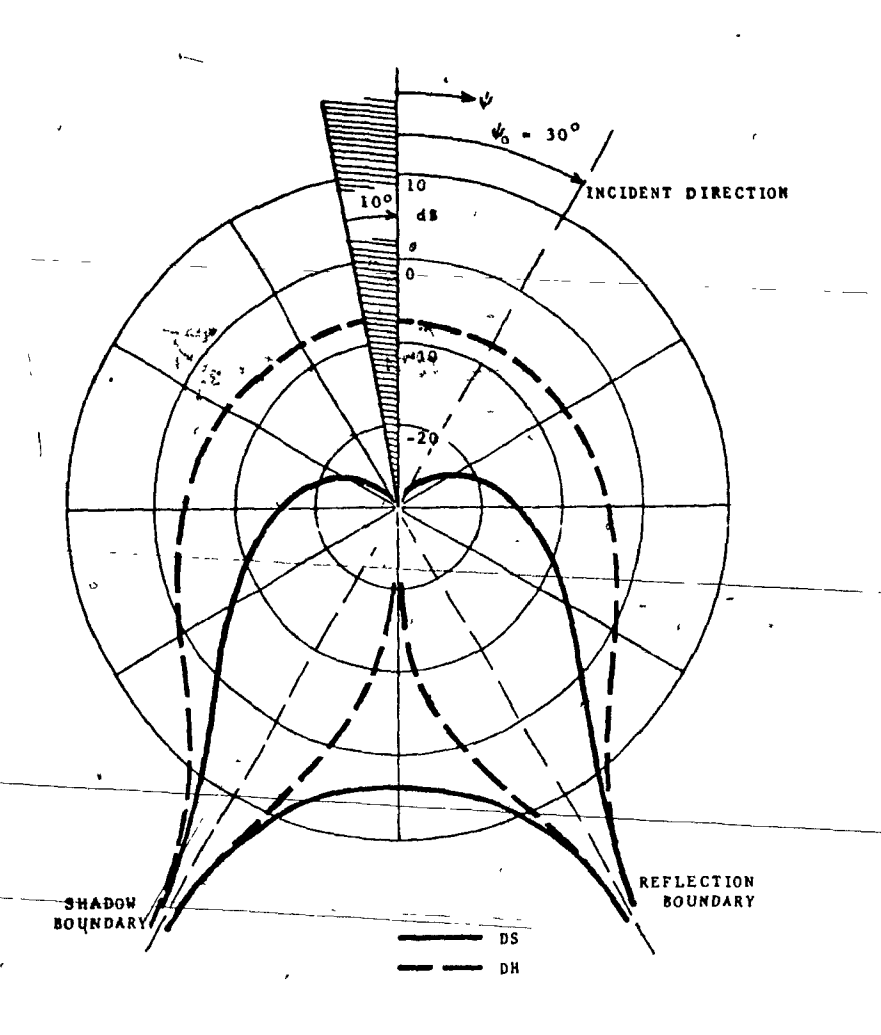


Fig. 3.5 The simple diffraction coefficients for a plane wave incident at 30° on a 10° wedge.

In Fig. 3.5 the diffraction coefficients D_s and D_h are plotted as functions of the diffraction angle ψ for incident angle $\psi_0 = 30^\circ$, $\beta = 90^\circ$, and a 10° wedge, on a dB scale. The "soft" diffracted field falls to zero along the planes of the wedge, although the "hard" coefficient is only 7.5 dB down from the illuminating field.

The simple diffraction coefficient becomes unbounded near the

shadow and reflection boundaries. Near an SB, for example, ψ is nearly π - ψ_0 , and thus the second term in the diffraction coefficient becomes large. The simple diffraction coefficient is said to be valid "far" from RBs and SBs .

3.4 The Edge-Related Coordinates.

This section defines the edge-related coordinates (4,5) and shows that they allow the dyadic diffraction coefficient D to be written in its simplest form.

If the illuminating field \overline{E}_{i} is written relative to some "incident" coordinate system as

$$\overline{E}_{i}$$
 * (E_{i1} , E_{i2} , E_{i3})

and the diffracted field relative to some "diffracted" coordinates as

$$\overline{\mathbf{E}}_{\mathbf{d}} = (\mathbf{E}_{\mathbf{da}}, \mathbf{E}_{\mathbf{db}}, \mathbf{E}_{\mathbf{dc}})$$

which are not necessarily the same as the incident coordinate directions, the dyadic diffraction coefficient may then be written in full as

$$\begin{bmatrix} E_{da} \\ E_{db} \\ E_{dc} \end{bmatrix} = (E_{11}, E_{12}, E_{13}) \begin{bmatrix} D_{1a} D_{1b} D_{1c} \\ D_{2a} D_{2b} D_{2c} \\ D_{3a} D_{3b} D_{3c} \end{bmatrix}$$

3.4.1

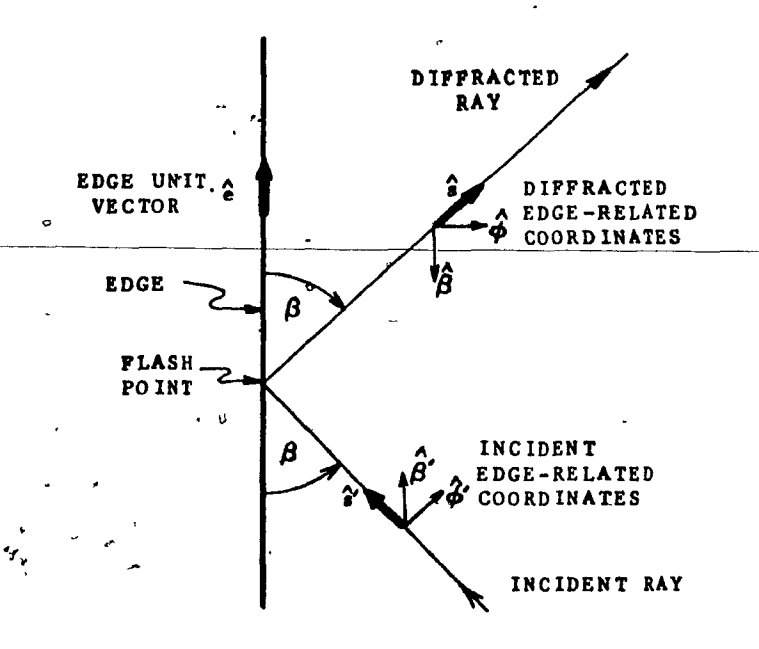


Fig. 3.6 The edge-related coordinates.

In general the elements of $\overline{\overline{D}}$ are all functions of the direction angles ψ , ψ_0 , β , of the distance to the field point, and the radii of curvature sof the incident wavefront.

It is apparent from Sect. 3.3 that the components of incident fields parallel and perpendicular to the edge are of fundamental importance to the diffraction process. Let ê be a unit vector in the direction of the edge, Fig. 3.6. If ŝ is a unit vector along the incident ray, a coordinate direction ê can be defined,

$$\hat{\phi}' = \frac{\hat{\mathbf{s}}' \times \hat{\mathbf{e}}}{|\hat{\mathbf{s}}' \times \hat{\mathbf{e}}|}$$

3.4.2

Unit vector $\hat{\phi}^{\dagger}$ is perpendicular to both the direction of incidence and the edge. If \hat{s} points along the diffracted ray, then unit vector

$$\hat{\phi} = \frac{\hat{\mathbf{e}} \times \hat{\mathbf{s}}}{|\hat{\mathbf{e}} \times \hat{\mathbf{s}}|}$$

is also perpendicular to the edge. The component of diffracted field along $\hat{\phi}$ obeys the "hard" boundary condition with respect to the component of incident field along $\hat{\phi}$. Thus

$$\frac{E_{d\phi}}{d\phi} = \overline{E}_{d} \cdot \hat{\phi} = D_{h} \overline{E}_{i} \cdot \hat{\phi} = -D_{h} E_{i\phi}, \qquad 3.4.4$$

The incident field cannot have a component in the direction of propagation. Thus its only other component must be in direction

$$\hat{\beta}_0^* = \hat{s}^* \times \hat{\phi}$$
 3.4.5

The magnetic field associated with the $\hat{\beta}_0'$ component of E_1 is perpendicular to the edge. The component of diffracted field in direction

$$\hat{\beta} = \hat{\mathbf{s}} \times \hat{\boldsymbol{\phi}} \qquad 3.4.6$$

has an associated magnetic, field perpendicular to the edge. Hence the $\hat{\beta}$ components of \overline{E}_{1} obeys the "soft" boundary condition with the $\hat{\beta}_{0}^{i}$ component of \overline{E}_{1} ,

$$\underline{E}_{d\beta} = \overline{E}_{d} \cdot \hat{\beta} = -D_{\overline{S}} \overline{E}_{i} \cdot \hat{\beta}' = -D_{S} E_{i \beta'_{O}}$$
3.4.7

The "incident edge-related coordinates" are (\hat{s} , $\hat{\phi}$, $\hat{\beta}_0$) given by (3.4.2) and (3.4.5), and are illustrated in Fig. 3.6. The "diffracted edge related coordinates" are (\hat{s} , $\hat{\phi}$, $\hat{\beta}$) given by (3.4.3) and (3.4.6). When the incident field and the diffracted field are resolved into the edge-related components, by virtue of (3.4.4) and (3.4.7) the general diffraction equation (3.4.1) can then be re-written in its simplest form

$$\overline{E}_d = (O, -D_h E_{i\phi'}, -D_s E_{i\beta'_o})$$
 3.4.8

By proper choice of coordinate systems, $\overline{\mathbf{D}}$ has only two non-zero elements.

3.5 The Transition Diffraction Coefficient

Consider the wedge diffraction problem of Fig. 3.4. At all field points the total field must be continuous. As the field point approaches a reflection or shadow boundary, where a component of the GTO field vanishes, the diffracted field must increase until its magnitude is comparable to the direct field. It must then exhibit a discontinuity at the boundary so that the total field remains smooth. As the field point moves away from the boundary, the diffracted field once again decreases. The four zones of space, where the diffraction coefficient exhibits this special behavior, are called "transition regions" and lie one on each side of the reflection and shadow boundary. The simple diffraction coefficient becomes unbounded in the transition regions, as illustrated in Fig. 3.5.

The best diffraction coefficient available in the literature to date is Kouyoumjian's "dyadic diffraction coefficient" (1,4,5,9) at which a specific function for the elements of $\overline{\mathbb{D}}$, and which shall be referred to as the "Transition Diffraction Coefficient" (TDC) in this thesis. It is valid at nearly all field points, including those inside the transition regions. This largely replaces other, more cumbersome methods such as: those evaluating series of Bessel functions; those using limiting expressions at certain field points (2); those postulating equivalent currents on the edge, (whose value must be found, and whose field is used inside the transition zones); or other tedious procedures valid only for special field points in specific problems. The TDC breaks down only when the field point is very near the point of diffraction, or when angle β (Fig. 3.1) is near 0° .

The TDC is derived in (9). An asymptotic solution to the wedge diffraction problem is obtained by the method of steepest descent. The leading term of the resulting generalized Pauli expansion is found to contain a simple correction factor or "transition function" which allows the diffracted field to be computed easily inside the transition regions. The transition function is unity valued away from the transition regions, making the TDC identical to Keller's simple coefficient there.

The TDC has a term containing the transition function for each of the four transition regions. When the field point under consideration enters a transition zone, the transition function in the appropriate term of the TDC "switches on". As the boundary is crossed, that transition function "switches off" and the correct one for the new region turns on, making the diffraction coefficient discontinuous at the boundary, and as a result the total

field remains smooth.

The Transition Diffraction Coefficient, which is described in greater detail in (1,4,5,9) which has the following form:

$$\frac{-k \, e^{r j \pi/4}}{2n \sqrt{2\pi k} \, \sin \beta_0} \times \frac{\pi + (\psi - \psi_0)}{2n} \, F \left[kL \, a^{\dagger} (\psi - \psi_0) \right] + \cot \frac{\pi - (\psi - \psi_0)}{2n} \, F \left[kL \, a^{\dagger} (\psi - \psi_0) \right] + \cot \frac{\pi - (\psi + \psi_0)}{2n} \, F \left[kL \, a^{\dagger} (\psi + \psi_0) \right] + \cot \frac{\pi - (\psi + \psi_0)}{2n} \, F \left[kL \, a^{\dagger} (\psi + \psi_0) \right]$$

$$\frac{a^{\dagger} (\psi + \psi_0)}{2n} = 2 \cos^2 \frac{2n\pi \, N^{\frac{1}{2}} - (\psi + \psi_0)}{2} \quad 3.5.2$$

where N * most nearly satisfy

$$2\pi \text{ nN}^+ - (\psi \pm \psi_0) = \pi$$
 3.5.3a
$$2\pi \text{ nN}^- - (\psi \pm \psi_0) = \pi$$
 3.5.3b

and L is a distance parameter dependent on the radii of curvature of the incident field.

In general, the reduced diffraction coefficient is related to the complete form by

$$D_{s} = D_{s}^{1} A(r) e^{-jkr}$$
 3.5.4

Kouyoumjian (1,4,5) gives expression for the divergence factor A (r) for various

incident waves. Thus for plane wave illumination with the field point far from the edge, $1/\sqrt{kr}$ is used as in Sect. 3.3. In antenna problems using a point source, the incident wave has spherical divergence, and for far field observation points, the divergence factor is

$$A(r) = 1/kr$$

F(X) is the transition function given by

$$F(X) = 2j \int X' e^{jX} \int_{X'}^{\infty} e_{i}^{-jt^2} dt$$

For X > 10, $F(X)' \simeq 1$. If all the transition function arguments in the TDC are greater than 10, then the TDC is the same as the Keller coefficient. Thus the region of validity of the simple form is clearly established.

A computer subroutine "DIFFLD", which evaluates the TDC, has been developed during this project and is listed in App.3. In addition, a simple, fast computational method for evaluating the transition function \(\mathbb{F}(\mathbb{X}) \) was developed, and is detailed in App.4.

In Fig. 3.7 the transition diffraction coefficient is plotted in dB as a function of the field angle ψ , for the same problem as in Fig. 3.5. Note that the TDC is bounded but discontinuous at the shadow and reflection boundary.

3.6 Evaluation of the Field Diffracted from a Straight Edge

A straight edge running between vertices at \overline{P}_1 and \overline{P}_2 as illuminated by a point source located at \overline{R}_c . Fig. 3.8 shows the plane containing

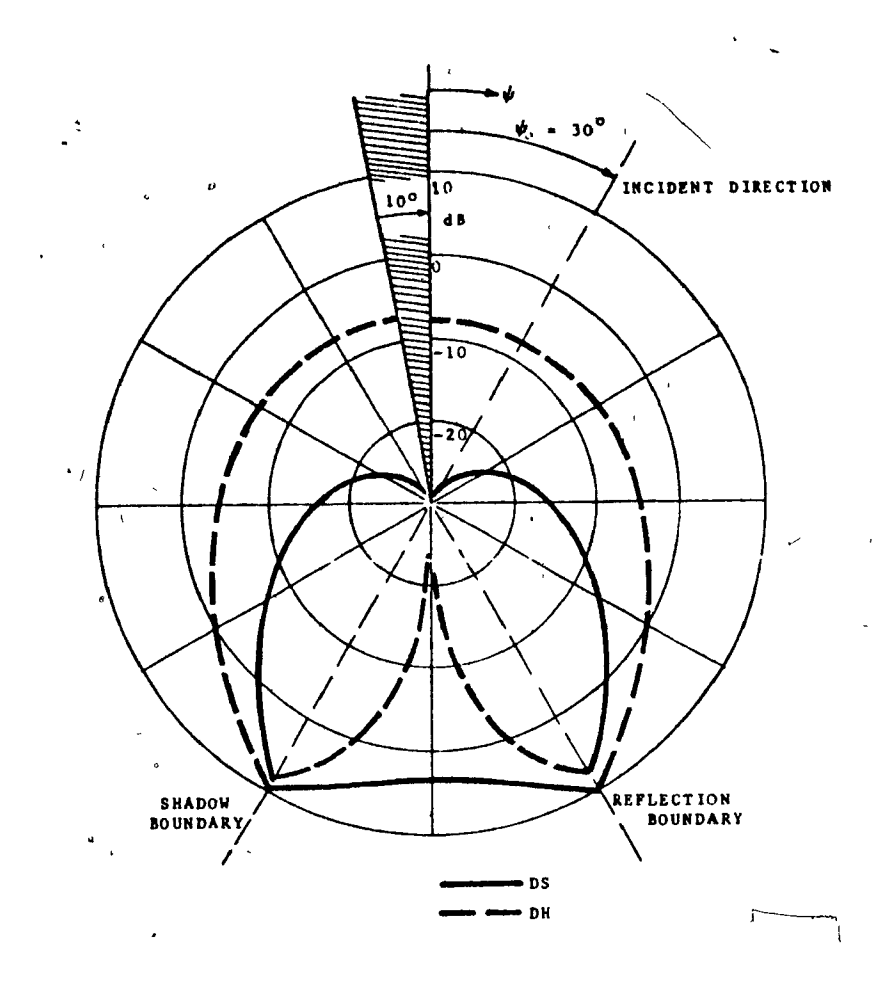


Fig. 3.7 The transition diffraction coefficients for a plane wave incident at 30° on a 10° wedge.

the edge and the source point $\overline{\mathbf{x}}$. The diffracted field at a distant point in direction f is to be found.

F. y.

A ray from the source incident on a point \overline{P} on the edge makes an angle

$$\cos \beta_{o} = \hat{s}' \hat{e}$$
 3.6.1

with the edge, where \hat{e} is the unit vector pointing along the edge from \overline{P}_1 to \overline{P}_2 , and unit vector \hat{s}' points from the source to \overline{P} . When \overline{P} coincides with \overline{P}_1 , β_0 assumes its greatest value β_1 , and for \overline{P} at \overline{P}_2 , β_0 is a minimum β_2 . Hence, for any \overline{P}

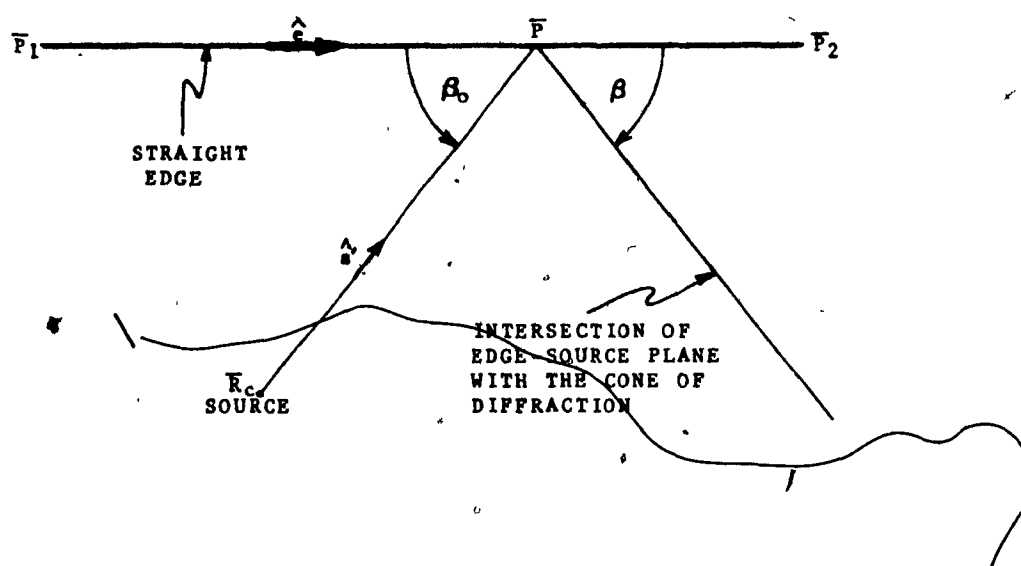


Fig. 3.8 The geometry of a far field diffraction calculation

$$\beta_1 > \beta_0 > \beta_2$$
 $\cos \beta_1 < \cos \beta_0 < \cos \beta_2$

Given a field direction f, the half-angle of the cone of diffraction is fixed as

$$\cos^2 \beta = \hat{f} \cdot \hat{e}$$

or

The flash point on the edge satisfies the Law of Edge Diffraction, which requires that angle β = angle β . There is a flash point on the edge only if the angle between the field direction and the edge, β , lies between the two extreme values for β , hence β must satisfy

4

....

$$\cos \beta_1 < \cos \beta < \cos \beta_2$$
 $\cos \beta_1 < \hat{f} \cdot \hat{e} < \cos \beta_2$

otherwise no flash point exists. In order to find the flash point, an iterative method is used. A test point \overline{P}_t on the edge is chosen, and the incident angle cosine, $\cos \beta_t$ is computed.

 \overline{P}_t lies too near to the \overline{P}_1 end of the edge, and a new test point is chosen, closer to \overline{P}_2 . The method converges rapidly.

Once the flash point \overline{P}_f is found, the edge diffracted field is readily calculated. The source field is evaluated at \overline{P}_{f} (Sect. 2.2)

where
$$\overline{\mathbf{E}}_{\mathbf{S}} (\overline{\mathbf{P}_{\mathbf{f}}}) = E_{\mathbf{o}} \frac{e^{-\mathbf{j}k\mathbf{R}_{\mathbf{SF}}}}{K\mathbf{R}_{\mathbf{SF}}} (\mathbf{\hat{p}} \times \mathbf{\hat{s}}') \times \mathbf{\hat{s}}'$$
where
$$R_{\mathbf{SF}} = |\overline{\mathbf{P}_{\mathbf{f}}} - \overline{\mathbf{R}_{\mathbf{c}}}|$$
and
$$\mathbf{\hat{s}}' = (\overline{\mathbf{P}_{\mathbf{f}}} - \overline{\mathbf{R}_{\mathbf{c}}}) / R_{\mathbf{SF}}$$

and

The incident edge-related coordinate unit vectors (Sect. 3.4) (β', ۴", β') are then found, and g is resolved into o and g components

$$\overline{E}_{s} = (0, E_{s\phi'}, E_{s\beta'})$$

The diffracted edge related components of the diffracted field are then found using (3.4.8)

$$\overline{E}_{d}$$
 * (0, $-D_{h} E_{s\phi}$, $-D_{s} E_{s\beta}$)

where D and D are the TDC evaluated for the appropriate incident and diffraction angles. The diffracted field vector $\overline{\mathbf{E}}_{\mathbf{d}}$ is rewritten relative to the base coordinates by evaluating the diffracted edge-related unit vectors (Sect. 3.4), ($\hat{s} = \hat{f}$, ϕ , $\hat{\beta}$). The diffracted field is then phase referred to the position of the source (Sect. 2.3), which completes the calculation.

Subroutine DIFEDG (App. 5) was developed to compute the field diffracted by a straight edge in a given field direction, by the method detailed above.

The work presented in this chapter provides the computational foundation for the analysis of a variety of specific problems. The remainder of this thesis is devoted to the study of one such problem, the horizontal plane radiation pattern of a current element centered in front of a rectangular conducting sheet, or "plate". It is found that the GDT provides great insight into the shape of the pattern as a function of the physical dimensions of the plate and the separation distance of the source, as is described in Chapter 4.

CHAPTER 4

THE FLAT PLATE PROBLEM

4.1 The Flat Plate Problem

A current element antenna radiates in the presence of a flat rectangular conducting sheet, or "plate", Fig. 4.1, of the width w and height h. The source is centered in front of the plate, spaced from it by the "separation distance", a, and is parallel to its vertical edges. The H-plane pattern of the current element is affected considerably by reflections and diffractions from the plate, and a systematic study of the resulting patterns is undertaken in this chapter. The computed patterns for a two-dimensional model of the plate are reduced to a small number of synoptic graphs which allow the original patterns to be reconstructed or new ones generated for any plate width and source separation distance within the range covered. The pattern of the full three-dimensional model is investigated as a function of plate height, and computations are compared with experimental results and published data.

.4.2 The Two-Dimensional Plate

If a radiating body is much larger in one dimension than in the others, the radiation field in the plate perpendicular to the long axis can often be found with sufficient accuracy by assuming that the body is infinitely long, and simply using a two-dimensional (2-d) model. Thus Burnside uses a 2-d model to find the roll plane pattern of an on-aircraft antenna (3). The essential

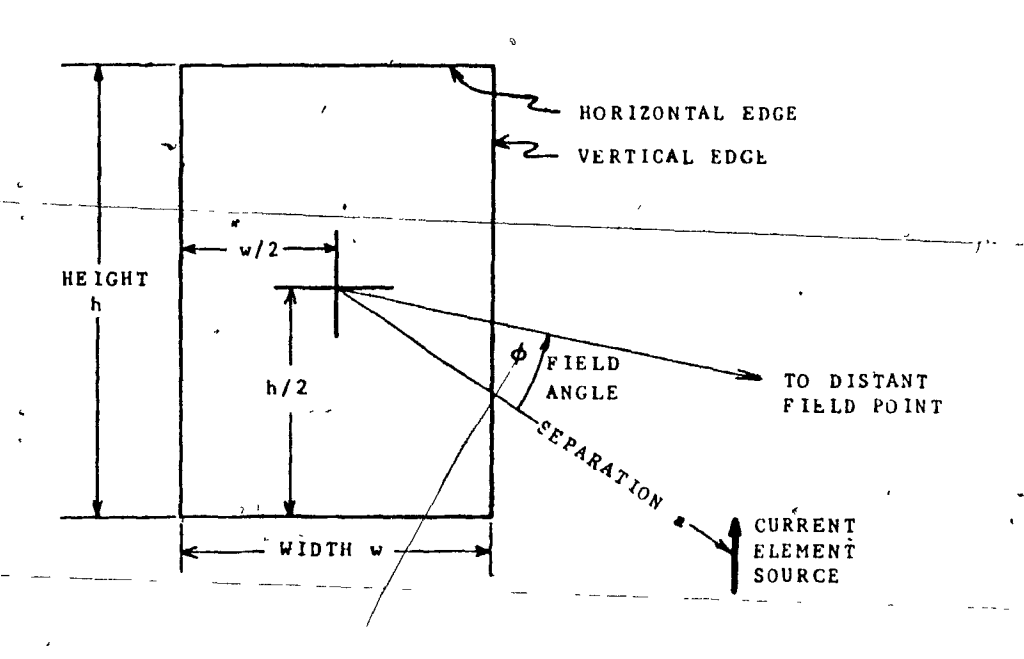


Fig. 4.1 The rectangular flat plate.

assumption is that the distant ends of the structure contribute only negligibly in the principle plane pattern to the total field.

The taiculation of the H-plane pattern may be approached by considering plates much taller than they are wide. The horizontal edges may then be neglected as they contribute insignificantly in the principle plane pattern to the total field, and an essentially two-dimensional plate remains, Fig. 4.2. The pattern of the three-dimensional plate of height h is a variant of the corresponding 2-d pattern, and is found by including the fields diffracted by the horizontal edges.

A similar problem was studied by Bavou (8), using the surface element method. The H-plane pattern of a right circular cylinder illuminated by a dipole antenna parallel to its axis was studied as a function of the cylinder diameter and the dipole separation distance. The pattern is smooth,

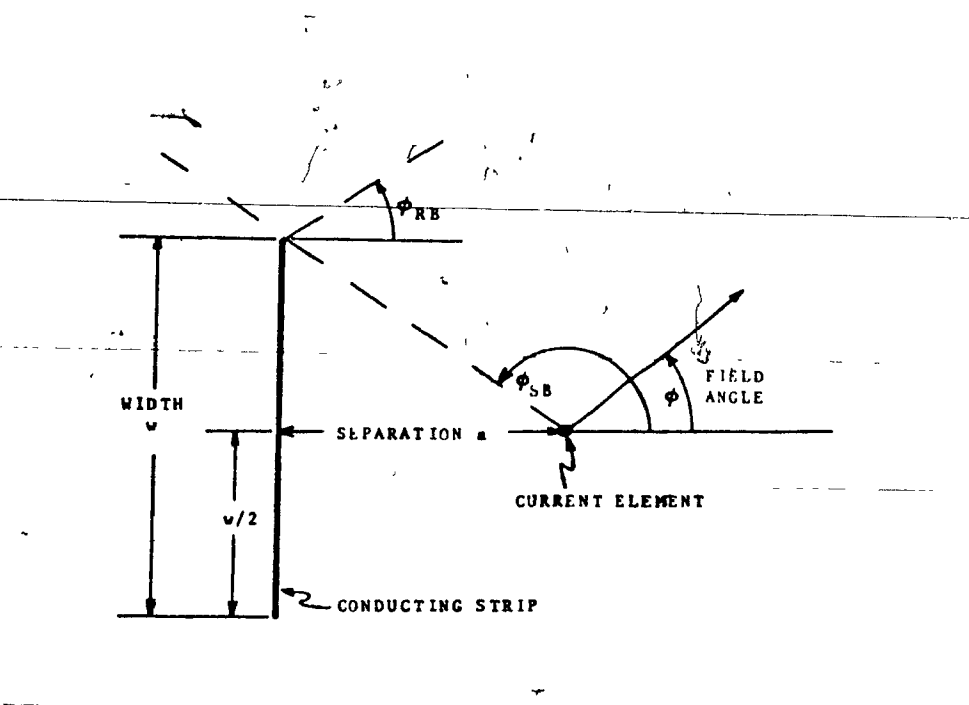


Fig. 4.2 The 2-d plate, plan view.

with low peaks and shallow vallevs. The number of minima is proportional to separation distance, a new pair being added for every half-wavelength increase in separation. Furthermore, the minima location angles for a given diameter move smoothly as a function of separation. Bayou compiled the results into "parametric curves" which give the number of minima, their location angles, and the maximum to minimum ratio, which may be used to sketch the H-plane for any diameter-separation combination. One objective of this study is to determine whether similar graphs can be constructed for the flat plate problem.

4.3 The GTO Solution to the Flat Plate Problem

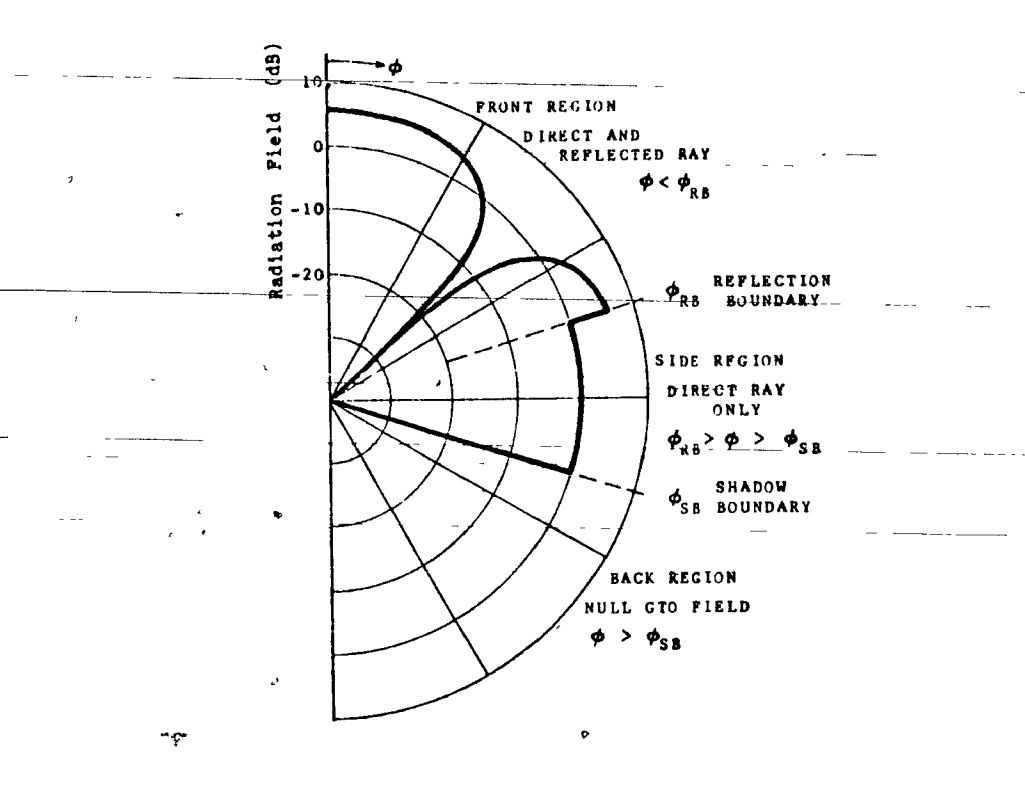


Fig. 4.3 . The GTO pattern for $w = 5\lambda$, $a = 0.75 \lambda$.

to find the Geometrical Optics fields (Sect. 2.1), and thus gain the insight into the problem that this simple method has to offer.

Because of the symmetry of the problem in Fig. 4.2, the field need only be found for

$$0^{\circ} < \phi < 180^{\circ}$$
 4.3.1

and all further discussion in this chapter refers to this half pattern.

A typical GTO pattern is shown in Fig. 4.3. There is a reflection boundary at

$$\phi_{RR} = \tan^{-1} (w/2a)$$
 4.3.2

and a shadow boundary at

$$\phi_{SB} = 180^{\circ} - \phi_{RB}$$
 4.3.3

At the reflection boundary angle ϕ_{RB} , the reflected component of field vanishes abruptly, and in the "side region" ($\phi_{RB} < \phi < \phi_{SB}$) the GTO field is the constant source field alone

$$\overline{E}_{GTO} = -1\hat{z}$$
 4.3.5

At the shadow boundary angle ϕ_{SB} , the source field vanishes, and the field in the "back region" or "shadow region" ($\phi > \phi_{SB}$) is zero, since the field point lies in the plate's shadow.

Although GTO patterns such as Fig. 4.3 can be computed by the direct evaluation of 4.3.4 and 4.3.5, the patterns were in fact calculated by calling the general reflection subroutine REF (App. 2), which automatically finds the reflected field normed and phase referred to the source. The main program is listed in Appendix 6.

The direct and reflected fields are in phase at angles given by

$$\cos \phi = \frac{1}{4a}, \frac{3}{4a}, \frac{5}{4a}, \dots$$
 4.3.6

At these angles there is a 6 dB peak in the GTO pattern. The nulls occur at angles given/by

$$\cos \phi = \frac{1}{2a}, \frac{2}{2a}, \frac{3}{2a}, \dots$$
 4.3.7

These peak and null angles are graphed as a function of source separation distance in Fig. 4.4, along with the reflection boundary angle for a variety of widths.

Fig. 4.4 illustrates that a new maximum is added to the pattern at $\phi = 0^{\circ}$ for each λ / 2 increase in separation. The maxima have been numbered in their order of appearance as separation increases. After the

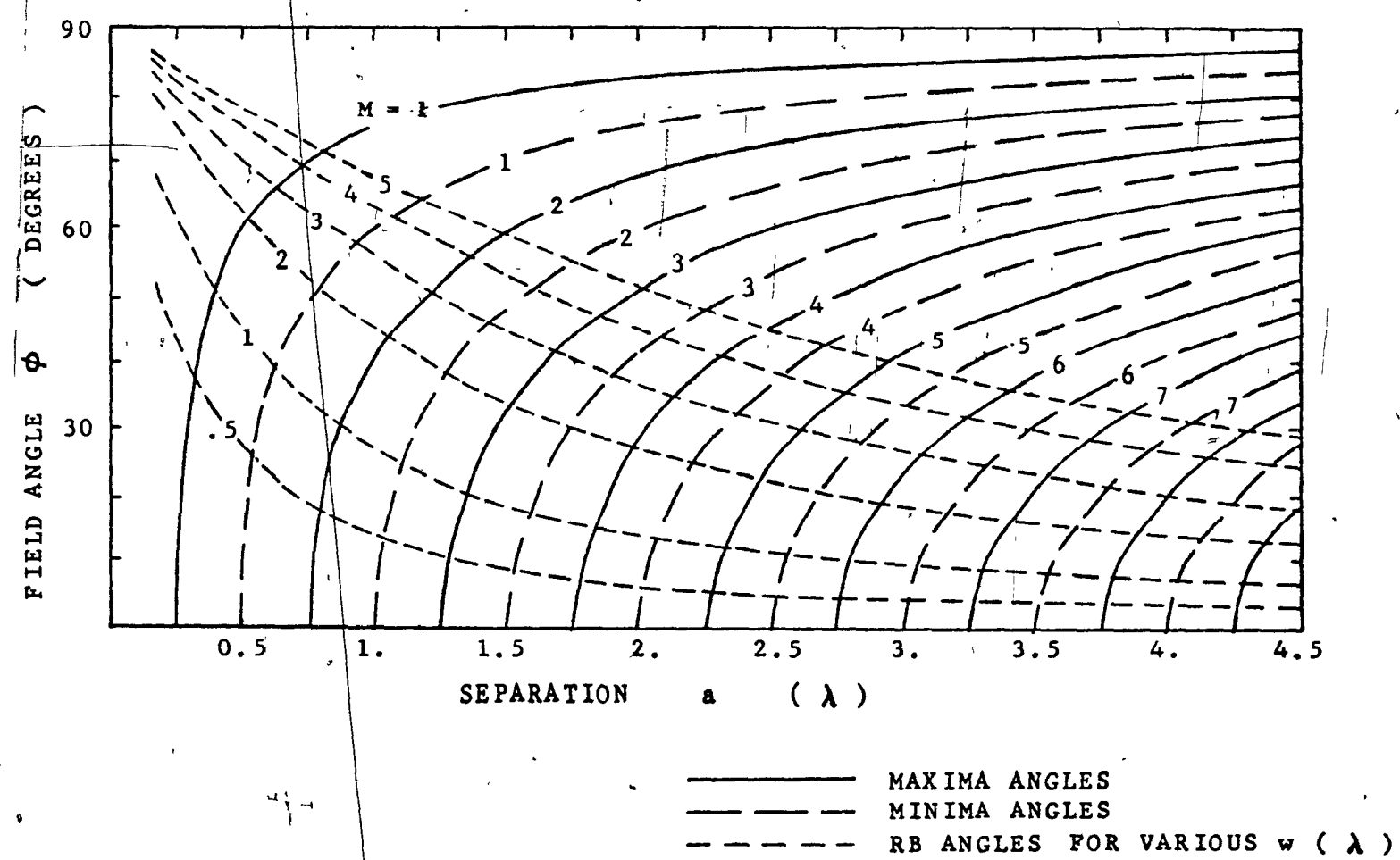


Fig. 4.4 The location angle diagram for the GTO pattern minima.

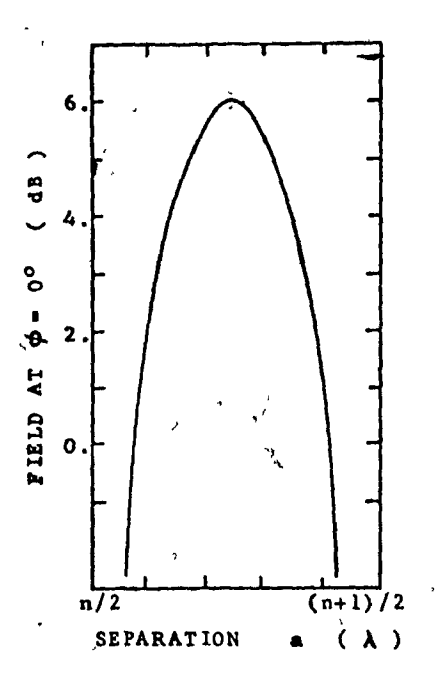


Fig. 4.5 Value of the GTO field at $\phi = 0^{\circ}$ between two minima.

Mth maximum has appeared at $\phi = 0^{\circ}$, it moves smoothly through the pattern with increasing separation, until it coincides with the reflection boundary, where it disappears. A vertical line drawn in Fig. 4.4 for a particular separation 'a', intersects the curves giving the angles of the 6 dB peaks and the nulls in the front region of the pattern, and the angle of the reflection boundary.

Fig. 4.5 gives the field at $\phi = 0^{\circ}$ when neither a maximum nor a minimum occurs at that angle. The value is given as a function of the source to plate separation distance within any half-wavelength interval between minima. Thus Fig. 4.4 and 4.5 provide enough information to sketch the GTO pattern with reasonable accuracy for any plate width and source separation distance in the range covered. This graph and others like it may be useful to the designer, in

ಜ

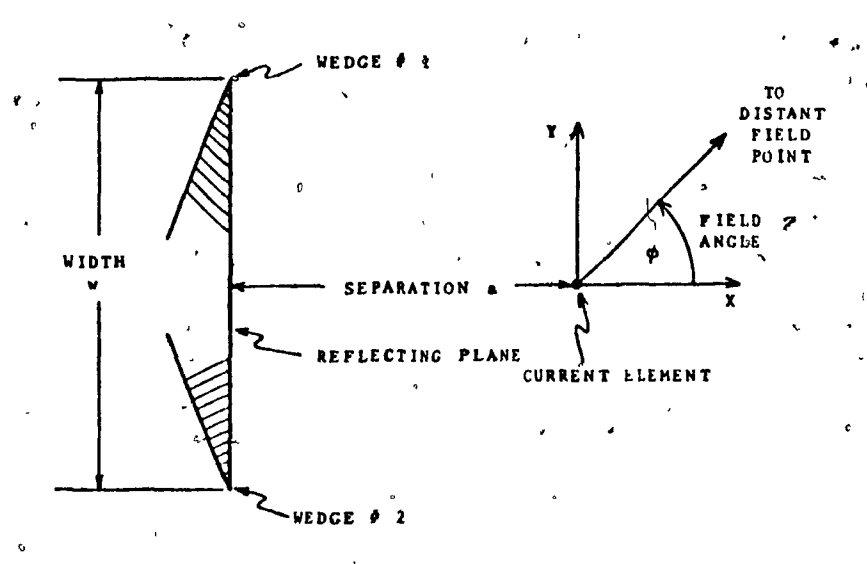


Fig. 4.6 The GDT model of the 2-d plate radiating system.

predicting the type of pattern to be expected.

4.4 The GDT Model of the 2-d Plate

The GTO plate is extended to a 2-d GDT model by accounting for the fields diffracted from the two vertical edges, (Fig. 4.1). The GDT 2-d plate model is shown in Fig. 4.6. Although the half-plane solution can be used to calculate the edge diffracted fields, in this thereis these fields are calculated by modelling each edge with a small angle wedge, since the plate is thin. For H-plane field points, the flash point on each edge is its intersection point with

Š

the x-y plane. The source field evaluated at the flash point is

$$\overline{E} = -E_0 \frac{e^{-jkR}SE}{kR_{SE}} \hat{z}$$

4.4.1

where

$$R_{SE} = \sqrt{w^2/4 + a^2}$$

4.4.2

Since \overline{E}_s is parallel to the edge, the "soft" diffraction coefficient is used. Hence, at large distances from the edge, the diffracted fields are given by

$$\frac{E_{d1}}{E_{d2}} = -E_{o} \frac{e^{-jkR_{SE}}}{kR_{SE}} D_{S1} \frac{e^{-jkR_{E1}}}{kR_{E1}} \hat{z} \qquad 4.4.2$$

$$\frac{E_{d2}}{E_{d2}} = -E_{o} \frac{e^{-jkR_{SE}}}{kR_{SE}} D_{S2} \frac{e^{-jkR_{E2}}}{kR_{E2}} \hat{z} \qquad 4.4.3$$

where R_{E1} and R_{E2} are the distances from the flash points to the field point, and D_{S1} are the "soft" diffraction coefficients evaluated for the incident and diffraction angles for each wedge. The diffracted fields are phase referred and normed to the source field, (Sect. 2.3)

$$\overline{E}_{d1} = \frac{-e^{-jkR}SE}{kRSE} \qquad D_{S1} = e^{jk(\overline{r}_{d1} \cdot \hat{f})} \quad \widehat{z} \qquad 4.4.4$$

$$\overline{E}_{d2} = \frac{-e^{-jkR}SE}{kRSE} \qquad D_{S2} = e^{jk(\overline{r}_{d2} \cdot \hat{f})} \quad \widehat{z} \qquad 4.4.5$$

where \overline{r}_{d1} and \overline{r}_{d2} are vectors from the source point to the flash points on the edges.

Edge interaction gives rise to second and higher order diffracted rays emanating from each edge (21). These fields were neglected in this thesis. The validity of this assumption is established by comparison with measurements for plate widths greater than $2\lambda/3$ in Sect. 4.15. Thus the GDT total field is taken to be

$$\overline{E}_{T} = \overline{E}_{GTO}$$
 + \overline{E}_{d1} + \overline{E}_{d2} 4.4.6

CTO field fields diffracted by the vertical edges

The expressions detailed above could be directly evaluated to compute the pattern of the 2-d plate radiating system, using subroutine DIFFLD (App.4) to evaluate the diffraction coefficients. However, subroutines REF and DIFEDG have been developed to facilitate the programming of simple problems such as the flat plate. Their use is detailed in whe next section.

4.5 Computing the Radiation Pattern.

A special subroutine package has been developed for this project to facilitate the computation of the pattern of a general class of simple radiating systems, with current element illumination. The complete package consists of

Subroutine	र प्राचित्र प्र	Section 2.3	Appendix	2
(dbrode, inc	REF	Scotton 213		_
	,		-	
	(DOTA)	(
	(UVE€)	\(\)		
				
	STDFLD	Section 3.5	Appendix	3 ,
1	DIFFLD	4	-	•
•	(INTN)	•	*	
				•
	FRESIN FRESIN	Section 3.5	Appendix	4
	FRESNL ,	and Appendix 4-		
 -	FRE1		•	
	U			
	STEDG	Section 3.6	Appendix	5
	DIFEDG		•	
	(DOT)	، ن		
•	SFLD	Section 2.2	Appendix	-1

ج٠.

The principal subroutines are underlined, and the section where the theory is found is given, along with the appendix number containing the program listing. These subroutines are not claimed to be the fastest or most accurate possible, but are adequate for this work. The purpose and use of these subprograms for finding radiation fields is detailed in this section, using the 2-d plate problem as an example. The main program for the 2-d plate radiation pattern calculation is listed in App. 7. Descriptions and details of all the subprograms are in the appendices.

Fig. 4.7 Computing the radiation pattern of the 2-d plate by GDT.

A radiation pattern is calculated as flowcharted in Fig. 4.7. Field angle φ is swept through the full 180° of the pattern in sufficiently small angle increments $\Delta\varphi$. For each φ , field vector \hat{f} is computed, and the radiation field determined.

The first step in the computation is to find the direct field \overline{E}_s . If the ray originating at the source point \overline{s}_o and travelling outward in direction \hat{f} encounters a conducting plane, such as the surface of the plate, it is reflected and consequently there is no direct field at a distance point in the \hat{f} direction. Then $E_g = 0$. Otherwise, the source field is found, normalized to the field of an isotropic radiator and phase referred to point \overline{s}_o by Eqn. 2.2.4 as

$$\overline{E}_{q} = (\hat{p} \times \hat{f}) \times \hat{f}$$

where p is the polarization vector of the source.

The reflected field is found simply by calling subroutine REF. REF calculates the field reflected in the \hat{f} direction in the horizontal plane, from a planar conducting surface perpendicular to the horizontal plane, illuminated by a current element in that plane, with any polarization. Subroutine STREF inputs the start end points of the line of intersection of the conducting sheet with the horizontal plane, and finds the "edge cosines" $\cos\theta_A\cos\theta_B$, and unit vector \hat{u}_1 (Sect. 2.3). Subroutine REF determines the presence of a reflected ray in direction \hat{f} by the condition (2.3.8)

$$\cos \theta_{B} > \hat{f} \cdot \hat{u}_{1} > \cos \theta_{A}$$

If no reflected ray exists, REF sets \overline{E}_r to zero. Otherwise, \overline{E}_r is found by the

method of images as detailed in Sect. 2.3, and is normed to an isotropic source, and phase referred to point s.

The next step in the calculation of the 2-d plate's GDT fields

(Fig. 4.7) is to determine the field diffracted from the plate's vertical edges, \overline{E}_{d1} and \overline{E}_{d2} , (Fig. 4.6) . This is accomplished by a CALL DIFEDG statement for each edge, with the appropriate angle arguments. Subroutine DIFEDG is a specialized antenna radiation pattern calculation subprogram which finds the field diffracted from a straight edge in the field direction f with point source illumination. STEDG inputs the endpoints of the edge, which may be any two points in three dimensional space, and the angle α of the wedge which will be used to model the edge. STEDG computes the angle cosines $\cos \beta_1$ and $\cos \beta_2$, the edge unit vector $\hat{\mathbf{e}}$, and other quantities used by DIFEDG. DIFEDG calculated the diffracted field \overline{E}_d , by evaluating the edge-related coordinates and by using the Transition Diffraction Coefficient, as detailed in Sect. 3.6. The value of the current element's field at the flash point is found by calling subroutine SFLD, which evaluates ($\hat{p} \times \hat{r}_{d}$) $\times \hat{r}_{d}$ and distance R, where, if R, is a vector from source point s to the flash point, then $\overline{R}_d = |\overline{R}_d|$, and $\hat{r}_d = \overline{R}_d / R_d$. The TDC is evaluated as required by subroutine DIF,FLD, which uses certain constants dependent on the wedge angle, generated by calling subprogram STDFLD at the beginning of the main program. Finally, DIFEDG norms \overline{E}_d to the field of an isotropic radiator, and phase refers it to point $\frac{1}{5}$. If no flash point exists for field direction f,DIFEDG sets \overline{E}_{a} to zero. Thus DIFEDG computes the field diffracted by a straight edge by the best methods available.

The last step in the calculation is the summing up of the component fields to find the total field (Fig. 4.7).

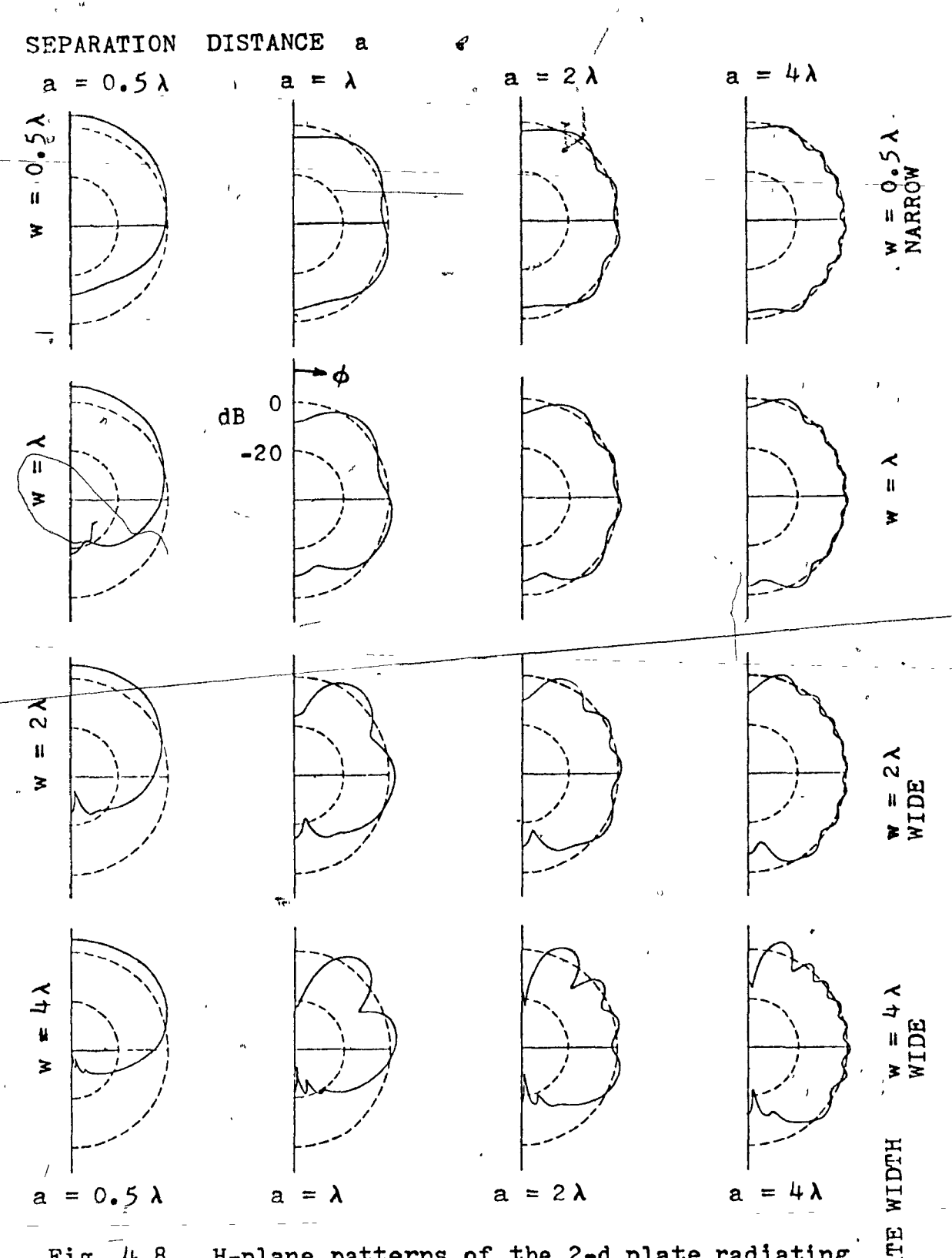


Fig. 4.8 H-plane patterns of the 2-d plate radiating system, computed by GDT.

The same

$$\overline{E}_{t} = \overline{E}_{s} + \overline{E}_{r} + \overline{E}_{d1} + \overline{E}_{d2}$$

If the effect of a particular component of the field on the pattern is to be evaluated, that component is set to zero, and the resulting pattern compared with the complete version.

In this way, the radiation field is found for each angle ϕ , and a complete pattern is calculated.

4.6 The Geometrical Diffraction Fields

In the following sections, the radiation pattern of the 2-d plate radiating system will be studied extensively over the range of dimensions

$$\lambda$$
 / 4 < a < 5 λ
 λ / 4 < w < 5 λ

although larger or smaller widths and separations could have been used. The number of graphs of radiation patterns needed did not justify the use of automatic plotting. Fig. 4.8 shows a matrix of patterns over this range of parameters, which serves to illustrate the behavior to be described.

The GDT model of the 2-d plate employs a wedge to model each of the two vertical edges as illustrated in Fig. 4.6. The angle of the wedges used was set at 10, after exploratory calculations indicated that the pattern is not critically dependent on this parameter, and does not change greatly if the wedge is made as large as 100.

When the fields diffracted from the vertical edges of the 2-d plate are included in the calculation, the resulting patterns are continuous across both the reflection and the shadow boundary. The front region behavior of maxima and minima is carried over into the side region as a ripple on the constant GTO field. The field in the plate's shadow is no longer zero but decreases smoothly across the shadow boundary.

When the pattern of the 2-d plate is studied as a function of separation, a distinctly different behavior for narrow plates (small w) and wide plates is found. The patterns for narrow plates are smooth, with no pronounced nulls, as shown in Fig. 4.8 for $w = \lambda / 2$. If the plate is more than a wavelength wide, the diffracted fields are weak in the front region and the total field is nearly the same as the GTO field. The shadow region field for the wide plate is the result of the interference of the diffracted fields from the two edges. It has a structure of peaks and nulls, and is at a substantially lower level than the front region fields. Wide plate patterns are shown in Fig. 4.8 for plates of width 2λ and 4λ .

The significant difference between a narrow plate pattern and one for a wide plate is that the former are reminiscent of isotropic antenna patterns, while the latter are directional, resembling a cardioid for small separations. Although this classification of "narrow" or "wide" plates is useful over the range of separations covered here, it breaks down at very large separations, where the pattern becomes isotropic for any width. The changeover from "narrow" to "wide" occurs sharply near $w = \lambda$, and the patterns at that width resemble "wide" plate patterns for small separation, and "narrow" for large source spacing, as illustrated in Fig. 4.8.

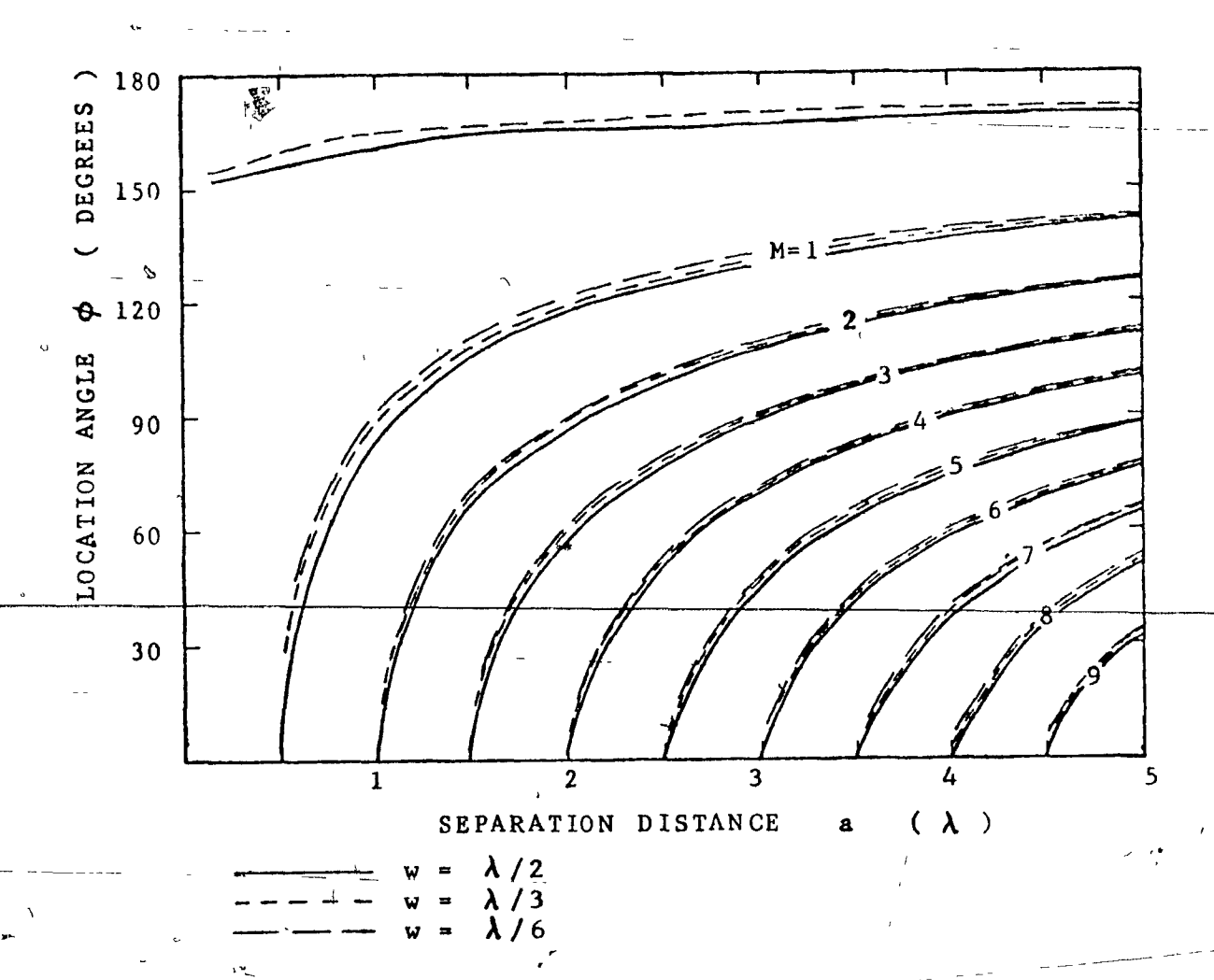


Fig. 4.9 Minimum location angle diagram for narrow plates.

4,7 Narrow Plate Patterns

The narrow plate patterns are remarkably similar to Bayou's cylinder patterns (8). By computing patterns for a range of widths and separations, the angles at which the minima occur can be plotted as a function of separation, Fig. 4.9, and have been numbered in their order of appearance, as in Fig. 4.4. Note that the minima location angles are now a function of width,

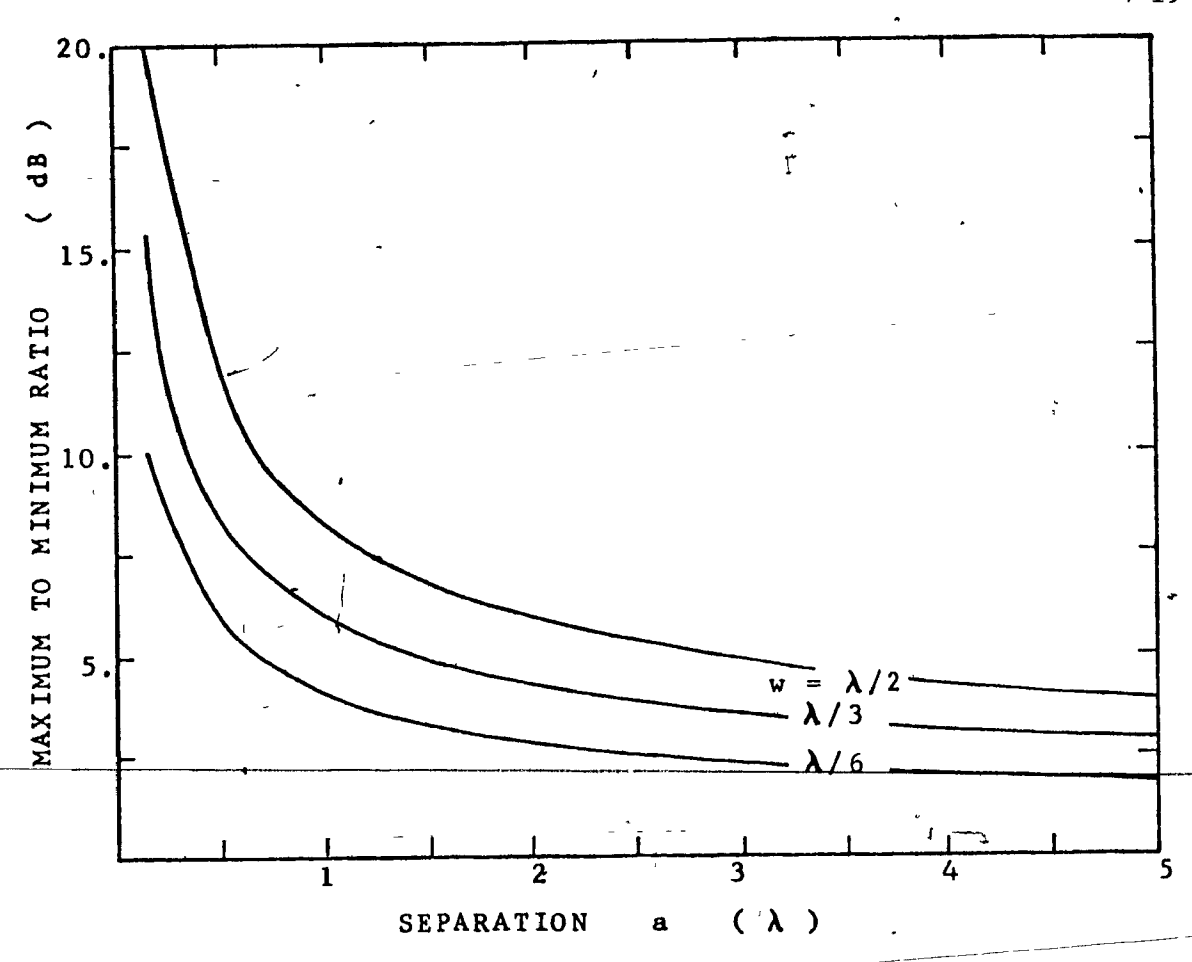


Fig. 4.10. Maximum to minimum ratio for narrow plates.

whereas the GTO angle diagram, Fig. 4.4, uses the same curves for all widths. Also, the maximum to minimum ratio in dB can be plotted for various widths as a function of separation, Fig. 4.10. Any narrow plate pattern can now be sketched, by finding the minima location angles from Fig. 4.9, and the amplitude variation from Fig. 4.10, and recalling that the pattern is smooth. Fig. 4.8 for w $\pm 0.5 \lambda$ could be reconstituted this way.

4.8 Minima Location Angles for Any Plate Width

It is possible to draw a minimum location diagram similar to Fig. 4.9 for a plate of any width, but the exact curves are a function of the

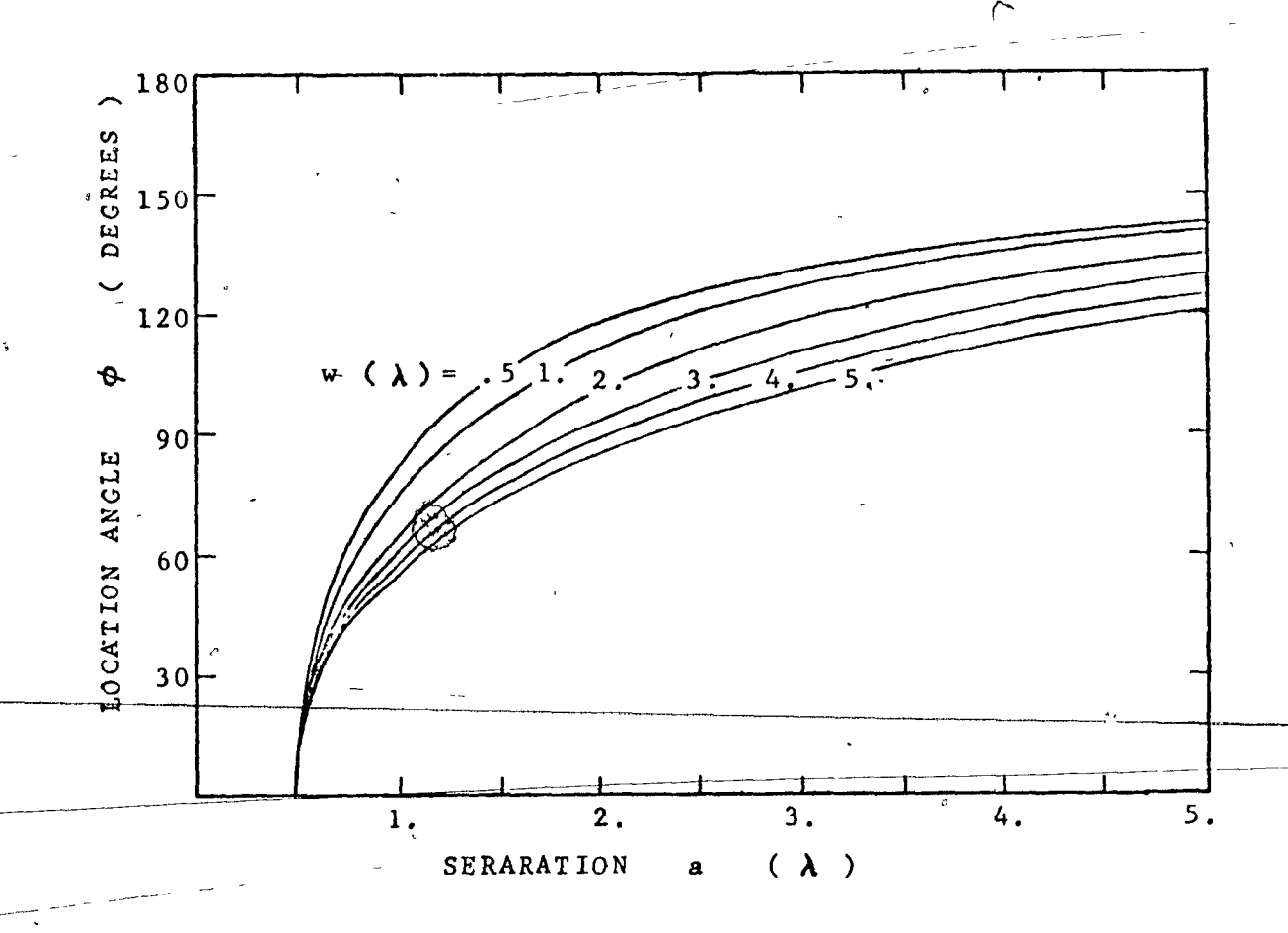


Fig. 4.11 Location angle diagram for the first
(M = 1) minimum.

width, and change considerably as the width is increased from 0.5 to 5. wavelengths, thus requiring a new family of curves for each plate width.

Rather than plot the minima angle curves for all the minima

(all M) for a particular width, the angle of the Mth minimum can be graphed

for a range of widths on the same axes, giving a separation-angle diagram such

as Fig. 4.11, drawn for the first minimum. From Fig. 4.11 the angle of the first

minimum can be estimated over a range of separations and widths. To find the

angle of all the minima for separations up to five wavelengths, nine separat
ion-angle diagrams like Fig. 4.11 would be needed, one for each minimum up to

M = 9.

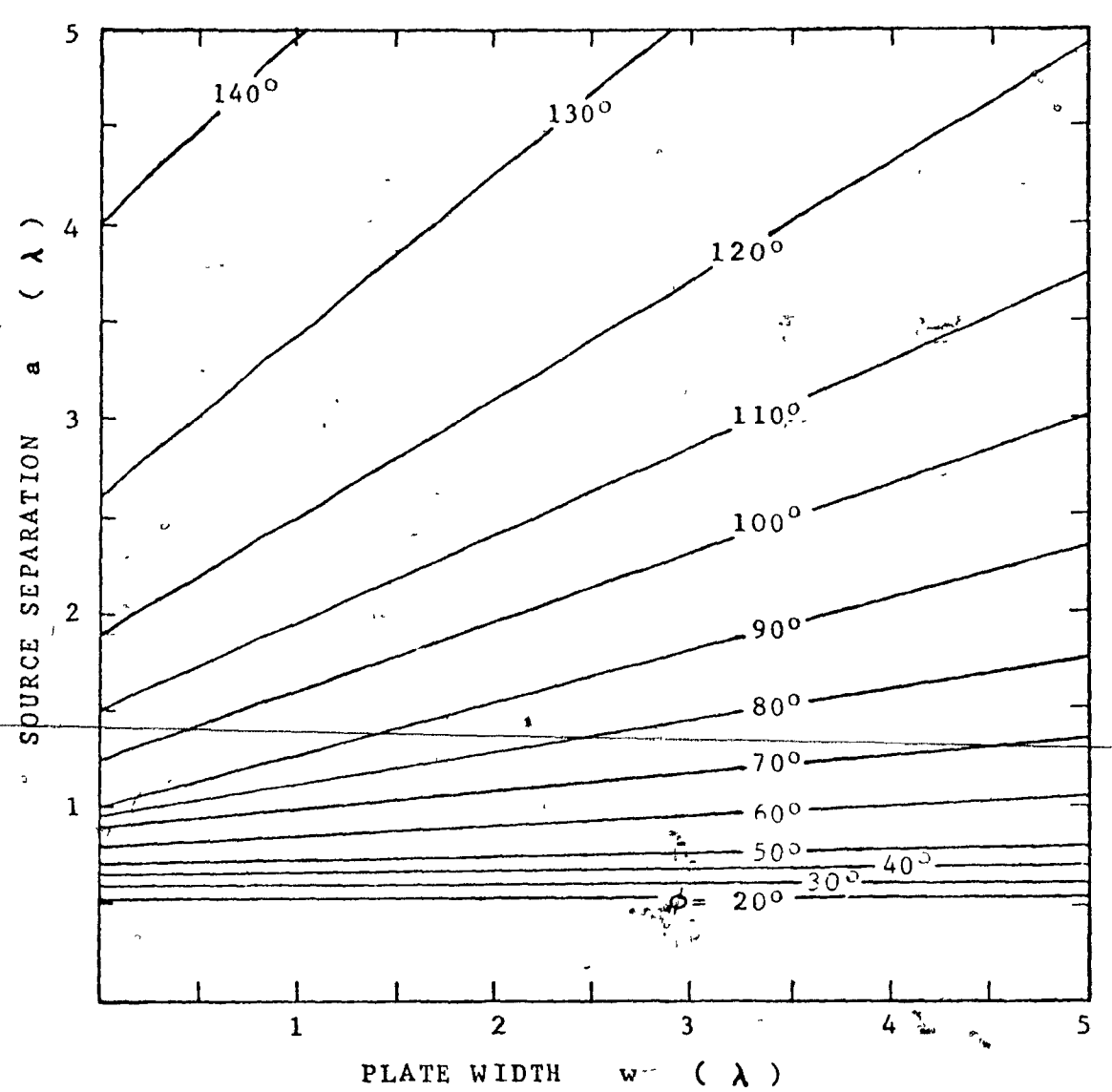


Fig. 4.12 ϕ -line diagram for the first (M=1) minimum .

A horizontal line drawn on the separation-angle diagram, Fig. 4.11, for a particular φ value, intersects the set of curves at width-separation (w,a) pairs having the first (M=1,Sect. 4.3) minimum at angle φ. These (w,a) pairs for each φ can be plotted, Fig. 4.12, and all lie very nearly on a straight line, which shall be called a "φ-line". A separation-angle diagram such as Fig. 4.11 and hence a φ-line diagram like Fig. 4.12 can be drawn for any minimum "M". A φ-line on the Mth diagram defines widths and separations of 2-d plate radiating systems which have the Mth minimum at the angle of the φ-line, or as nearly so as this linear approximation allows.

Each ϕ -line has slope "s" and intercept. "a" and relates width and separation according to

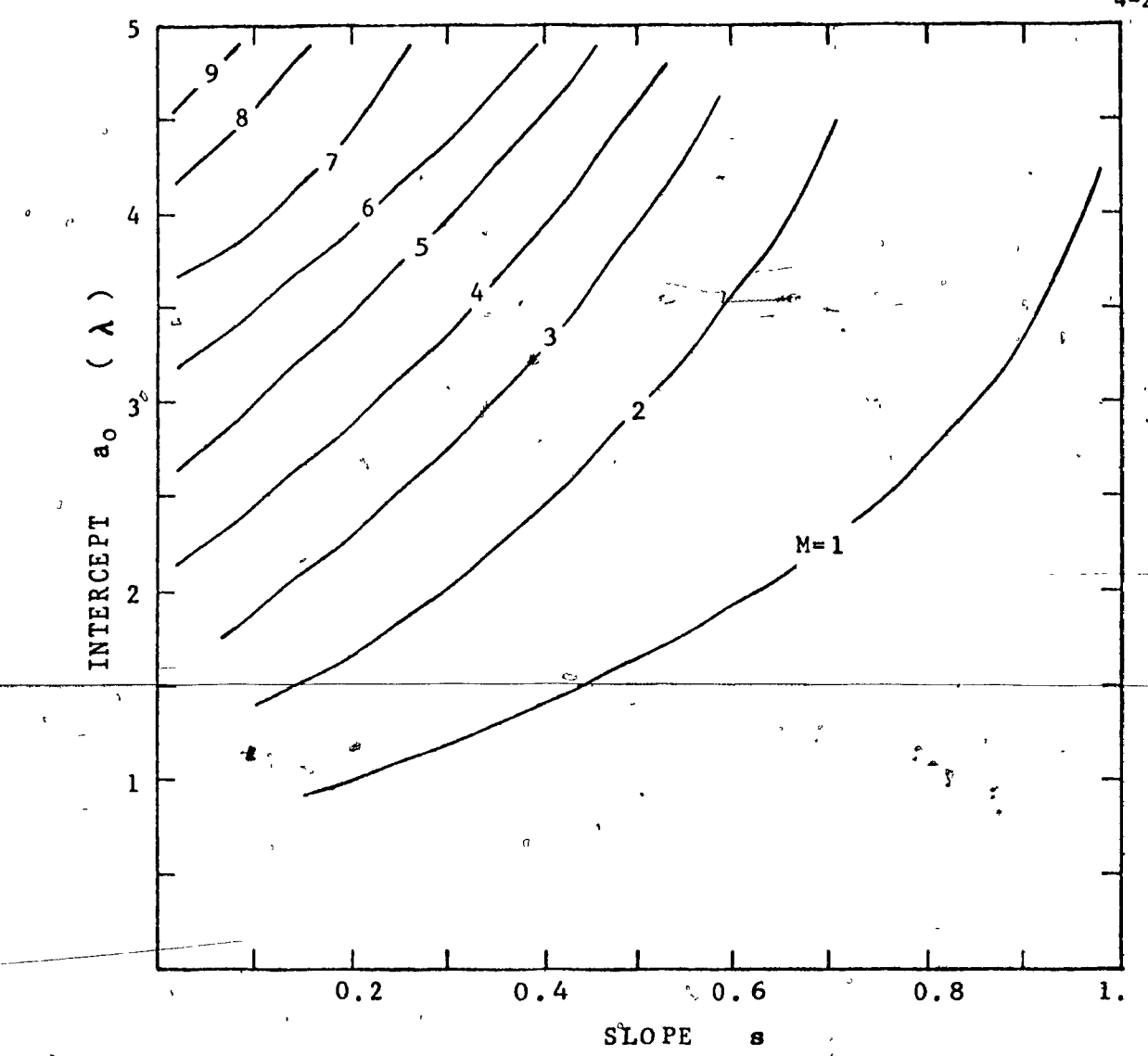


Fig. 4.13 The slope-intercept (s,a_o) diagram or M-curve diagram.

Note in Fig. 4.12 that as \$\phi\$ increases, both slope and intercept increase monotonically. If the slopes and intercepts of Fig. 4.12 are plotted on (s,a_0) axes, then the M = 1 curve of the slope-intercept diagram, or M-curve diagram, Fig. 4.13 is obtained. Other \$\phi\$-line diagrams for M = 2,3,... can be plotted to give slope-intercept data for the remaining M-curves of Fig. 4.13. Also, plotting the \$\phi\$ value against the intercept gives an intercept-angle diagram. Fig 4.14.

4.14

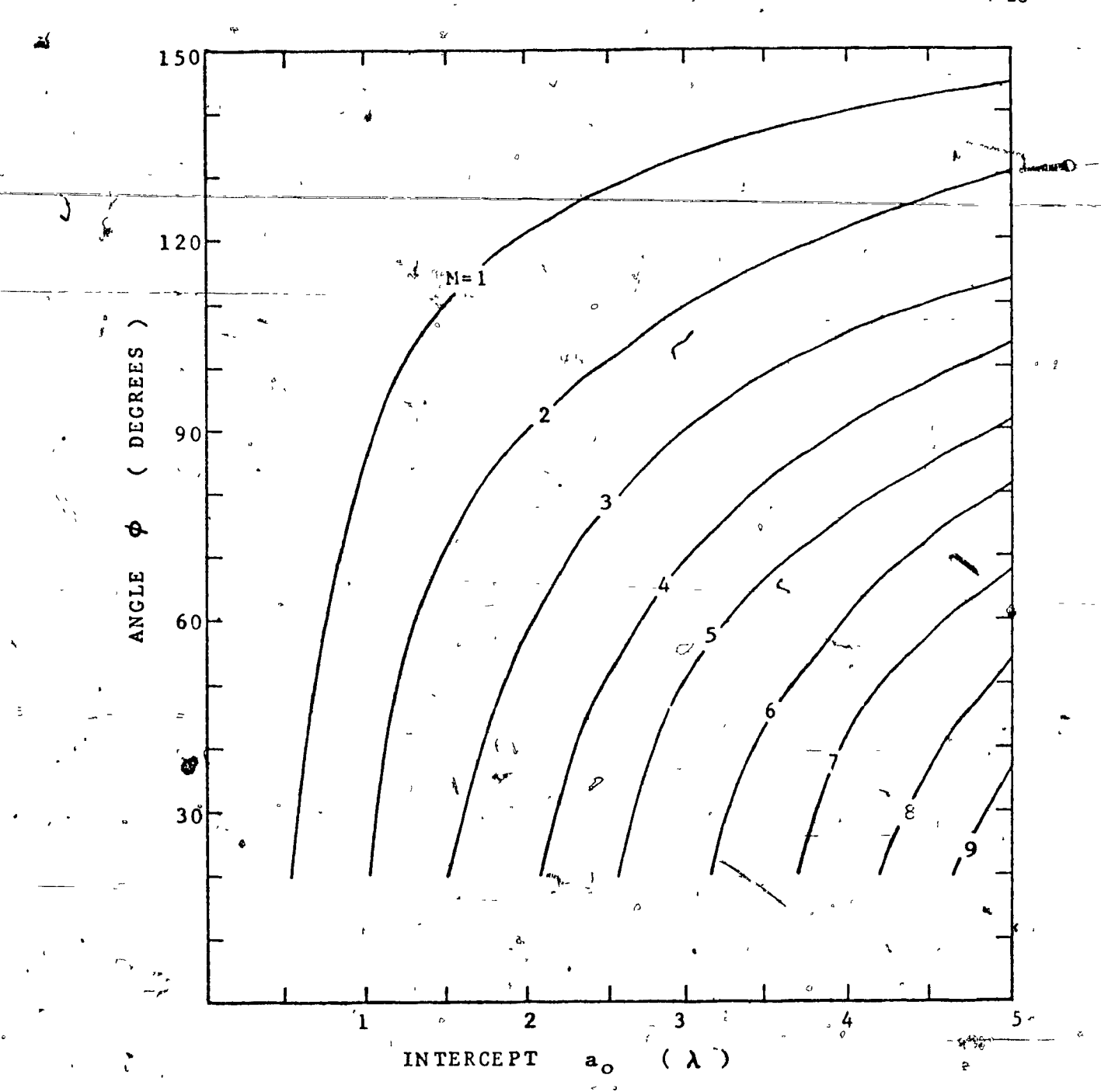


Fig. 4.14 The intercept-angle (a_ο,φ) diagram.

Given a particular width and separation, the angles of the front and side region minima can now be found.

Specifying (w,a) locates a point on the Mth ϕ -line (such as Fig. 4-12 for M=1). The ϕ -value of the ϕ -line through that point is the angle ϕ at

1

which the Mth minimum falls. In order to identify the φ-value, an interpolation must be made, using Figs. 4.13 and 4.14 as described below. With
"w" and "a" fixed, the φ-line equation represents a constraint on slopes and
intercepts,

$$a_0 = -ws + a$$

When this "characteristic line" is plotted on the slope-intercept diagram (Fig. 4.13), it will cut as many M-curves as there are minima in the front and side region of the pattern. The intersection point of the characteristic line with each M-curve gives the desired intercept value and hence the angle of the Mth minimum, via Fig. 4.14.

The characteristic line concept immediately shows that the separation alone determines the number of M-curves which the characteristic line will cut, and thus gives the number of minima in the pattern, since change ing the separation moves the line up or down on the slope-intercept diagram.

The plate width corresponds to the slope of the characteristic line and influences the location angles of the minima, but not the number of minima.

4.9 Moment Method Comparison

The reliability of the GDT solution to the 2-d plate-problem is best judged by comparison with results obtained by an independent method. Shafai and El-Moazzen (11) have solved the antenna-near-a-conducting-strip problem by the moment method, by representing the current on the strip by a truncated fourier series and finding the unknown coefficients by point matching an integral

TABLE I COMPARISON OF FRONT AND SIDE REGION MINIMA ANGLES OBTAINED BY
THE MOMENT METHOD(11), THE GDT PROGRAM, AND FROM THE SYNOPTIC
GRAPH FIGURE 4.13 .

DIMENSIONS MINIMA LOCATION				ANGLES	
kw	. ka	MOMENT METHOD	GDT DIRECT COMPUTATION	SYNOPTIC GRAPH	
10	3	O	0	0	
	10	. 20	18	24	
		60 '	5 59	` 64	
		93	94	95	
	20	20	21,	16	
-	45	46	52		
		67	65 ,	65	
		80	83	84	
		101	101	1/02	
-		120	122	123	
2	3	0 +	0	0	
	5	.70	71	. 58	
10	· 28	23	28		
	75	73	73		
		<u> 110</u>	110	109	
20	28	26	26		
	57	54	56		
	. 74	74	73		
	92	93	· 92		
	110	111	111		
		132	132	133	

equation. Col. 1 of Table I gives the angles of the front and side region minima estimated to about $\pm 3^{\circ}$ from the published moment method patterns of (11). Col. 2 gives the minima angles computed by the GDT 2-d plate program for the same dimensions. Comparing the numbers shows the degree of agreement. The numbers of minima for the very large separation ka = 60 (a = 9.6 λ) obtained by the moment method and by the GDT are completely different, being 10 and 20 respectively.

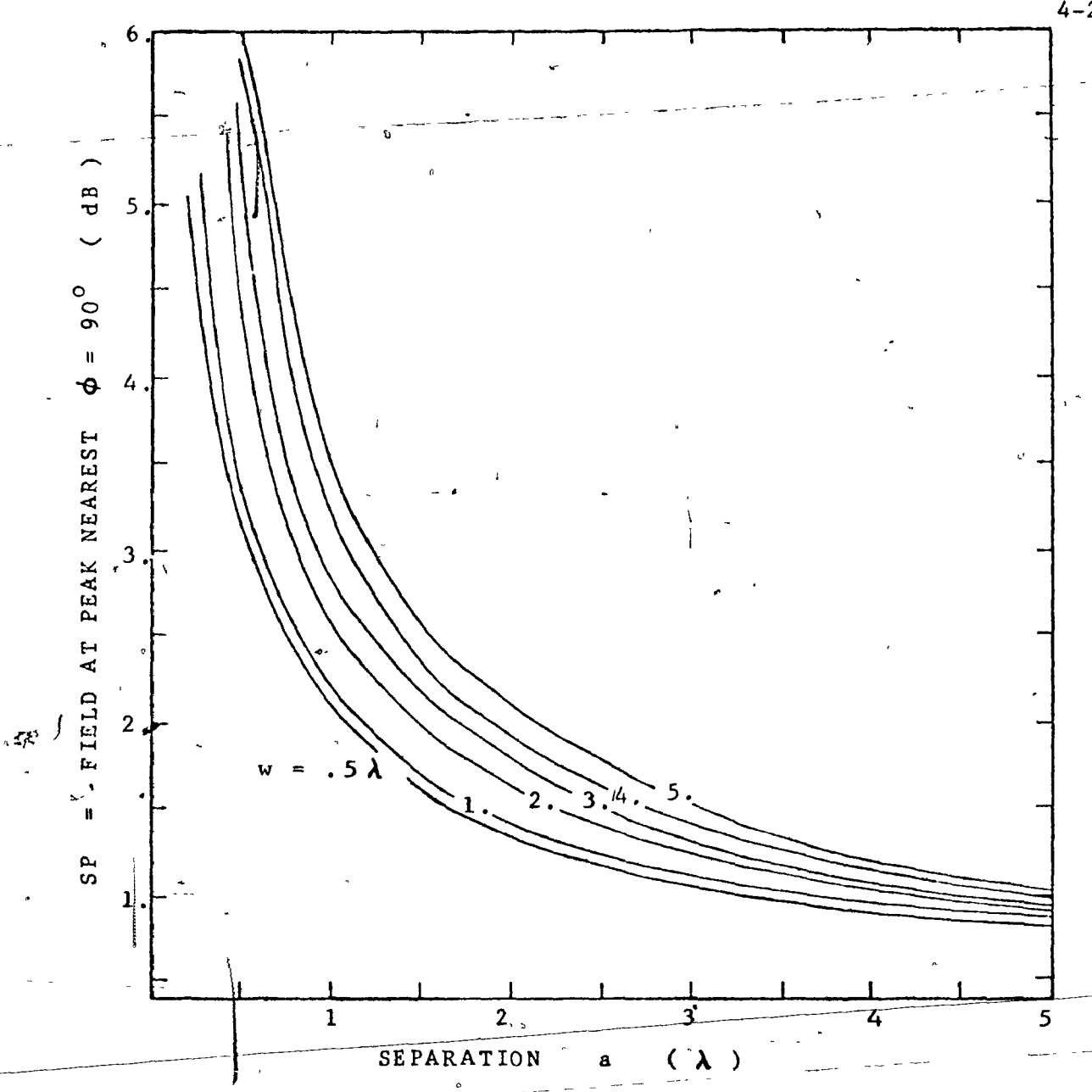
The accuracy of the graphical summary of the GDT method minima angle behaviour, Figs. 4.13 and 4.14, can be judged by comparing the minima angles given in Col. 3 obtained directly from the program, Col.2. There is little loss of accuracy, and the agreement with the moment method angles, Col.1 is still very good.

4.10 Pattern Amplitude Parameters

For the narrow plate, the angles of the front and side region nulls are given by Fig. 4.9, and in order to reconstitute the pattern adequately it is sufficient to use the maximum to minimum ratio, from Fig. 4.10. For wide plates, however, the pattern has more structure. While the front region resembles the GTO field, the side region has a ripple of unknown amplitude, with a mean value of 0 dB and the shadow region field decreases to an unknown value.

Some means is needed to specify these unknowns to determine the patterns for arbitrarily chosen widths and separations.

A suitable side region amplitude parameter "SP" is the height of the side region peak nearest 900. For large separations, the GTO field is used to



The "side peak" SP amplitude parameter. - Fig. 4.15

sketch the front region field, with the nulls partly filled in, and SP gives the amplitude of the side region ripple. The location angles of the minima are obtained from Fig. 4.13 and 4.14. For smaller separations, where there are one or two peaks in front and side region, SP specifies the height of the one nearest 90°. For very small separations for which only one peak occurs, its height is still given by SP. Thus, SP is a useful narameter for all widths and separations. Fig. 4.15 shows that parameter 8P is a smooth function, tending

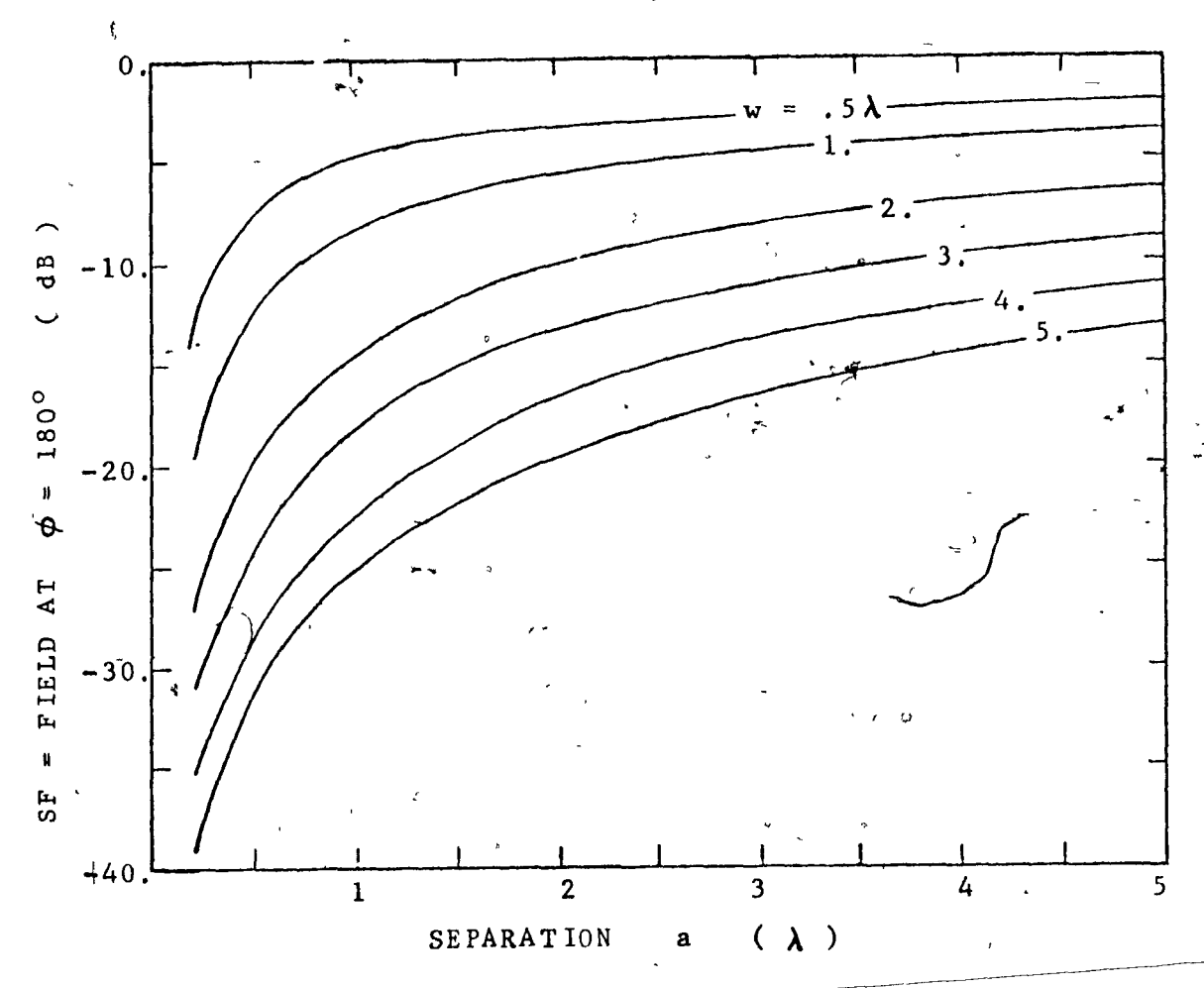


Fig. 4.16 The "shadow field" SF amplitude parameter.

towards 0 dB for large separations, and 6 dB for small source spacing.

The shadow region field is the result of the interference of the two vertical edge diffracted fields. The nulls are not given by previous graphical data, but the exact structure of the back region field is usually unimportant, and is adequately described by its peak value, given by the "shadow field" parameter, SF, Fig. 4.16. As may be expected, for wide plates SF is lower than for narrow ones, and as the source separation distance becomes large, SF tends to 0 dB and the field tends to that of an isotropic radiator.

4)

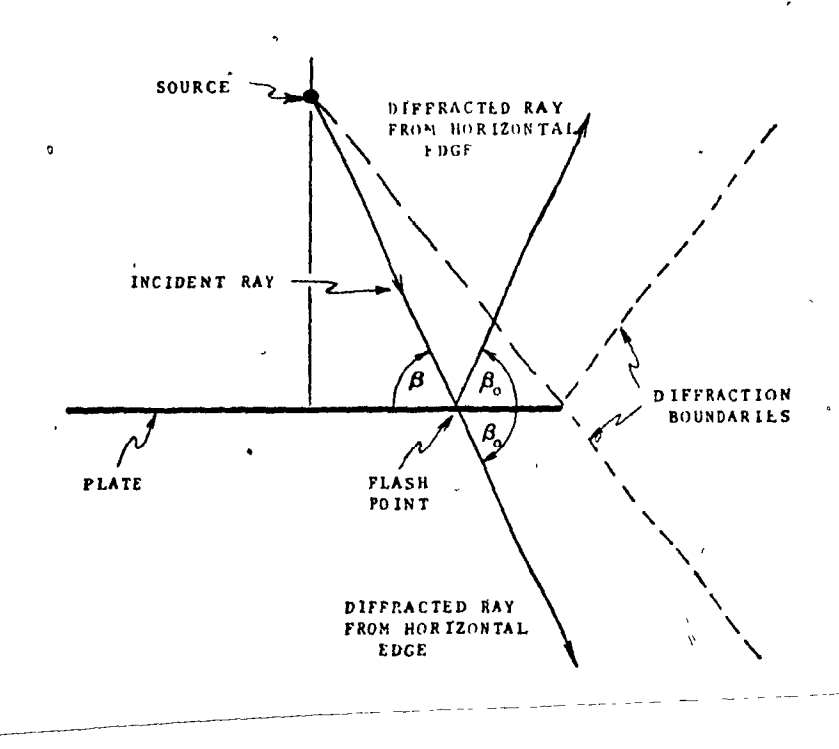


Fig. 4.17 Geometry of diffraction from a horizontal edge.

4.11 The Three Dimensional Plate

Previous discussion concerned the patterns of the "tall" plate and are valid as long as the diffracted fields from the two horizontal edges can be neglected. When the plate height is reduced, the contributions from the horizontal edges must be included.

The computation of the diffracted field for a horizontal edge is not as simple as for the vertical edges, where the point of diffraction is already known, and the source field is parallel to the edge. The diffraction point, or "flash point" must be found for each field angle by making angle β equal angle β_0 in Fig. 4.17. As the field angle increases from 0° , the flash point moves from the center of a horizontal edge, towards its end. The angle

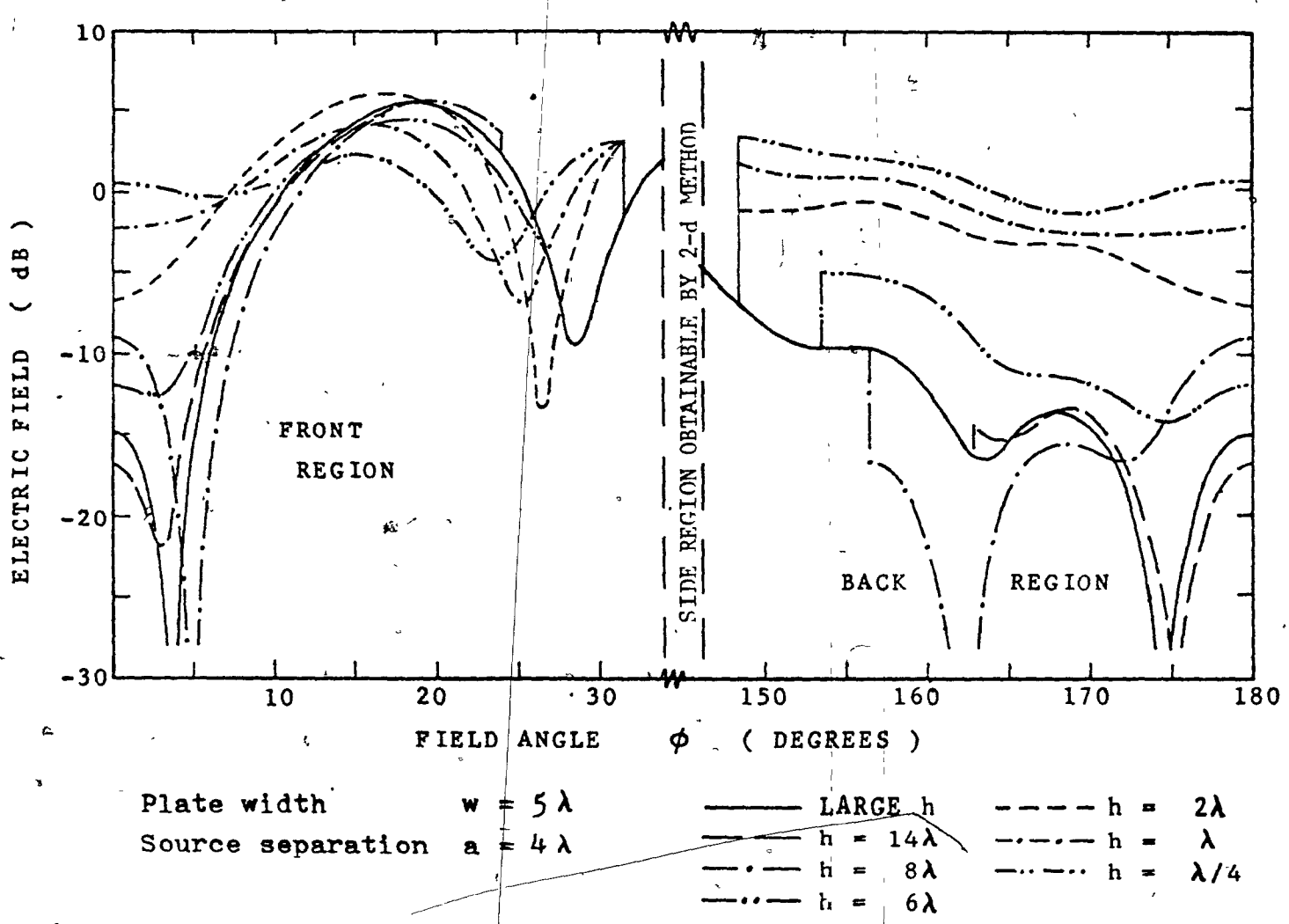


Fig. 4.18 The front and back region of an H-plane pattern, as a function of plate height.

7-4

which makes the flash point move off the end of the edge is the "diffraction boundary" (DB), Sect. 3.2. At this angle, the horizontal edge diffracted field contribution vanishes abruptly. This results in a second diffraction boundary near the shadow boundary, where the diffracted field reappears. Thus the horizontal edges contribute to the pattern only in the front and back regions, and, neglecting vertex diffractions, the side region fields are independent of plate height.

A further complication is introduced by the fact that the source field is not generally perpendicular to the horizontal edges. Thus the diffractions are neither pure "hard" nor "soft", and must be computed using the "edge-related" coordinates (Sect. 3.4).

The horizontal edge diffracted fields are included in the computer program simply by adding a CALL DIFEDG statement for each horizontal edge to the flow chart in Fig. 4.7. Subroutine DIFEDG automatically finds the flash point and computes the diffracted field, or if the field point lies beyond the diffraction boundary, sets the diffracted field to zero. Then the total field is

$$\overline{E}_{T}$$
 = \overline{E}_{S} + \overline{E}_{R} + \overline{E}_{d1} + \overline{E}_{d2} + \overline{E}_{d3} + \overline{E}_{d4}

GTO field Fields diffracted by the horizontal edges \mathcal{C} edges

4.12 The 3-d Plate Patterns

The front and back region of the pattern for a five wavelength

wide plate, with the source four wavelengths away is shown as a function of plate height in Fig. 4.18. For h > 20 wavelengths, the pattern including the horizontal edge diffracted rays, is identical to the corresponding 2-d plate pattern. The horizontal edges are so far from the source that their diffracted field is weak, and also, the diffraction boundaries fall near 0° and 180° and so these edges only contribute over a very narrow range of angles. As h is reduced, the diffraction boundaries move towards the reflection and shadow boundary. At h = 14 λ the DB's are 17° and 163° , and the pattern is almost the same as for a tall plate. At 8 λ , the front region fields are not greatly dhanged, but the chief back region null angle has moved considerably. By h = 6 λ this null has disappeared and the fields are smoothing out. As the height is further reduced, the fields tend towards the isotropic pattern which would be expected for a very short plate.

The discontinuity in the patterns at the DB angles is due to the abrupt vanishing of the diffracted fields of the horizontal edges. Reducing the height of the plate causes the four corners or vertices to be strongly illuminated. At present no coefficient has been developed to represent the vertex diffraction process. The field would have to be found by a hybrid technique using equivalent currents on the corner. The jump in the pattern at the DB would be smoothed out if the vertex diffracted fields were included in the calculation.

If the 3-d pattern is studied as a function of height for a large number of widths and separations, then three different regions of pattern behavior can be identified. Tall plate patterns are insensitive to plate height, with the DB angles near 0° and 180°. As the height is reduced, the DB angles move relatively quickly to coincide with the reflection and shadow boundaries,

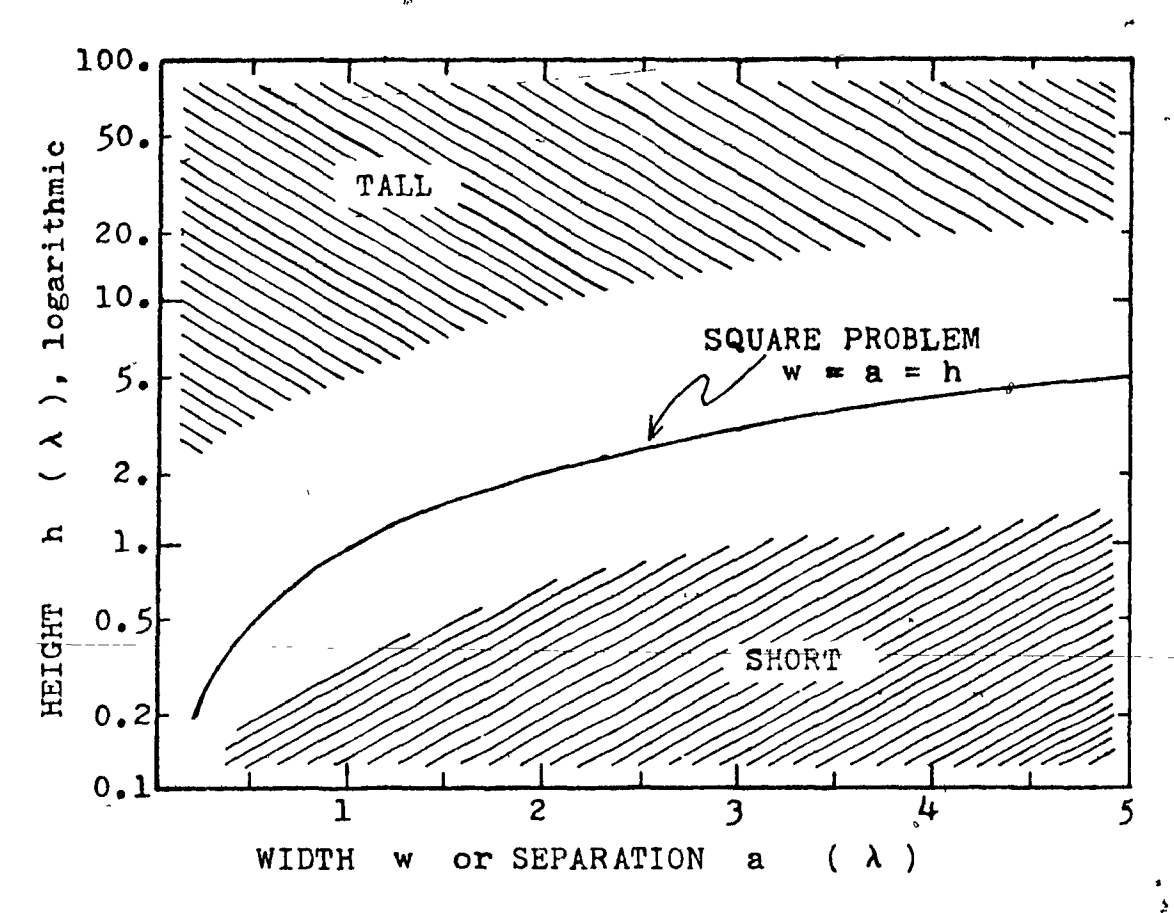


Fig. 4.19 The three regions of height for the case where width = separation.

and in this intermediate range of heights, the back region pattern changes very quickly with height. In Fig. 4.19, the three regions of height have been established for the square problem with width = separation, as a function of width. The case of height = width = separation, always fails in the intermediate zone of height.

_4.13 Comparison with Burnside

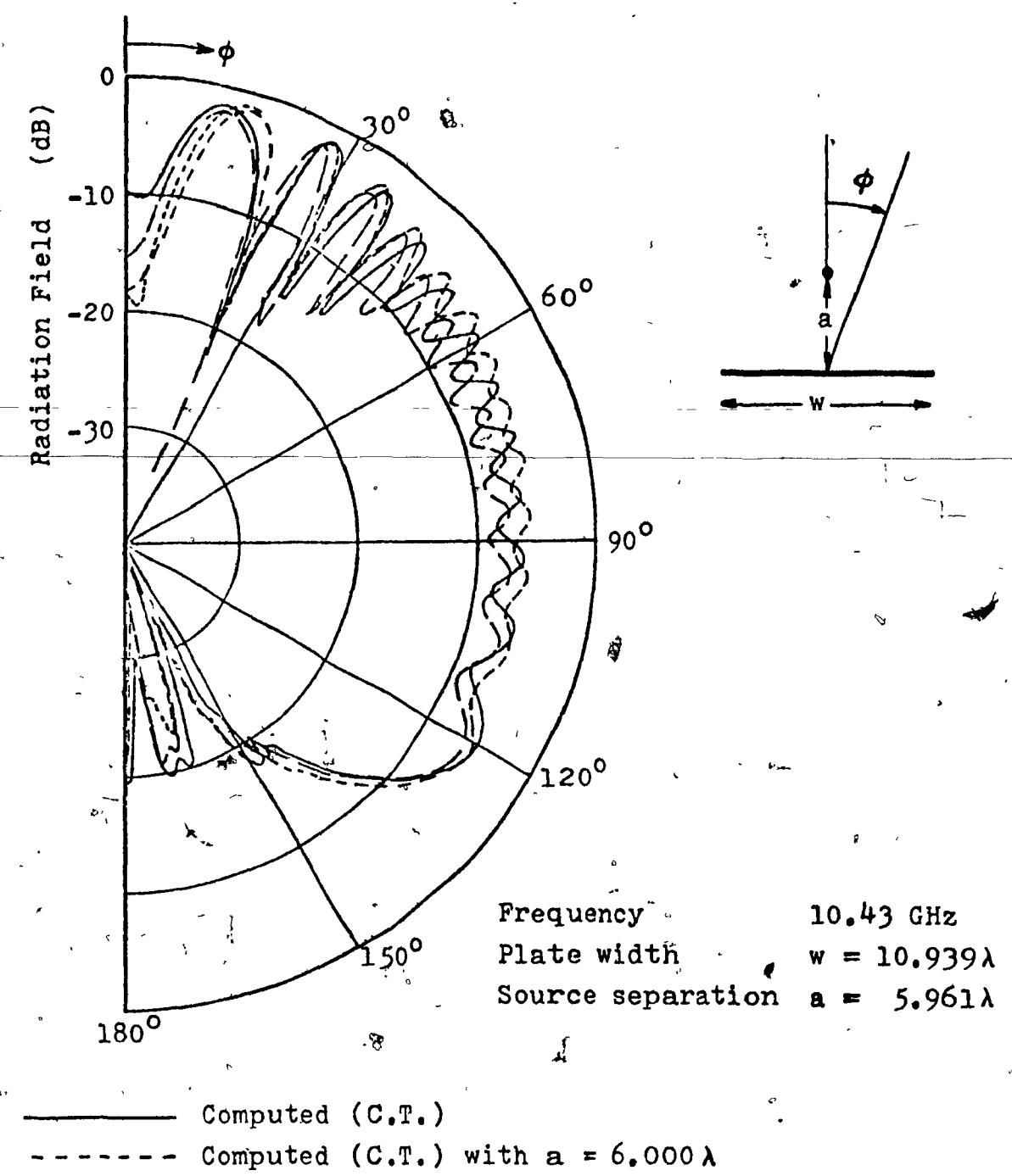
Burnside (3) has developed a GDT program to compute the fields of a plate with n sides, and in order to verify his program, he compares his computations with measurements for a 12 inch square plate at 10.43 GHz, which makes the plate 10.939 λ on a side. Figs. 4.20 and 4.21 compare our comput-

ations with Burnside's results. The Burnside (3) curves as shown here can differ by up to + 1dB due to the copying process used.

Fig. 4.20 compares our computations with Burnside for a current element source centered in front of the plate, separated from it by 5.961 λ . All patterns are normed to have the same value at the peak near 15° . Our computations are remarkably similar to Burnside's computations. The depth of the minimum at 0° is a poor point of comparison, as it is critically dependent on the source spacing. Thus if the spacing is increased by 0.039λ to 6.000λ , then as shown in Fig. 4.20 the depth of the minimum changes drastically. Thus the only significant difference between our computations and Burnside's is that his patterns have 7 minima in the side region where ours have 8, as is predicted by the foregoing sections. It is not known why Burnside's GDT calculations in Fig. 4.20 differ from our computations in this way.

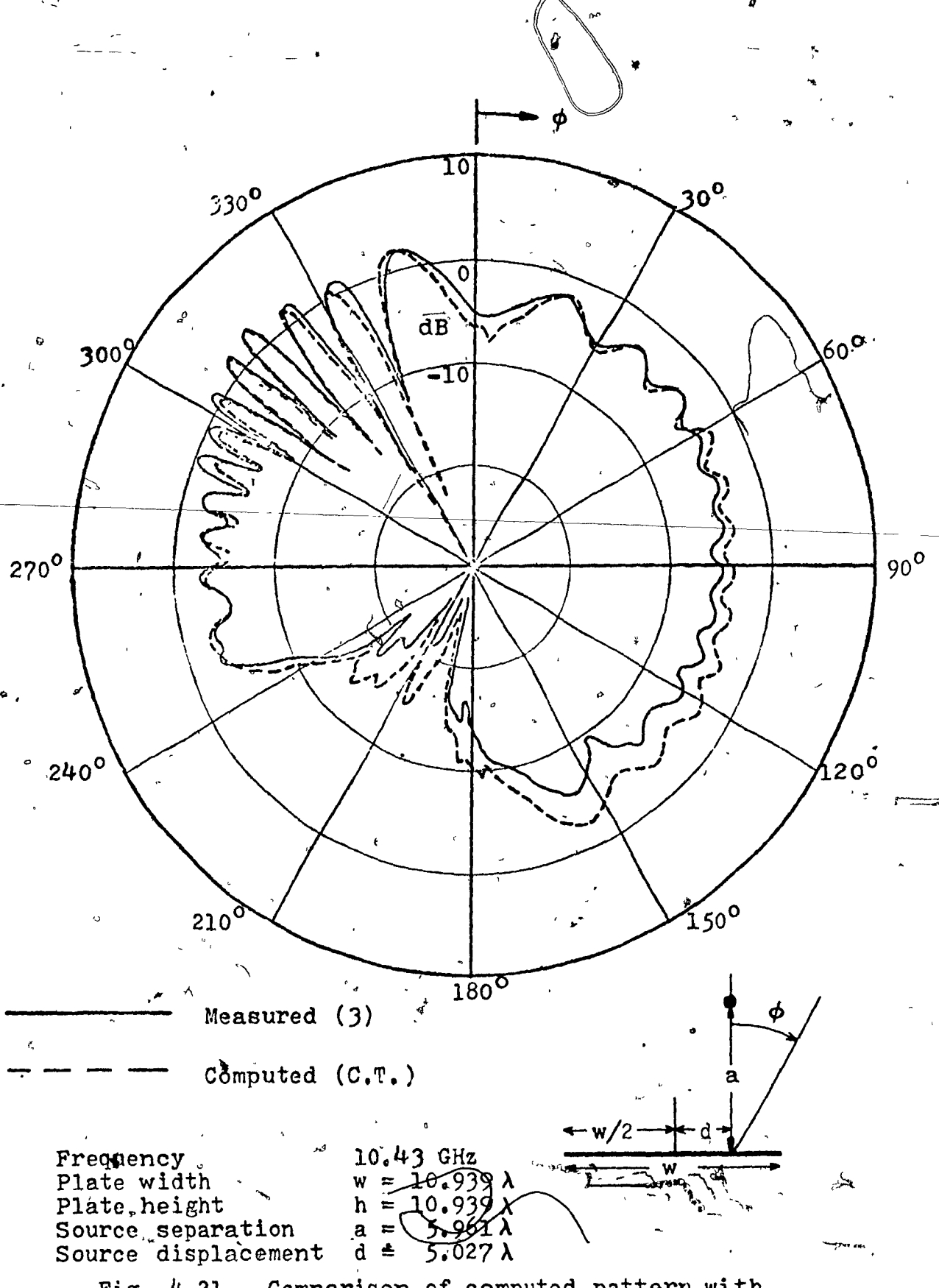
In Fig. 4.21 our computations are compared with Burnside's experimental pattern for the current element separated from the plate by 5.961 λ , but off-center by 5.027 λ . For this source location, our computations are almost identical with Burnside's, so only-his measured pattern is shown in the figure.

It is instructive to ask why the pattern with the Burnside dimensions and the centered source, Fig. 4.20, does not appear to have discontinuities at the diffraction boundaries, as do the patterns of Fig. 4.18. If the back region of Fig. 4.20 is plotted for a range of heights near $h = 10.939\lambda$, Fig. 4.22, it is found that the discontinuity is very much present at h = 12 and 11λ , and is a step up with increasing angle, whereas at $h = 10\lambda$, it is a step down. The Burnside height is very near the changeover from step up to step down, and so the discontinuity is not readily apparent, being effectively cancelled out, due to the fortuitous choice of the dimensions used.



Computed (3) Measured (.3)

Comparison of computed pattern with Burnside's (3) Fig. 4.20 measurements and computations with centered source.



Ü

Fig. 4.21 Comparison of computed pattern with

Burnside's measured pattern(3) for the

off-center source.

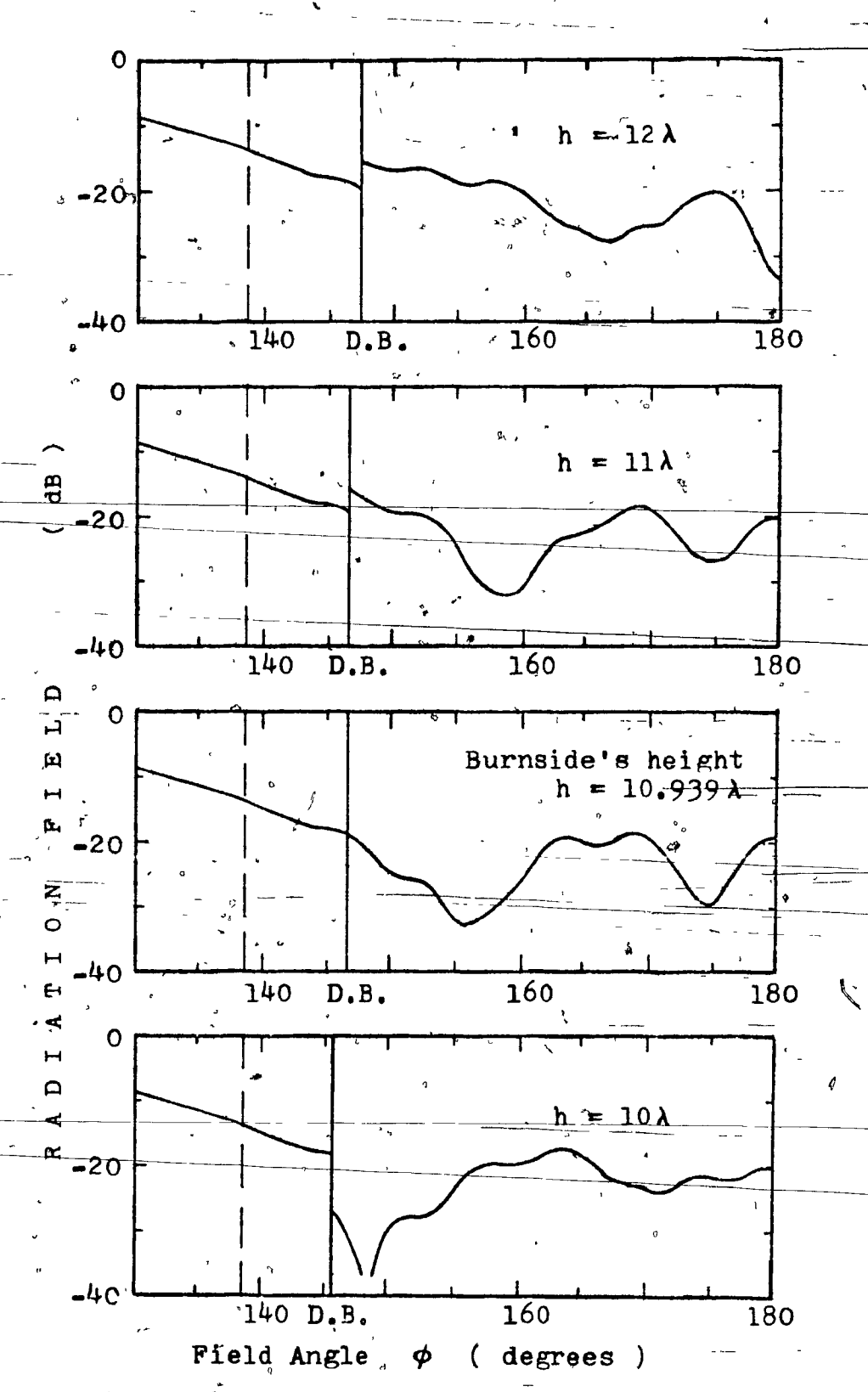


Fig. 4.22 The back region of Burnside's centered source pattern, as a function of plate height h.

.,

ı

- -

- - -

٩

· ____

.

4.14 Radiation Pattern Measurements

To provide a sound verification of the computed radiation patterns, experimental patterns were obtained in a 300 MHz - 3 GHz anechoic chamber designed especially for radiation pattern measurement. The anechoic chamber and associated instrumentation is described by Kubina (12).

The experimental model, Fig. 4.23, capitalized on the x-y plane symmetry of the problem. It consisted of a circular ground plane of 0.16 cm (1/16") thick aluminum, supported at the center by a 30 cm square "support plate" of 1 cm thick aluminum, to ensure the ground plane's flatness. The source antenna was a monopole 1.5 cm high mounted at the center of the ground disc. A 0.32 cm (1/8") thick aluminum plate mounted at right angles to the ground plate was used to model the flat plate. The ground disc and support plate were drilled and threaded so that the flat plate could be mounted with plate to monopole separation distances of a = 10,18.45, and 21.9 cm. Two flat plates' were used, of 10 and 30 cm square. Thus the plate width was w = 10 or 30 cm, and because of the ground plane configuration, the effective heights were h'= 20 and 60 cm.

Measurements were carried out at 2.0 and 2.4 GHz. Recieving patterns were taken. The antenna model was illuminated by an open ended rectangular waveguide mounted in the plane of the ground disc, about 2 m from the source antenna. The ground plane configuration was used to minimize the effect on the radiation pattern of the cable carrying the received signal from the monopole to the detection equipment.

The experimental error in the measured patterns is estimated to be ± 1 dB in amplitude in the front and side region, and ± 2 degrees in the

1

angular position of any feature of a pattern. Larger experimental errors are present in certain regions of the patterns:

- (1) In the front region at $\phi = 0^{\circ}$, when the separation is near that for a GTO null, the depth of the null is very sensitive to separation distance, and operating frequency. In such cases the experimental error is large near 0° .
- (2) Similarly, the depth of any front region null due primarily to GTO effects, is subject to a large experimental error.
- (3) In the back-region of the pattern, the field is the sum of edge andvertex diffracted components. These fields are sensitive to departure
 from the ideal in the physical model such as ground plane flatness and
 levelness, and to the illuminating waveguide position and angular alignment inaccuracies.

The measured patterns were found to symmetric to within ± 1 dB and ± 1 degree in the front and side region, but only very roughly symmetric in the back region. In the next section, measured patterns are shown only for $0^{\circ} < \phi < 180^{\circ}$, and in general the better half of the back region is shown in the diagrams.

4.15 Comparison with Measured Patterns.

rigs. 4.24 and 4.25 compare the patterns measured at 2.0 and 2.4 GHz with computations made with both the two- and the four-edge plate models with dimensions corresponding to the physical dimensions of the ex-

the calculations conform to the measurements. The agreement is best in the side region of the patterns, good in most of the front regions, but is often poor in the back region.

It has been emphasized throughout this chapter that the vertex diffracted components of field have been neglected in the calculations. These components of field are expected to be large near the diffraction boundaries, where the computed patterns with the four-edge model are discontinuous. Thus in the side region, the vertex diffracted components on field are expected to be negligible, and indeed the measured and calculated patterns agree best in the side region. For this reason, in every case the experimental pattern has been normalized to the same peak value as the computed pattern in the side region.

Front region agreement in many patterns is verw good, Fig. 4.24 (a), (b), and Fig. 4.25 (c), (d), and (f). In some patterns, Fig. 4.24 (f) and Fig. 4.25 (e), the disagreement occurs at Ø = 0° and can be attributed to a GTO effect (see last section). In general, however, the vertex diffracted components of field in the front region are not negligible, especially near the diffraction boundary, and can explain certain disagreements. Thus the increased front lobe width in Fig. 4.24 (d) and (e) might be due to vertex diffractions. In other patterns, especially for the 10 cm plate, the D.B.s are near 0° and the vertex diffracted components of field may have a considerable effect in a region near 0°. In Fig. 4.24 (c) the horizontal edge diffracted fields are apparently cancelled by the vertex diffracted fields. But in Fig. 4.25 (a) the vertex diffractions smooth out the D.B. discontinuity and somewhat reduce the field value near 0°. In Fig. 4.25 (b) the dis-

continuity is smoothed out but the computed level near 0° including the horizontal edge diffractions is confirmed.

In the back region of the patterns, the total GDT field is the sum of the four edge diffracted and the four vertex diffracted components. The vertex components can have a magnitude comparable to the edge diffracted fields, so the measured patterns might be expected to display behavior completely different from the computed patterns, which only include edge dif-It is found, however, that in most of the measured patterns; Fig. 4.24 (a), (e), (f), and all of Fig. 4.25, that the measurements and calculations distilay similar behavior, although "agreement" cannot be claimed Measurements often have a back region null not found in the computations, (24) (a), (f), and Fig. 4.25 (a), (b), (c), and (d), which could be due to the interference of the vertex and the edge diffracted fields. Fig. 4.24 (c), note the measured pattern does not display the back region lobe due to horizontal edge diffractions which is seen in the calculated pattern. The front region lobe due to these edges was also not found in the measured pattern. But the measured pattern in Fig. 4.25 (b) tends to confirm the lobe due to the horizontal edge diffractions in both the front and the back regions.

Other disagreements in this set of patterns are worthy of note. The calculated minimum in Fig. 4.24 (d) at $\emptyset = 40^{\circ}$ is not well confirmed by the measured minimum which occurs at 48° and is not nearly as deep. This is primarily a GTO minimum and is not expected to be reliably measured, as discussed in the last section.

In Fig. 4.24 (a) the measured and experimental minimum near 50 does not agree well. The reason for this difference is not apparent. Also,

the back region in Fig. 4.25 (d) is grossly in disagreement. Again, the cause of this error is unknown.

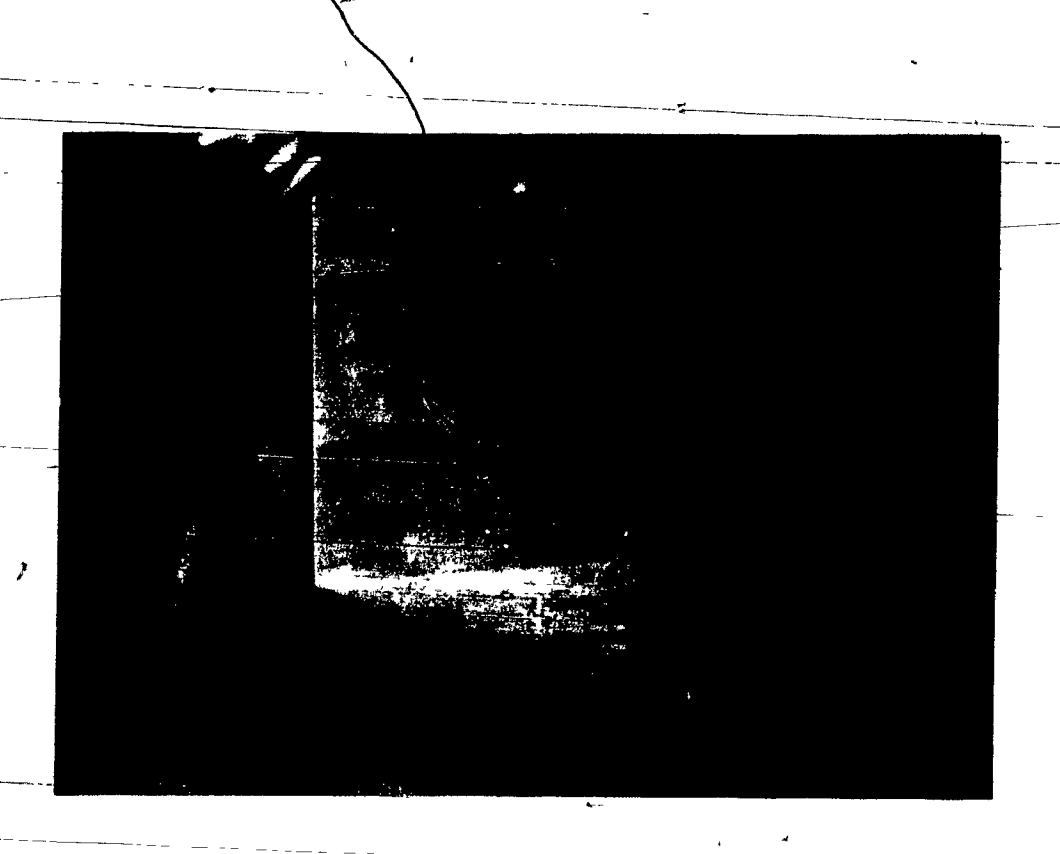
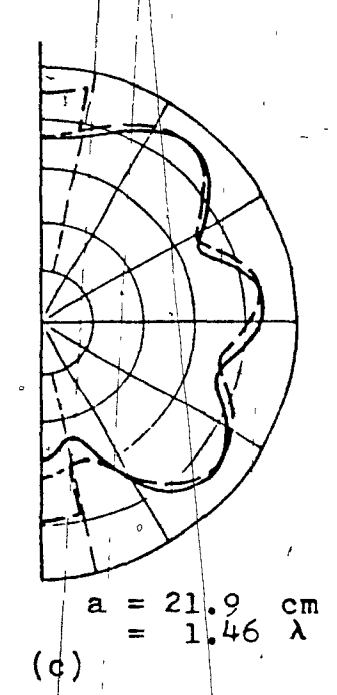


Fig. 4.23 The experimental model. A square aluminum plate is fastened at right angles to a large circular ground plane, and is illuminated by

a short monopole antenna fed from below .

(dB) a = 10 cm $= 0.6666 \lambda$ (a) PLATE WIDTH w = 10 cm

a = 18.45 cm= 1.23 λ



0.6666 λ

Frequency

Wavelength 15 cm

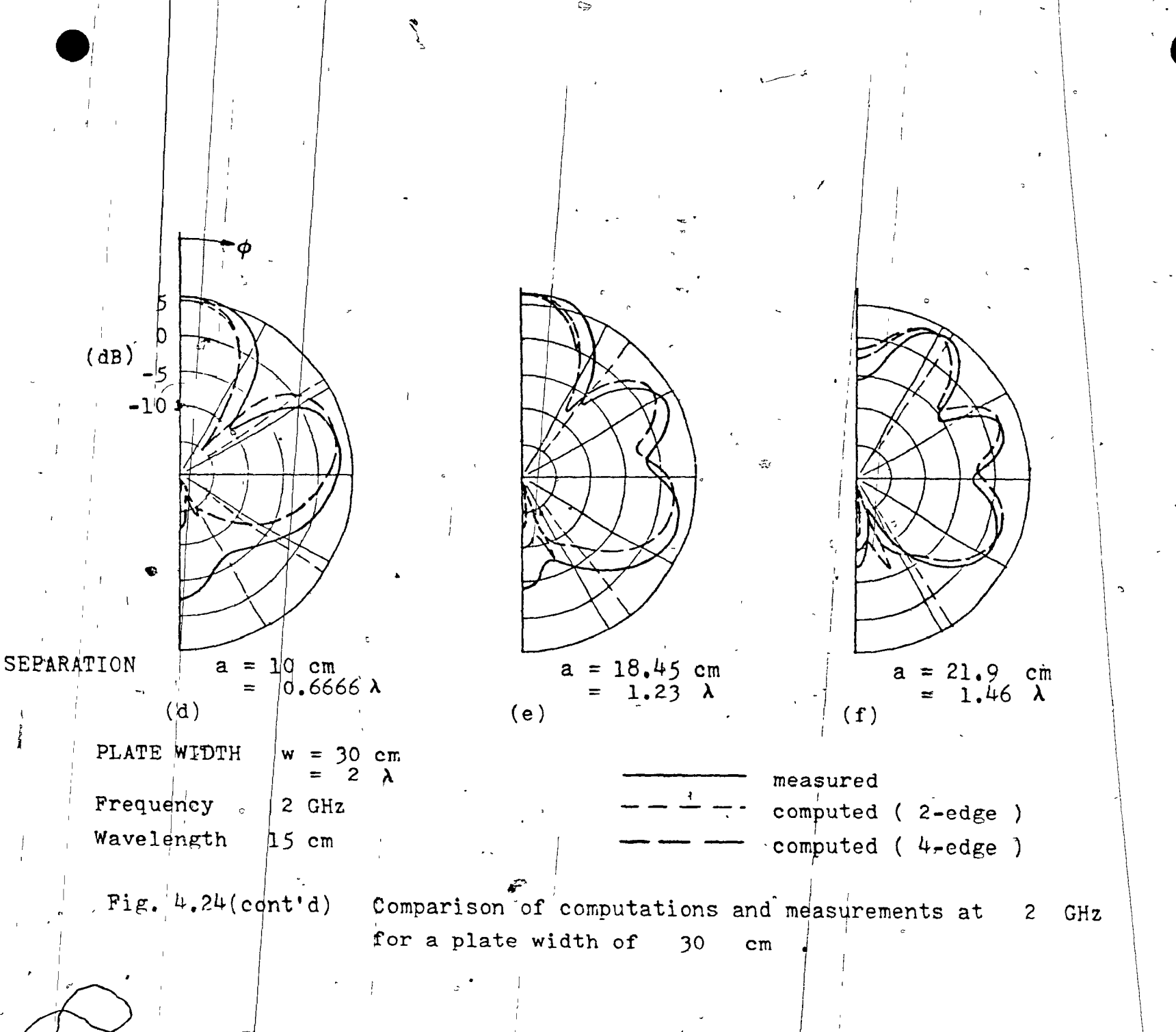
measured

computed (2-edge)

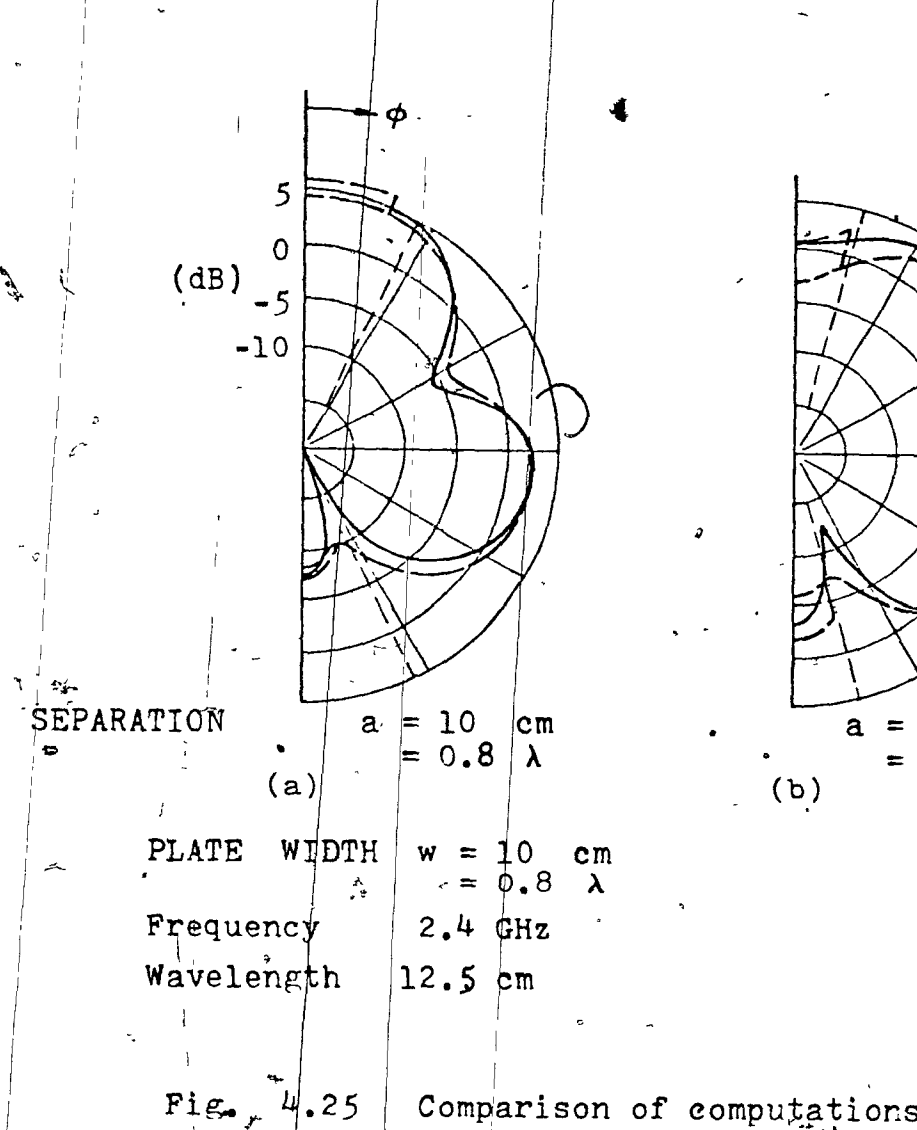
computed (4-edge)

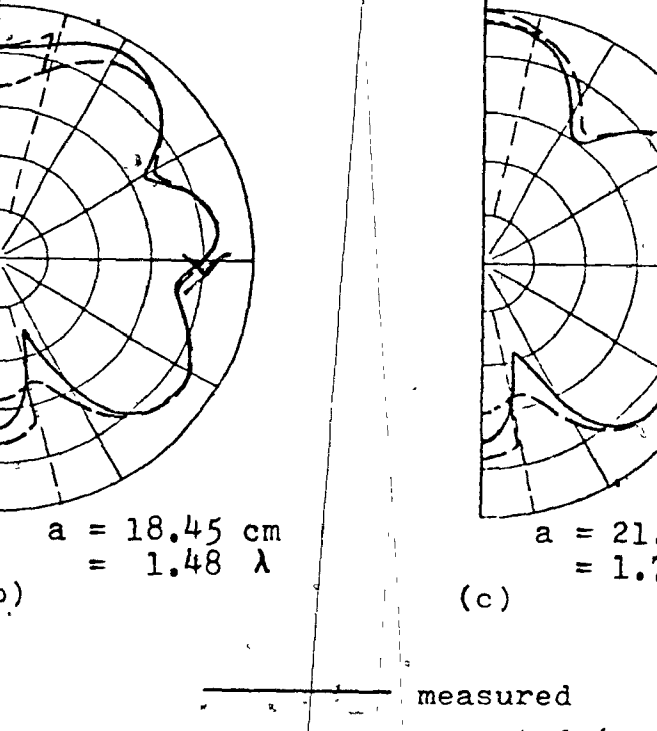
Fig. 4.24 Comparison of computations and measurements at 2 GHz for a plate width of 10 cm .

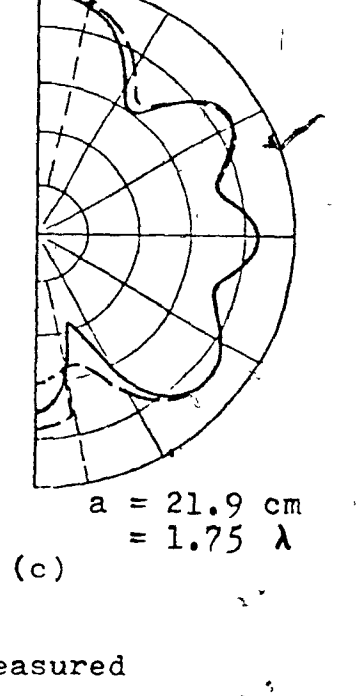
(b)



1-45

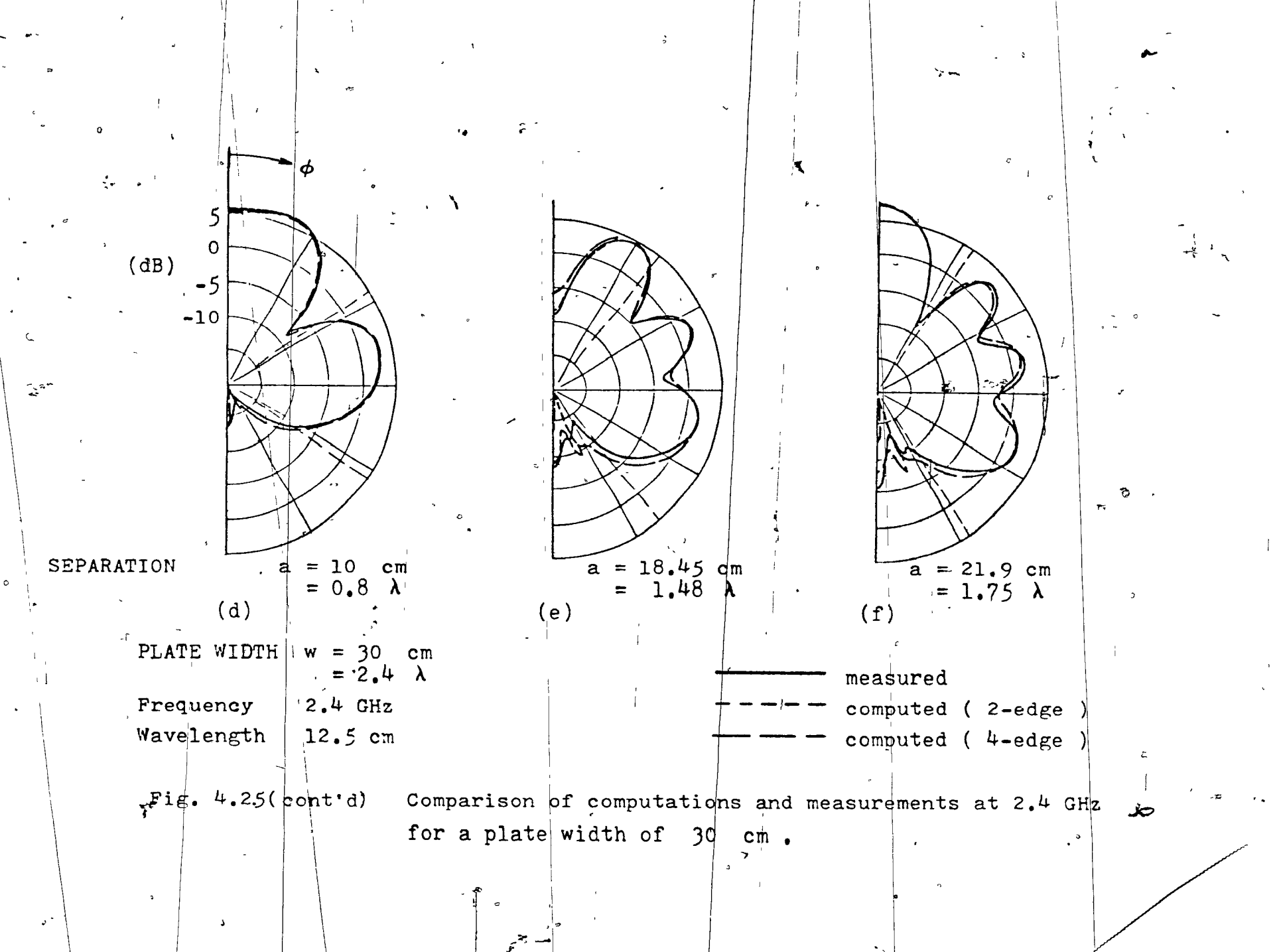






computed (2-edge) computed (4-edge)

Comparison of computations and measurements at 2.4 GHz for a plate width of 10 cm.



CHAPTEP 5

SUMMARY AND CONCLUSIONS

5.1 Parametric Graphs, Parametric Families, and Synoptic Graphs

The investigation of an antenna by classical techniques seeks the "pattern function" which gives the radiated field in terms of the direction of the field point and the physical dimensions of the particular antenna geometry under consideration. Such an explicit function provides considerable physical insight into the behavior of the radiation pattern as the antenna's dimensions are varied. Within a fixed antenna geometry, an analytic pattern function generates the pattern for any dimensions immediately and directly with a minimum of calculation. Unfortunately, the class of antenna geometries in which pattern functions have been found is severely limited.

At the opposite extreme, the pattern for any antenna geometry whatsoever can be obtained by measurement with a suitable model. Such measurements provide little insight into the behavior of the pattern as a function of the antenna's dimensions, unless an extensive atlas of patterns is compiled for many sets of dimensions. This is a difficult and expensive undertaking since most antenna models cannot have their dimensions changed easily.

Flectronic computers allow the solution of radiation problems with complex antenna geometries, but this "solution" is in the form of numerically generated radiation patterns. The computer program allows the numerical investigation of the radiation pattern over a wide range of antenna dimensions within a given geometry, but the results of such a study come in the form of large numbers of numbers that are hard to interpret. The insight of an explicit

pattern function is lost. The difficulty lies in condensing this numerical pattern information to a succinct form which aids in understanding the physical processes governing the antenna system. Resorting to graphical presentation, whether by manual means or computer graphics, and plotting an extensive atlas of patterns is a primitive first step towards such interpretation.

behavioral traits of the radiation pattern in terms of the physical dimensions of the particular antenna geometry.

In this thesis, an attempt is made to cope with this information diagnization problem. The significant features of the radiation pattern of the antenna system are first identified. For example, for an antenna with a broadly directional pattern, the number of maxima and the number of minima in the pattern, the angles at which these maxima and minima occur, and the relative heights of the maxima and minima might be considered to be significant features. For a highly directive antenna, the height of the main lobe, the beamwidth, and the maximum sidelobe level might be considered as the important pattern features. The behavioral traits exhibited by these features as a function of the antenna dimensions can be extraoted from the numerical patterns and expressed graphically. Thus for example the number of maxima or the angles at which the maxima occur in the pattern as a function of an antenna size dimension could be plotted.

Consider the problem of fully documenting in graphical form the behavior of one pattern feature "f" as a function of two antenna physical dimensions s_1 and s_2 , over a specified range

s_{21.} < s₂ < s_{2H}

For a fixed value of one dimension, say s_1 , the value of feature f (the height of the main lobe, for example) can be plotted against the other dimension, s_2 .

A curve giving (f,s_1) pairs can be drawn for N values of s_2 over the range under consideration. The data for these curves is extracted from the computed numerical radiation patterns. The result is a "parametric graph" describing the behavioral traits of feature f as a function of size variable s_1 for N different values of s_2 .

Parametric graphs represent a considerable reduction of the computer's raw numerical radiation pattern data. A set of such parametric graphs describes the behavior of the significant pattern features in a way that lends itself to interpretation and hence understanding of the physical processes of the antenna system much better than does an atlas of patterns.

The parametric graph described above does not display the data in its most meaningful form. The independent variables are the antenna physical dimensions s_1 and s_2 . The value of the dependent variable f should be plotted on a z-axis against s_1 and s_2 on the x and y axes. This displays the values of s_1 and s_2 which give a particular value of f. The information for such a graph is available directly from the parametric graph described above. Several constant f contours can be plotted, for different values of f. Such .

feature f against the independent variables s₁ and s₂. Although parametric family contours contain the same information as a parametric graph, this information is displayed in a much more meaningful way.

ametric family by an analytic function determined empirically from the parametric family graph, of the form

$$s_2 = function of (s_1, p_1, p_2)$$

where p₁ and p₂ are "family parameters" which are functions of f, then a further distillation of the numerical radiation pattern is readily achieved.

Thus, for example, if the curves in the parametric family are straight lines, then the "parametric family law" would be

$$s_{2} = p_{1} s_{1} + p_{2}$$

where the family parameters p₁ and p₂ are the slope and the intercept of the straight line.

In general, the family parameters p_1 and p_2 will be different for each contour in the parametric family, and hence are functions of the feature value f. Family parameter p_2 can be graphed against parameter p_1 , and because p_1 and p_2 are both functions of f, the feature value f will be a known function of position along the curve. Thus N separate curves on the parametric family graph can be reduced to one curve on the (p_1, p_2) graph. This single curve contains all of the information of the N parametric graph

curves, and so the (p_1, p_2) graph will be called a "synoptic graph". A synoptic graph is based on the parametric graphs and hence on the computed data, and also on an empirical function describing the curves of the parametric family. The form of this empirical relationship determines the dependence of the family parameters p_1 and p_2 on the antenna dimensions s_1 and s_2 . This procedure is illustrated by the current element - plate radiating system analysis in the next section.

constructed describing the behavior of the significant features of the pattern on the antenna physical dimensions s_1 and s_2 , the graphs can be used to reconstruct the pattern for any values of the size variables s_1 and s_2 over the range covered. If the "significant features" of the pattern have been carefully selected, then the "reconstructed" pattern should be accurate enough for practical purposed. Thus parametric graphs and/or synoptic graphs can be used to generate patterns for antenna dimensions s_1 and s_2 for which no explicit run of the computer program has been made, and so constitute a "Pattern Generator Function" (PGF) for the antenna system. The classical pattern function is only one form of the radiating system's PGF.

Even if an analytic pattern function can be obtained for a particular antenna geometry, the design of the antenna to meet predetermined

specifications is still an iterative procedure requiring many calculations and comparisons, based on the assumption that it is possible to realize the specifications with the given antenna geometry. However, if a formal "inverse" of the pattern function is possible, then the realizability of specifications is immediately apparent, and the choice of physical antenna dimensions to achieve the design is available directly. Unfortunately few antenna geometries have mathematical pattern functions, and fewer till have an identified formal inverse.

Parametric and hence synoptic graphs can be plotted from numerical radiation patterns, or from patterns obtained experimentally, or even generated by a mathematical pattern function, by the systematic procedure described above. These graphs have a powerful pattern generation capability in that approximate patterns can be sketched immediately from parametric or synoptic graphs for any antenna physical dimensions in the range covered. The graphs make apparent at once the realizability of a given set of specifications with the antenna geometry under consideration. Further, the choice of antenna dimensions to obtain a given performance is obtained directly from the parametric or synoptic graphs. Parametric and synoptic graphs may be useful for design purposes.

5.2 Parametric Graphs and a Synoptic Graph for the Flat Plate Problem.

In this thesis the H-plane radiation pattern of a current element centered in front of a rectangular plate, parallel to the "vertical" edges, is studied in detail by the Geometrical Diffraction Theory method of analysis. General information about the behavior of the radiation pattern as a function of plate height, width, and source separation distance is readily generated. Regions of height are established (Sect. 4.12) for which the plate can be considered:

- i) tall, where the horizontal edge diffracted fields have little effect on the pattern, or
- intermediate, in which case the front and back regions of the pattern are sensitive to plate height and the horizontal and vertical edge diffracted fields are of comparable magnitude, or
- iii) short, in which case the horizontal edge diffracted fields dominate the front and back regions and the pattern is again insensitive to plate height. These results are summarized in table II. It is also found that, as a function of width, the pattern behavior is different in two regions, for which the plate can be considered "narrow" or "wide" (Sect. 4.6). Narrow plate patterns are often reminiscent of isotropic patterns, whereas wide plate patterns are directional (Fig. 4.8).

The pattern of the current element - plate radiating system for any plate height h can be derived from the pattern for large h and the same plate width and source separation, by the addition of the components of field diffracted from the horizontal edges (Sect. 4.11). Thus a systematic investigation of the "tall" plate pattern yields useful information for all heights.

TABLE II: Regions in which horizontal (H) and vertical (V) edge contributions dominate.

Region of Angle	Front	Side.	Back
Region of Plate Height			
Short	Н	v .	, Н
Intermediate	: н + -v	v	`H + V
Tall	V °	v ·	v

The tall plate pattern is studied in Chapter 4 by the parametric graph - synoptic graph approach over the range of widths and separations

The significant results are summarized below.

The investigation of the tall plate radiation patterns is begun with a study of the simpler "narrow" plate patterns and then extended to include plates of any width over the range covered. The significant features of the narrow plate pattern are identified as the number of minima in the pattern, the angles at which these minima occur in the pattern ("location angles"), and the ratio of the pattern maximum to the pattern minimum. The behavior of

these features as a function of the plate width and the source separation distance is determined by running the computer program for a set of discrete values of width and separation.

It is found that the number of minima in the front and side region of the pattern is stepwise proportional to the source separation distance

o# minima = 2 x Separation

where the separation in wavelengths is rounded down to the nearest half wavelength. The parametric graph shown in Fig. 4.9 gives the number of minima and their location angles as a function of an antenna size variable, the separation, for various fixed values, the second antenna size variable, the width which fall in the "narrow" range. This parametric graph is readily derived from the computed radiation patterns. The parametric graph shown in Fig. 4.10 gives the maximum to minimum ratio as a function of separation for various widths and is also readily obtained from the numerical patterns. These two parametric graphs represent a considerable reduction of the raw computed data and present the behavior of the significant features of the pattern in a way which aids in understanding the physical processes of the radiating system. contain enough information to reconstruct the narrow plate radiation pattern for any separation over the range covered, and for a small range of "narrow" widths.

The shape of the plate pattern as a function of separation and width when the width does not fall in the narrow range can now be considered. The significant features of the pattern are identified as the number and location angles of the minima in the front and side region of the pattern, the relative height of the maxima and the minima in the side region as represented

hev

by parameter SP (see Sect. 4.10), and the value of the field in the plate's shadow as given by parameter SF (Sect. 4.10). Parametric graphs showing the functional dependence of amplitude parameters SP and SF as a function of the source separation distance for various values of plate width are readily derived from the computed patterns and are shown in Fig. 4.15 and 4.16.

The number of minima in the plate pattern for any width is found to be stepwise proportional to the separation distance, exactly as in the "narrow" plate case. It is helpful to sequence the minima in order of appearance as the separation distance increases as detailed in Sect. 4.3 and Fig. 4.4, and to consider each minimum M as a separate "significant pattern feature". A parametric graph giving the location angle in the pattern of each minimum M as a function of source separation distance for various fixed widths is easily plotted from the computed numerical data. Fig. 4.11 is such a parametric graph for the first minimum (M=1). Similar parametric graphs for M = 2,3,....,9 would be necessary to describe the behavioral traits of all the minima over the complete range of separations under consideration.

Any of the above parametric graphs, Fig. 4.9, 4.10, 4.15, 4.16, or the set represented by Fig. 4.11, could be replotted as a parametric family graph as discussed in Sect. 5.1. This work pursues this study only for the parametric graphs for the minimum location angles. The results of this study are discussed below.

The parametric family graph for the Mth minimum consists of contours of constant location angle ϕ of the Mth minimum, plotted against the independent variables, namely the source separation distance on one axis, and the plate width on the other. Fig. 4.12 shows the parametric family contours

for the first minimum (M=1), and is easily derived from the parametric graph Fig. 4.11 as detailed in Sect. 4.8. Each contour on the parametric family graph for the Mth minimum is for a different value of the location angle ϕ of the Mth minimum, and so the contour represents widths and separations for which the radiation pattern has the Mth minimum at the angle ϕ of the contour.

One parametric family graph is derived from the parametric graph for each of the nine minima for M = 1,2,....9. Thus, although the parametric family contours aid in understanding the physical processes of the radiating system by graphing the value of the dependent variable against the independent variables, the parametric family graph itself does not represent any further compacting of the computed data of the original parametric graph. However, the significant contribution of the parametric family contours plotted in Fig. 4.12 is that they bring to light a simple relationship between the variables width and separation, for constant location angle of the Mth minimum. The "curves" in Fig. 4.12 are found to be straight lines, as precisely as can be determined from the computed data.

The next step in the data distillation procedure described in Sect. 5.1 is the determination of an empirical "parametric family law" to describe the contours on the parametric family graph. The "law" can then be exploited to derive a "synoptic graph".

The parametric family graph for the location angle ϕ of the Mth minimum displays a linear relationship between widths and separations which make the Mth minimum fall in the pattern at a particular angle ϕ , and so the parametric family law has the form

a = sw + a

4

0,

The "family parameters" discussed in Sect. 5.1 are now identified as the slope and intercept of the straight line. A synoptic graph can now be prepared. The value of the slope s and the intercept a of each straight line on the parametric family graph for the Mth minimum is determined graphically. Since each line has an angle of associated with it, each slope-intercept pair also carries an associated angle o. If the intercepts are plotted against the slopes, then the Mth curve on the "synoptic graph" Fig. 4.13 is obtained. This procedure reduces the set of curves on the parametric family graph for the Mth minimum to one curve on Fig. 4.13. The parametric family graph for each minimum $M = 1, 2, \ldots, 9$ has been reduced to the Mth curve on Fig. 4.13. Thus nine graphs have been summarized in one "synoptic graph". The ϕ value associated with each point on each curve on the synoptic graph Fig. 4.13 could be indicated on the diagram. For greater accuracy in finding the location angles of the minima given a width and separation by the method discussed below, a separate graph has been plotted relating minimum location angle ϕ to the intercept value a, and is shown in Fig. 4.14. This graph explicitly displays the dependence of family parameter a on the location angle of the Mth minimum.

The synoptic graph Fig. 4.13 can be used to obtain the number, and location angles of all the minima in the front and side region of the pattern for any plate width and source separation over the range covered. The parametric family law is rearranged to read

$$a_0 = -ws + a$$

Given a value of separation a and width w, this equation relates the intercepts and slopes possible for this system. The straight line will intersect as many

of the synoptic curves on the synoptic graph Fig. 4.13 as there are minima in the front and side region of the pattern. Further, the intercept values of the intersection points of this straight line with the synoptic curves can be determined, and then the actual location angles of the minima read from Fig. 4.14.

Thus new information about the behavioral traits of the H-plane pattern of the current element centered in front of a rectangular plate radiating system has been discovered. A systematic procedure has been developed which allows such information to be extracted from a large numerical "atlas" of computed H-plane patterns for discrete values of width and separation, and expressed as simple, continuous "parametric graphs". This concept has been extended via a empirically determined "parametric family law" which allows a set of curves on a parametric graph to be reduced to a single curve on a "synoptic graph". The parametric graphs and the synoptic graph found for the current element-plate system allow a continuum of new patterns to be obtained without further computation, and hence are considerably more useful than the original numerical atlas of patterns. The graphs display the system's behavioral traits in a form that is easy to understand and which lends itself to the interpretation of the physical processes of the radiating system. Such graphs may be useful for design purposes.

5.3 Vertex Diffractions

It was found that when the height of the plate is such that the horizontal edges contribute a significant field, the calculated pattern

then exhibits a discontinuity at angles where the Law of Edge #iffraction forces the horizontal edge diffracted fields to vanish abruptly (Sect. 4.11-4.13).

This observation and others similar to it lead to the conjecture that the current stage development of the GDT technique is still incomplete, even with the Kouyoumjian dvadic diffraction coefficient. In seeking possible physical explanations it is reasonable to consider the effect of vertices and their possible dontribution to the diffracted field. The discontinuity noted above may be due to the neglected components of field diffracted from the plate's four corners of "vertices". If the vertex diffracted fields were included in the computation, then the discontinuity might be smoothed out. It was not possible to include these vertex diffracted fields in the calculation since no vertex diffraction coefficient has been developed to date.

In this thesis, a comparison is made of 12 experimental patterns with patterns computed with the four-edge GDT plate model. (Sect. 4.15). It is found that the best agreement is obtained in the side region of the patterns where the vertex diffracted components of field may be expected to be insignificant. In the front region, the vertex diffracted fields could also be important, even though this region is dominated by the GTO fields. While in many patterns the front region agreement is good, some patterns indicate that the neglected vertex diffracted fields might have considerable effect. In the pattern's back region, the vertex diffracted components of field might be expected to have magnitudes comparable to the edge diffracted fields, and in some patterns a considerable disagreement is seen in the back region, as suggested.

Thus the plate study has identified the need for a more intensive investigation of vertex diffraction and possibly the development of a vertex

diffraction coefficient. Such a vertex diffraction coefficient D would be a 3 x 3 dyadic which would generate vertex diffracted fields from incident fields

 $\overline{E}_{dv} = \overline{\overline{D}}_{v}$

Just as "edge related" coordinate systems have been found which simplify
the edge dyadic diffraction coefficient D so that it has only two non-zero
elements, so special "vertex related" coordinates might be sought.

5.4 The GDT Method

The GDT method of analysis offers several significant advantages.

There is a direct correspondence between body features such as reflecting surfaces, or edges, and components of field which allows the effect of any feature of the body on the radiation pattern to be readily assessed.

Thus great insight into the behavior of the pattern is gained.

There is considerable ease of analysis. The total field is the sum of several easily evaluated components, which are identified by simple ray tracing techniques.

Subroutines of general application, such as REF for reflected fields and DIFEDG for edge diffractions, are possible, which, once available, greatly simplify the analysis of any particular problem.

A numerical model of a radiating system can be programmed and debugged in stages. If a simple model shows promising results, further

diffracted rays can be included in the computation to improve the agree-

Since the solution of large matrix equations is not necessary, potentially there may be a reduction in computer running time, over moment method techniques.

5.5 Hybrid Modeling

The opportunity to merge the currently known computational methods in order to solve a more general class of problems, now becomes apparent. Attempts at hybridization of some moment methods are already known (20). A hybrid of the wire grid moment method with the GDT accounting for interactions between the wire segments of an antenna and a nearby reflecting-diffracting body is a first step in this direction (19). Additional terms are included in the impedance matrix to account for the field at the j-th wire segment due to the field of the i-th segment being reflected or diffracted by the body. Such a hybrid method could be used to study the plate illuminated by a half-wave dipole rather than a current element.

Hybrid modelling also offers a computational method to evaluate diffraction effects where no closed-form diffraction coefficient exists. Thus, vertex diffracted fields might be computed by putting a small number of surface patches or wire elements of current near the vertex, and finding the values of the currents by matrix inversion.

In conclusion, this thesis has

- 1. Studied the current element centered in front of a rectangular conducting plate radiating system, by the Geometrical Diffraction Theory method of analysis;
- 2. Developed and described a systematic procedure for obtaining parametric graphs from computed data, and deriving from them synoptic graphs which succinctly describe the behavior of the radiation pattern as a function of the physical dimensional parameters of the radiating system;
- 3. Obtained parametric and a synoptic graph for the current element plate radiating system;
- 4. Recognised that these parametric and synoptic graphs may be a representation of a simple, direct functional relationship, defined herein as the "pattern generator function", which provides significant pattern information in terms of the physical dimensions of the radiating system;
- 5. Shown that, while the GDT method provides a solution to this type of problem which promotes insight into the physical processes governing the radiating system, it has an important shortcoming at present in that the diffracted fields of vertices cannot be taken into account.

REFERENCES

- (1) R.G. Kouyoumjian, "An Introduction to the Geometrical Theory of Diffraction," notes from Short Course on Application of GTD and Numerical Techniques to the Analysis of Electromagnetic and Acoustic Radiation and Scattering, The Ohio State University, Columbus, Ohio, 1974.
- (2) R.C. Rudduck, "Application of Wedge Diffraction and Wave Interaction Methods to Antenna Theory," Notes from Short Course, The Ohio State University, 1974.
- (3) W.D. Burnside, "Principle Plane Pattern Analysis of On-Aircraft Antennas," notes from Short Course, The Ohio State University, 1974.
- R.G. Kouyoumjian, and P.H. Pathak, "The Dyadic Diffraction Coefficient for an Edge, Part I and Part II," private communication to be published.
- (5) R.G. Kouyoumjian, and P.H. Pathak, "A Uniform Geometrical Theory of Diffraction for an Edge in a Perfectly Conducting Surface," Proc. IEEE, Vol 62, pp. 1448-1461, November, 1974.
- (6) J.B. Keller, "Geometrical Theory of Diffraction," <u>Jour. Optical Society</u>
 of America, Vol. 52, pp.116-130, February, 1962.
- (7) ... Abramowitz and Stegun, eds. "Handbook of Mathematical Functions," Dover.

T. Bayou, "Surface Element Analysis of the Far Field Behavior of a
Dipole Antenna Near a Conducting Cylinder," Masters Thesis, Department
of Electrical Engineering, McGill University, Montreal, Quebec, March,
1972.

37

- (9) P.H. Pathak, and R.G. Kouyoumjian, "The Dyadic Diffraction Coefficient for a Perfectly Conducting Wedge," Report 2183-4, Electroscience Laboratory, The Ohio State University, Columbus, Ohio, 1970.
- (10) R.F. Harrington, "Time Harmonic Electromagnetic Fields," McGraw-Hill,

 1961.
- (11) L. Shafai, and Y.S. El-Moazzen, "Radiation Patterns of an Antenna

 Near a Conducting Strip." IEEE Trans. Antennas and Propagation, Vol.

 AP-20, pp 642-644, September, 1972.
- (12) S.J. Kubina, "Radiation Characteristics of Vehicle-Mounted Antennas and their Application to Comprehensive System Design," Ph.D. Thesis, Department of Electrical Engineering, McGill, University, Montreal, Quebec, August, 1972.
- (13) W. Wolde-Ghiorgis, "Wire-Grid Analysis of Antennas near Conducting Surfaces," Ph.D. Thesis, Department of Electrical Engineering, McGill University, Montreal, Quebec, March, 1972.

î

- (14) J.H. Richmond, "A Wire-Grid Model For Scattering by Conducting Bodies,"

 IEEE Trans. Antennas and Propagation, Vol. AP-14, pp. 782-786, November

 1966.
 - (15) K.K. Chan, "Projective Solution of Antenna Structures Assembled From Arbitrarily Located Straight Wires," Ph.D. Thesis, Department of Electrical Engineering, McGill University, Montreal, Quebec, August, 1973.
- (16) J.B. Keller, "The Geometrical Optics Theory of Diffraction," from "The McGill Symposium on Microwave Optics (1953), Part II, Diffraction and Scattering," Karasik and Zuker, editors, Bedford, Massachusetts, April, 1959, p.207.
- (17) W.T. Sedgwick, and H.W. Tyler, "A Short History of Science," revised by
 Tyler and R.P. Bigelow, MacMillan, New York, p.189.
- (18) J.H. Richmond, and N. Wang, "Sinusoidal Reaction Formulation for Scattering by Conducting Bodies of Arbitrary Shape," notes for Short Course on Application of GTD and Numerical Techniques to the Analysis of Electromagnetic And Acoustic Radiation and Scattering, The Ohio State University, Columbus, Ohio, 1974.
- G.A. Thiele, "A Hybrid Technique for Combining Moment Methods with the Geometrical Theory of Diffraction," IEEE Trans. Antennas and Propagation,
 Vol. AP-23, pp.62-69, January, 1975.

- (20) N.C. Albertsen, J.G. Hansen, and E.N. Eilskov Jensen, "Computation of Spacecraft Antenna Radiation Patterns," Contractor Report ESRO CR-207, ESTEC contract No. 1340/71, Technical University, Lyngby, Denmark.
- (21) L.L. Tsai, D.R. Wilton, M.G. Harrison, E.H. Wright, "A Comparison of Geometrical Theory of Diffraction and Integral Equation Formulation for Analysis of Reflector Antennas," <u>IEEE Trans. Antennas and Propagation</u>, Vol AP-20, pp. 705-711, November, 1972

App. 1 Subroutine SFLD

Given the position vector of a field point, R_p (RP), subroutine SFLD finds the distance RSM and the unit vector $\hat{\mathbf{r}}_s$ (RS) from the current element source located at s (S) with polarization $\hat{\mathbf{p}}(P)$. SFLD then evaluates vector TH whose components are given by the cross product ($\hat{\mathbf{p}} \times \hat{\mathbf{r}}_s$) at $\hat{\mathbf{r}}_s$. In Sect. 2.2 it is shown that this double cross-product gives the source field vector normalized to an isotropic source of magnitude 1. RSM may be used to remove the normalization, and is also the radius of curvature of the source's spherical wavefront.

```
SUBROUTINE SFLD( RP, RSM, TH )
 FINDS THE DIRECTION AND DIRECTIVITY OF A POINT SOURCE AT S
      REAL RP(3),P(3),S(3),RS(3),PH(3),TH(3)
      COMMON / SOURCE / S.P.
            : UNIT VECTOR IN THE DIRECTION OF THE CURRENT ELEMENT .
C
            : POSITION VECTOR OF THE SOURCE .
 FIND THE DISTANCE AND DIRECTION FROM SOURCE TO FIELD POINT :
      00 \ 1 \ I = 1,3
    1 RS(I) = RP(I) - S(I)
      CALL UVEC( RS,RSM )
C DIRECTION OF THE FIELD :
      PH(1) = {}_{\mathcal{L}}P(2)*RS(3) \Leftrightarrow P(3) * RS(2)
      PH(2) = -P(1)*RS(3) + P(3)*RS(1)
      PH(3) =
                P(1)*RS(2) - P(2)*RS(1)
      TH(1) = PH(2)*RS(3) - PH(3)*RS(2)
      TH(2) = -PH(1)*RS(3) + PH(3)*RS(1)
      TH(3) =
                PH(1)*RS(2) - PH(2)*RS(1)
      RETURN
      END
```

The name of the corresponding variable in the computer program is given in the brackets.

ಡಾ~^{ಕ್ಕಿ}

App. 2 Subroutine REF

If a planar conducting sheet is perpendicular to the (x,v) plane, subroutine REF finds the reflected field at a distant point in the (x,y) plane in direction \hat{f} (F). As shown in Sect. 2.3 there will be a reflected ray at the distant field point if

$$\cos \theta_{B} > \hat{f} \cdot \hat{u}_{1} > \cos \theta_{A}$$

Subroutine STREF calculates and stores the location of the image source SI, its polarization POLI, unit vector $\hat{\mathbf{u}}_1$ (U1), the direction cosines $CGI = \cos \theta_A$ and $CG2 = \cos \theta_B$. Then for a given field direction $\hat{\mathbf{f}}$, subroutine REF evaluates the dot product $\hat{\mathbf{f}}$: $\hat{\mathbf{u}}$ to determine if a reflected ray exists. If so, the location and polarization of the image are used to find the reflected field as given in Sect. 2.3, normed to an isotropic source, and phase referred to the position of the primary source $\hat{\mathbf{s}}$ (S).

Subroutine STREF:

Suproutine STREF:

CALCULATES THE 2AIA WEEDED TO FIND THE REFLECTED FIELD FROM
EACH PLANE.

CHAPLES

THE NUMBER OF REFLECTING PLANES.

CHAPLES

S. LICEATION OF THE SCURCE.

COLIDOTES:

THE NUMBER OF REFLECTING PLANES.

S. LICEATION OF THE SCURCE.

COLIDOTES:

ARRAYS OF STATE TO ALGO BE THE THAGE SOURCE OF THE THAGE.

COLIDOTES:

ARRAY OF LOCATIONS OF THE IMAGE SOURCE TO THE 1-TH IMAGE.

COLIDOTES:

ARRAY OF LOCATIONS OF THE IMAGE SOURCE TO THE 1-TH IMAGE.

COLICCES:

YESTERS OF LISTING ANGLES.

COMMAN / STREE!

ARRAY OF LOCATIONS OF THE 1-TH EDGE:

COLICCES:

YESTERS OF LISTING ANGLES.

COLICLIST OF COLICISMENT OF THE 1-TH EDGE:

COMMAN / STREE!

ARRAY OF LOCATION OF THE 1-TH EDGE:

COLICLIST OF COLICISMENT OF THE 1-TH EDGE:

COLICLIST OF COLICLISMENT OF THE 1-TH EDGE:

CALL UNCCIONALLY OF CLICLISMENT OF THE 1-TH EDGE:

CALL UNCCIONALLY OF CLICLISMENT OF THE 1-TH EDGE:

CFIND THE POLICISMENT OF THE 1-TH EDGE:

CFILL OF THE POLICISMENT OF THE 1-TH EDGE:

CFIND THE POLICISMENT OF THE 1-TH EDGE:

CCCITIC THE POLICISMENT OF THE 1-TH EDGE:

CCCITIC THE THE THE THE THE THE THE 1-TH EDGE:

CCCITIC THE THE THE THE THE THE T

```
Subroutine STREF (cont'1):
   11 \ U2(I,J) = -U2(I,J)
   10 CONTINUE
C FIND POINT P WHICH IS CLOSEST TO THE SOURCE ON THE 1-TH EDGE :
      D1 7 0.
      D2 = U1M
      TOL = 0.01
    5 DP = D1 + ( D2 - D1 ) / 2.
      00 6 J = 1.3
    6 P(J) = PA(I,J) + OP = U1(I,J) = S(J)
      CALL UVEC ( P.PM )
      CG = -DOTAL U1.P. 1 1
      IFT ABSCICG F .LT. TOLET GO TO 7
      IFI CG .GT. O. 1 GO TC 8
C CP TOO LARGE :
      D2 # DP
      GO TO 5
    8 CONTINUE
C DP TCO SMALL :
      D1 = OP
      GO TO 5 -
    7 CONTINUE
C L'CCATE THE IPAGE SOURCE :
  1. D(I) = 2. + PF o r
      009J = 1.3
    9 SI(I,J) = S(J) + D(I) + P(J)
      D(I) = D(I) + 2. + 3.1415926
      I = I + 1
      IF( I .GT. NR ) RETURN
      GO TO 1000
      END
Subroutine
      FUNCTION DCTA( E.R.I )
C FINDS THE DOT PRODUCT OF THE 1-TH ROW OF E. AND THE VECTOR R .
      REAL E16,31,R(3)
      DOTA = Q.
      001J = 1.3
    1 DOTA = DOTA + E(1,1) & R(J)
      RETURN
      END
```

Subroutine REF

```
SUBROUTINE REF( F.ER. 1 )
C FINDS THE VALUE OF THE FIELD REFLECTED FROM THE I-TH PLANE .
C INPUTS :
              : UNIT VECTOR IN THE DIRECTION OF THE FIELD POINT .
CF
CI
             : REFLECTION PLANE EDGE NUMBER .
C OUTPUT :
C ER
              : THE COMPLEX VECTOR COMPONENTS OF THE REFLECTED FIELD
                PHASE REFERENCED TO THE SOURCE .
      COMPLEX ER (3) , ERP
      REAL PI(6,3), PH(3), TH(3)
      REAL F(3), U1(6,3), U2(6,3), SI(6,3), D(6), CGI(6), CG2(6)
      COMMON / STREFZ / LI.UZ.SI.D.CGI.CGZ.PI
C DETERMINE IF THERE IS A REFLECTED FIELD :
C DOES THE FIELD POINT LIE ON THE SOURCE SIDE OF THE PLANE ?
      DOTUZF = DOTA( U2,F,[ )
      IF ( DOTUZF -LT. 0. ) GO TO 1001
C DOES THE REFLECTION POINT LIE WITHIN THE FINITE PLANE ?
      CA = -DOTAL -U1.F.I 1
      IF( ( CA .LT. CG1(I) ) .AND. ( CA .GT. CG2(I) ) ) GO TO 1000
C NC REFLECTED FIELD :
 1001 CONTINUE
      D0 2 J = 1,3
    2 ER(J) = ( 0..0. )
      RETURN
 1000 CONTINUE
C FIND THE REFLECTED FIELD :
      RC = D(I) + DCTU2F
      ERP = CEXP( CMPLX( 0.,-RD ) )
C DIRECTION OF THE REFLECTED FIELD INCLUDING SOURCE DIRECTIVITY :
      PH(1) = PI(1,2)*F(3) - PI(f,3)*F(2)
      PH(2) = -PI(I,1)*F(3) + PI(I,3)*F(1)
      PH(3) = PI(1,1)*F(2) - PI(1,2)*F(1)
      TH(1) = PH(3)*F(2)
      TH(2) = -PH(1) + F(3) + PH(3) + F(1)
      TH(3) = PH(1)*F(2) - PH(2)*F(1)
      DO 1.4 = 1.3
    1 ER(J) TH(J) # ERP
      RETURN
      ENO
```

120

į

App. 3 Subroutine DTFFLD

Subroutine DIFFLD evaluates the Transition Diffraction Coefficients DS and DH (Sect. 3.5), given the angles of incidence BETAO = $\beta_{\rm O}$, PSIO = $\psi_{\rm O}$, and PSI = ψ , and the distance RSM from the source to the point of diffraction. Subroutine DIFEDG (App. 5) finds the point of diffraction on the edge and evaluates BETAO, PSIO, PSI, and RSM, and calls DIFFLD to find the value of the TDC. DIFFLD calls subroutine INTN to find N -, and then determines if the simple diffraction coefficient applies, which is used if possible to save computational effort. If the TDC is needed, DIFFLD calls subroutine FRESNL to evaluate the transition function F (X). Subroutine STDFLD finds certain constants used by DIFFLD, which are related to the wedge angle.

```
Subroutine
                                                                          Subroutine DIFFLD
       SUBROUTINE STOFLO
 C CCMPUTES SUBROUTINE DIFFLO PARAMETERS .
 C INPUTS :
 C NE
               : THE NUMBER OF WEDGES IN THE MODEL .
                                                                        C OLTPUT :
               : THE ANGLE PARAMETER FOR EACH EDGE .
                                                                        C CS, DH
      COMMON / STED3 / C1.TPN.C3.C4
                                                                        C INPUTS :
       COMPLEX C1(6),C3(6)
                                                                        C BETAD
       REAL TPN(6),N(69,C4(6)
                                                                        C PSIO
       COMMON / STED4 / N.NE
                                                                        C PSI
       COMMON / CONSTS / PI.TPI.PI2.PI4.RTD.DTR
                                                                        CI
       STP1 = SQRT( TP1 )
                                                                        C RSM
-- CCMPUTE FOR EACH EDGE, I=1.NE :
                                                                                         FIELD POINT .
       1 = 1
                                                                              REAL KL. TPN(6).N(6).C4(6)
  1000 CONTINUE
 C TRANSITION ZONE FORMULA PARAMETERS :
       TPN(I) = TPI + N(I)
      C1( I ) = -CEXP( CMPLX( 0.,-P14 ) ) / ( 2. * STPI * N(I) )
                                                                              COPMON / STED4 / N.NE"
 C SIMPLE FORMULA PARAMETERS :
                                                                              TN = 2. + N(1)
      C3(1) = 1.7 (N(1)+STPT) + SIN(PI/N(1))
                                                                              RSMK = RSM + TPI
                 * CEXP( CPPLX( 0..-PE/4. 1.1
      C4(1) = COS( PI / N(1) )
                                                                              SBO = SIN( BETAO )
       1 + 1 = 1
                                                                              PHIL = PSI - PSIO
       IF( I .GT. NE ) RETURN
                                                                              PH12 - PS1 + PS10
       GO TO 1000
       END
                                                                              TP = TPN( [ )
                                                                              RNP1 = {PI + PHII} / TP
                                                                              RNP2 = (PI + PHI2) / TP
                                                                              NP1 = INTN( RNP1 )
                                                                              NP2 = INTN( RNP2 )
                                                                              NM1 = INTN( RAM1 )
 Sebroutine UVEC
                                                                              NM2 = INTN( RAM2 }
       SUBROUTINE UVEC( A.AM )
       REAL A(3)
      AM = SQRT( A(1)**2 + A(2)**2 + A(3)**2 )
       00 1 1 = 1.3
    1 A(I) = A(I) / AM
      RETURN
       END
 Subroutine INTN:
      FUNCTION INTNE P 1
C THIS FUNCTION IS USED IN EVALUATING THE TRANSITION DIFFRACTION
C CCEFFICIENTS BY SUBROUTINE DIFFLD
      INTN = INT(P)
      R = P - FLCAT(INTN)
                                                                         1000 CONTINUE
      IFF R .GE. 0.5 ) INTN = INTN + I
      RETURN
      END
```

```
SUBROUTINE DIFFLD( DS.DH.BETAO.PSIC.PSI.I.RSM )
C CCMPUTES THE DIFFRACTION COEFFICIENTS USING FORMULAE VALID EVERYWHERE.
C INCLUDING IN THE TRANSITION REGIONS .
               : THE SOFT AND HARD DIFFRACTION COEFFICIENTS .
              : THE DIFFRACTION CONE HALF-ANGLE .
              : THE INCIDENT ANGLE .
              : THE DIFFRACTION ANGLE .
              : THE WEDGE NUMBER .
               : THE DISTANCE FROM THE POINT OF DIFFRACTION TO THE
     COMPLEX C1(6), ESA.P1,P2.DS.DH,C3(6),FRESNL
     COMMON / CONSTS / PI, TPI, PI2, PI4, RTD, DTR
     COMMON / STED3 / CL.TFN.C3.C4
     ESA = CEXP! CPPLX! O.,-RSMK ) ) / SQRT( RSMK )
    ~KL = PI + RSM + { SB0++2 }
     RNH1 = (-PI + PHII) / TP
      RNM2 = { -PI + PHI2 } / TP
      AP1 = 2. *(( COS( (TP *NP1-PHT11/2. ) )**2 ) * KL
      AP2 = 2. #({ COS( (TP *NP2-PH[2]/2.) )**2 ) * KL
      AMI = 2. *(( CCS( (TP *NM1-PH[1)/2.) 1**2 ) * KL
     AM2 = 2. *( COS( [TP *NM2-PH[2]/2.] ]*+2 ] * KL
C CETERMINE IF THE SIMPLE FORMULA MAY BE USED :
     IF( (AP1.GT.10.) .AND. (AP2.GT.10.) .AND. (AM1.GT.10.)
           .AND. ( AM2.GT.10.) ) GO TO 1000
C THE TRANSITION ZONE FORMULA MUST BE USED : "
     P1 = COTAN( (PI+PHI1)/TN ) = FRESNL( AP1 )
                + COTAN! (PI-PHIL)/TN ) + FRESNL! AM1 )
     P2 = COTAN( (PI+PHI21/TN ) + FRESNL( AP2+)
               + COTANI (PI-PHIZ)/TN ) * FRESNLI AMZ )
     DS = C1(1) / SBO + ( P1 - P2 ) + ESA
     DH = C1(1) / $80 + ( P1 + P2 ) + ESA
C THE SIMPLE FORMULA CAN BE APPLIED : 🍾
     P1 = 1. / ( C4(1) - COS( PHIL/N(1) ) ) / SBO
     P2 = 1. / ( C4(I) - COSI PHIZ/N(I) ) ) / S80
     DS = ( P1-P2 ) * C3(1) * ESA
     OH = (P1+P2) + C3(I) + ESA
     RETURN
```

END

App. 4 Evaluating the Transition Function:

Subroutines FRESIN; FRESNL, FREI

A4.1 Introduction

This appendix shows how to evaluate the transition function

$$F(X) = 2j \int X e^{jX} \int \frac{e^{-jt^2}}{X} dt$$

For X > 10, F(X) = 1. For X < 10, numerical integration will be used. A graph of F(X) will be found in (1).

A4.2 Relationship to the Fresnel Integral

The integral in the transition function may be rewritten as

$$\int_{\sqrt{X}}^{\infty} e^{-jt^2} dt = \int_{0}^{\infty} e^{-jt^2} dt - \int_{0}^{\sqrt{X}} e^{-jt^2} dt$$
 A4.2.1

The last integral is similar to a known and tabulated Fresnel Integral (7p.300)

$$\frac{f(\Delta)}{f(\sqrt{2X/\pi})} = \int_{0}^{a} e^{\frac{1}{3}(\pi/2)u^{2}} du$$

$$= \int_{0}^{\sqrt{2X/\pi}} e^{-\frac{1}{3}(\pi/2)u^{2}} du$$

hence \

where the bar denotes conjugate. Let $t = \sqrt{\pi/2}$ with when

 $u = \sqrt{2X/\pi}$, then $t = \sqrt{X}$ and the integral becomes

$$f(\sqrt{2X/\pi}) = \int_{\pi}^{2} \int_{0}^{\sqrt{X}} e^{-it^2} dt$$

which is the same as the second integral on the RHS of Eqn. A4.2.1. Thus

$$\int_{-\overline{X}}^{\infty} e^{-jt^2} dt = \int_{\overline{Z}}^{\overline{T}} \int_{u\to\infty}^{1im} f(u) - \int_{\overline{Z}}^{\overline{T}} f(\sqrt{2X/\pi})$$

The limit is easily found (7)

$$\lim_{y \to \infty} f(\psi) = \frac{1}{2} + j\frac{1}{2}$$

hence the transition function becomes

$$F(X) = 2i \sqrt{X} e^{i X} \left[\sqrt{\frac{\pi}{2}} \left(\frac{1}{2} + i \frac{1}{2} \right) - \sqrt{\frac{\pi}{2}} f \left(\sqrt{2X/\pi} \right) \right]$$

$$= \sqrt{\pi X} e^{i X} (1 + i) - \sqrt{2\pi} X e^{i X} f \left(\sqrt{2X/\pi} \right)$$

Thus evaluating the transition function is reduced to finding the Fresnel Integral, f $(\sqrt{2X/\pi})$.

A4.3 Finding the Fresnel Integral

The Fresnel Integral must be evaluated for arguments $a = \sqrt{2X/\pi}$ where X < 10, that is, for a < 2.5231.................... (7) uses a polynomial approximation for a > 5, and tables for smaller a . For computer application, tables are inconvenient and a numerical integration is preferred.

Expanding f (a) as real and imaginary part,

f (a) =
$$\int_0^a \cos((\pi/2) u^2) du + \iint_0^a \sin((\pi/2) u^2) du$$

The kernels are rapidly varying functions and so cannot be integrated accurately with low-order quadrature. Let \mathbf{u}_k be the points where the kernels are zero, or "nodes",

$$u_k = \sqrt{k}$$

(Hence either cos ($(\pi/2)$ k) or sin ($(\pi/2)$ k) is zero.) Between any consecutive u_k both kernels are slowly varying, and can be integrated easily.

Let

$$g_k = \int_{u_{k-1}}^{u_k} e^{1 (\pi/2) u^2} du$$

k = 1, 2, ...

Then for any argument a , we can write

$$f(a) = \sum_{m=1}^{n} g_m + \int_{u_n}^{a} e^{j(\pi/2)u^2} du$$

where u_n is the largest u_k less than a . Let f_k be the value of the Fresnel Integral at the nodes u_k , then the "node values" are

$$-\mathbf{f}_{\mathbf{k}} = \sum_{\mathbf{m}=1}^{\mathbf{k}} \mathbf{g}_{\mathbf{m}}$$

and

$$f(a) = f_n + \int_{u_n}^{a} e^{j(\pi/2)u^2} du$$

where the integral can be evaluated quickly and accurately by low order Gauss-Legendre Quadrature .

A4.4 Subroutines FRESIN, FRESNL, FRE1

Subroutine FRESIN generates the nodes of the kernels, u_k (Z(k)), and finds the node values, f_k (FS(k)). Function FRESNL evaluates the Transition Function for any argument, using the expressions obtained above. The value of the Frensel Integral is found by function FREI, for any argument, using the polynomial approximation (7) where valid, and otherwise the numerical integration technique detailed above. The nodes and node values found by FRESIN must be included in the main program's BLOCK DATA segment.

Subroutine FRESIN : SUBROUTINE FRESIN C THIS SUBROUTINE FINDS THE FRESNEL INTEGRAL EVALUATION CATA . REAL Z(26), PCN(8), PCH(8) CCMPLEX F1241,Fh,F5(25),C1,C2 CGPMCN / CUAD / BGW.RCN.NG CCMMCN / FREST / Z.FS.C1.C2.SPI2 COMMON / CONSTS / PI,TPI,PI2,PI4,RTC,CTR SPI2 = SCRT(PI2) C1 = CMPLX(1.,-1.) + CMPLX(0.,SP12) C2 = CMPLX4 C.,-2. +SP12) C GENERATE THE NCCES : CC 1 1 = 1,26 RT = 1 - 1 1 Z(1) = SCRT(RI) C EVALUATE THE F-PONSTANTS : CC 2 I = 1,24 Fh = (C.,C.) (1)5 = A B = 2(1+1)AME = (A-E), / 2. APB = (A+B) / 2. 1 CC 3 J = 1.NG U = AME + EGN(J) - APE Fh = Fh + CEXF(CPPLX(C., PIZ*(L**2))) + EGW(J) 3 CCATINUE F(I) = -AME + FW 2 SCATINUE C EVALUATE THE FS CONSTANTS : FS(1) = (0..C.) ' ... FS(2) * F(1)0041 = 1,23FS(1+2) = FS(1+1) + F(1+1)4 CONTINUE RETURN ENC Subroutine FRESNL:

FUNCTION FRESHL(X) C EVALUATES THE TRANSITION FUNCTION FOR ANY ARGUEHENT X . COMPLEX FR,C1,C2,FRE1,FRESHL COMMON / FRE21 / C1,C2,SP12 IF(X .6T. 10.) GO TO 1 C FCR SMALL ARGUEMENTS: SX = SQRY(X) Y = SX / SP12 FR = FRE1(Y) FRESHL=SX + CEXP(CMPLX(0.,X)) + (C1+C2+CONJG(FR)) RETURN 1 FRESHL = 1. RETURN

Subroutine FRE1 :

```
FUNCTION FREE ( X )
C EVALUATES THE FRESNEL INTEGRAL AT X .
      REAL BN(E), RH(8)
COPMON / QUAD / BH, BN, NG
      COMMON / CONSTS / PI. TPI.PI2.PI4.RTD.DTR"
      COMMON / FRESI / Z.FS
      COMPLEX FS(25), FW, FRE1
      REAL 2(26)
      IF( X .LT. 5. ) GO TO 4
      XS = X * X
      X4 = XS * XS
      C1 = (0.3183099 - 0.0968 / X4) / X
      C2 = \{ 0.10132 - 0.154 / x4 \} / \{ x = x5 \}
      PXS = 3.1415926 / 2. * XS
      SPXS = SIN( PXS )
      CPXS = COSt PXS +
      CX = 0.5-+ C1+SPXS - C2+CPXS
      SX = 0.5 - C1 + CPXS - C2 + SPXS
      FRE1 = CMPLX( CX.SX )
      RETURN
    4 CONTINUE
C LOCATE THE INTERVAL IN WHICH X LIES :
      1 = 2
    1 IF( Z(1) .GT. X ) GO TO 2
      1 = 1 + 1
      GO TO 1
    2 CONTINUE
C EVALUATE THE INTEGRAL :
      A = Z(I-1)
      8 = X
      AMB = \{ oA-P \} / 2.
      APB = { A+B } / 2.
      FW = ( 0..0. )
      DO 3-J = 1.NG
      U = AMB + BN(J) - APR
      FW = FW + CEXP( CMPLX(0., PIZ+(U+2) )) * BW(J)
    3 CONTINUE
      FW = -AM8 + FW
      FRE1 = FS(I-1) + FW
      RETURN
      END
```

END '

```
Main program for calculating the Fresnel
                                                                  The Fresnel integral evaluation data generated by
integral evaluation data :
                                                                   the program at left: O
C GENERATE THE FRESNEL INTECRAL EVALUATION DATA
                                                                   *** FRESNEL INTEGRAL EVALUATION DATA ***
     CEMPLEX F5f251,C1,C2 °
     REAL ZfZE)
                                                                   * INCIVICUAL CONSTANTS : SPI2 =
                                                                                                    C-1253314E+01
     CCPMCN / FRESI / Z.FS.Cl.C2.SP12
                                                                                          C1 = { C.1253314E+01, C.1253314E+C1)
     COMMON / CONSIS / PI, TPI, PI2, PI4, RTC, CTR
                                                                                             = ( O.C
                                                                                                               . -Q.2506628E+C1)
     PI = 3.1415926
     TPI = 2, + PI
PI2 = PI / 2.
                                                                   * THE ACCES 2(K) AND THE ACCE VALUES OF 2(K) )
     PI4 = PI / 4.
                                                                          NCCE Z(K)
                                                                                            NOTE VALUE F( Z(K) )
     RTE = 18C. / FI =
     CTR = PI / 18C.
     CALL FRESIN
                                                                         C.1CCCCCE+01 C.7798924E+CO 0.4382589E+CO
     WRITF(6,1CC)
                                                                         C.1414213E+Cb C:5288522E+CC G.7139727E+CO >
 ICO FCRMAT(///. *** FRESNEL INTECRAL EVALUATION DATA ****) ;
                                                                         #RITE(6,1C1) SP12,C1,C2
                                                                         1C1 FORMAT(//, * * INDIVIDUAL CONSTANTS : SPI2 * ".E15.7.
                                                                         /+28X,*C1 = {',E15.7,',',E15.7,')',
                                                                         C.244949CE+01 C.5C66417E+CC ,C.62854C1E+CO
           /,28x,*C2 = d',E15.7,*,*,E15.7,*)*)
                                                                         C.2645751E+01 C.3803895E+CG C.5C532C9E+CO
     WRITE(6.102)
                                                                         C.28284278+0% C.49561768+CO O.38797CGE+CO
 102 FCRMAT(//, * * THE ACCES Z(K) AND THE ACCE VALUES F( Z(K) ).
                                                                        $C.3CCCCCE+G1 C.6C57197E+CC C.4963126E+CO
          /. K',5x, 'ACCE Z(K)',12x, 'ACCE VALUE F( Z(K) )',
                                                                         0.3162277E+01 C.50315P5E+6C C.6CC362PE+CC
          /,26%, 'REAL', 9%, "IMAG")
                                                                         C.3316625E+CL C.4042584F+CO 0.5027465E+CO
     CC 1 K = 1.25
                                                                         13
   1 WRITE(6,103) K,Z(K),FS(K)
                                                                    14
                                                                         103 FCRMAT( 1,13,2x,3615.7)
                                                                   15
                                                                         C.3741657E+01 "C.5C19199E+CC C.5849428E+CD
     STCP
                                                                   16
                                                                         C.3E72983E+01 C.4179262E+CC C.5C17356E+CC
     END
                                                                         C.4CCCCCCE+01 C.4984219E+CC
                                                                   17
                                                                                                   C.42C5166E+CC
                                                                   18
                                                                         C:41231C6E+01 C.57712CGE+CG 0.49856C3E+CC
                                                                    19
                                                                         C.424264CE+C1 C.5013230E+C0 0.5749575E+C0
                                                                         C.43588558+C1 C.427C3458+CC C.5C12217E+C0
                                                                         0.4472136E+01 C.49886#0E+CO C.42E87E7E+CO
                                                                         C.4592576E+C1 C.5694134E+C0 0.498949CE+C0
C SPECIFY GALSSIAN CLACPATURE DATA FOR THE FRESNEL INTEGRAL EVALUATION
                                                                         G.469C415E+C1 C.5CC9815E+CC C.5678215E+C0
     DIMENSION PIBLERW(P)
                                                                         0.4786832E+01 C.4336659E+CC C.5CC9183E+CO
     CCMMCM / CLAC / EM, E, NG
                                                                         0.4698979E+01 C.4991386E+CC 0.435C6C1E+CO
     DATA NG / 6 /
     EATA RW / .1713244923,.3607615730,.6679139345,
         .4679139345,.3607615730,.1713244923 /
     CATA 8º / -.5324655142,-.6612093864,-.238619186C.
           .238615186C,.6612093864,.9324695142 /
     ENC
```

A.10

Subroutine DIFEDG App. 5

Subroutine DIFEDG finds the complex vector field ED diffracted in field direction f(F), by a straight edge which starts at point \overline{P}_1 (PI) and ends at point \overline{P}_2 (P2), illuminated by a point source located at \overline{s} (S) The flash point is found as in Sect. 3.6 by the iterative method, then the edge-related coordinates are determined, and the source field vector evaluated at the diffraction point by Subroutine SFLD (App.1), is resolved into edge-related components. The edge-related components of the diffracted field ED are found by Eqn 3.4.8, using the Transition Diffraction Coefficient evaluated by Subroutine DIFFLD (App. 3). The diffracted field is then restored to base coordinates and phase referred to the location of the source.

For each edge in the GDT model, Subroutine STEDG computes the "edge cosines" cos β_1 and cos β_2 , the edge unit vector $\hat{\mathbf{e}}$, and other parameters , and stores them for later reference by DIFEDG.

```
Subroutine STEDG (cont'd)
    CG1(1) = -COTA(E,R1,1)
    00.5 J = 1.3
   5 R1(J) = P2(I,J) - S(J)
    CALL UVEC( RI.RIM )
   . CG2(1) = - DOTA( E.R1.127
    WA = {2. - N(1)} + 180.
    WRITE(6,100) [,WA, ( E([,J),J=1,3 ),RE([),( U111,J),J=1,3 ),
    1 ( U2(1,J),J=t,3 )
 1CO FORMAT(/, * + DERIVED WEDGE DATA EDGE 4',12.", ANGLE ',F5.1." DEG
   IREES',7, * * UNIT VECTOR ALONG EDGE ..
   23E15.7,/, * EDGE LENGTH *,E15.7,
   3 /. * REFERENCE VECTOR # 1 ',3E15.7,
   4 /. * REFERENCE VECTOR # 2 *.3615.7 )
    1 = 1 + 1
    IF( 1 .GT. NE ) RETURN
    GD TO 1001
    END
```

Sul routine DOT

```
FUNCTION DOT( A.B )

REAL A(3),B(3)

DOT = A(1)+B(1) + A(2)+B(2) + A(3)+B(3)

END
```

```
Subroutine DIFEDG :
       SUBROUTINE DIFEOGI F.I.ED )
C FINDS THE DIFFRACTED FIELD FROM EDGE I, IN DIRECTION F .
C REQUIRED SUBROUTINES : UVEC.DOT.DOTA.DIFFLD.SFLD .
C INPUTS :
       : UNIT VECTOR IN THE DIRECTION OF THE FIELD POINT .
       : EDGE NUMBER .
C OTHER INPUTS AS IS SUBROUTINE STEDGE .
C EC .: THE COMPLEX X,Y,Z COMPONENTS OF THE DIFFRACTED FIELD, PHASE
C REFERENCED TO THE SOURCE .
      COMMON & SOURCE / S.PCL
      COMMON / STED1 / P1.P2.P3
COMMON / STED2 / E.RE.U1.U2.CG1.CG2-
      REAL RE(6), POL(3), ES(3), N(6)
      COMPLEX ED(3).
                           ESE2, ESE3, OS, DH, ED2, ED3, PHASE
       REAL K.RC(3), ER12(3), ER13(3), ERF2(3), ERF3(3), RP(3), R1(3), E(6,3),
      15(3),U1(6,3),L2(6,3),CG1(6),CG2(6),P1(6,3),P2(6,3),P3(6,3),F(3)
      COMMON / STED4 / N.NE
      COMMON / CCNSTS / PI,TPI,PI2,PI4,RTD,DTR
C DETERMINE IF DIFFRACTION FROM THE I-TH EDGE TAKES PLACE FOR THIS FIELD.
C DIRECTION :
      CA = -DOTA(E,F,I)
      IF( | CA -GT. CG2(1) | AND. | CA .LT. CG1(1) | GO TO 1000
C NO DIFFRACTION :
      00 1 J = 1.3
    1 ED(J) = (0.,0.1)
      RETURN
C DIFFRACTION CCCURS . FIND THE DIFFRACTION POINT :
- 10C0 D1 = 0.
      DZ = RE(I)
      TOL = 0.01
    2 CONTINUE'
      D = D1 + (D2 - D1 ) / 2.
      00.3 J = 1.3
    3 \text{ RP(J)} = \text{P1(I,J)} + \text{D} + \text{E(I,J)}
      DO 4 J = 1.3
    4 R1(J) = RP(J) - S(J)
      CALL UVECT RIGHT
      CT = -DOTA( E.R1. I )
C DETERMINE IF THE DIFFRACTION POINT P HAS BEEN FOUND WITH
C ENOUGH ACCURACY :
      IF! ABS! CT - CA ) .LT. TOL ) GO TO 1001
      IFI CT .LT. CA ) GO TO 5
C D MUST BE INCREASED
      D1 = D
      GO TO 2
C D MUST BE DECREASED :
      GO TO 2
 1001 CONTINUE
C CALCULATE THE DIFFRACTED FIELD :
```

1.12

```
Subroutine DIFEDG (cont'd)
C DETERMINE THE VALLE OF THE SOURCE FIELD AT THE DIFFRACTION POINT P :
      CALL SFIDE RP, RPM, ES )
C FIND THE INCIDENT FOGE-RELATED COORDINATES :
      ERIZ(1) = RI(2)*E(1,3) - RI(3)*E(1,2)
ERIZ(2) = -RI(1)*E(1,3) + RI(3)*E(1,1)*
       ER[2(3) = R1(1)*E(1,2) - R1(2)*E(1,1)
      CALL UVEC( ER12, ER12M )
      ER[3(1) = R1(2) + ER[2(3) - R1(3) + ER[2(2)]
      ERI3(2) = -R1(1)*ERI2(3) + R1(3)*ERI2(1)
      ERI3(3) = R1(1)*ER[2(2) - R1(2)*ER[2(1)
      CALL UVEC( ER13, ER13H )
C RESOLVE THE INCIDENT FIELD INTO EDGE-FIXED COMPONENTS :
      ESE2 = ES(1)*ER(2(1) + ES(2)*ER(2(2) + ES(3)*ER(2(3)
      ESE3 = ES(1)*ER[3(1) + ES(2)*ER[3(2) + ES(3)*ER[3(3)
C DETERMINE THE DIFFRACTION ANGLES :
      BETAO = ABS( ARCOS( CA ) )
C FIND THE INCIDENT ANGLE :
      CP1 = DOTA( U1,R1,I )
      CP2 = DOTA( U2,R1,1 )
      IF( CP1 .NE. 0. ) GO TO 300
      PS10 = P12
      IF( CP2 .GT. C. ) PS(0 = 3. + P(2
      GO TO 8
  300-ADPH = ATAME CPZ / CPL )
     JF( CP1 .LT. C. ) GO TO 7
      PSID = PI + ALPH
      GO TO 8
    7 PSTO = ALPH
      IF/ CP2 .LT. C. ) GO TO 8
      PSIO = TPI + ALPH
    8 CONTINUE
C FIND THE DIEFRACTION ANGLE :
     CP1 = -DCTA( U1,F,I )
      CP2 = -DOTA( L2,F,I )
      IFI CP1 .NE. C. ') GO TO 302
      P$1 = P12
      IF( CP2 .GT. 0. ) PSI = 3. * PI2
      GO TO 10
  302 ALPH . ATANI CP2 / CP1 )
  303 CONTINUE
      IF( CP1 .LT. C. ) GQ TO 9
      PSI = PI + ALPH
      GO TO 10
    9 PSI = ALPH
      IF! CP2 .LT. C. 3 GO TO 10
      PSI = TPI + ALPH
   10 CONTINUE
C FIND THE DIFFRACTION CCEFFICIENTS :
      CALL DIFFLOI CS, DH, BETAO, PSIO, PSI, I, RP# 1
C FIND THE COMPONENTS OF THE DIFFRACTED FIELD IN EDGE-FIXED COORDINATES
     ;ED2 = -DH + ESE2
    "ED3 = -DS + ESE3
C FIND THE DIFFRACTED EDGE-FIXED COORDINATES :
      ERF2(1) = E(1,2)*F(3) - E(1,3)*F(2)
```

```
Subroutine DIFEDG
                           (cont'd)
       ERF2(2) = -E(1,1)*F(3) + E(1,3)*F(1)
      ERF2(3) = E(1,1)*F(2) - 'E(1,2)*F(1)
      CALL UVECI ERF2, FRF2F )
       ERF3(1) = F(2)*ERF2(3) - F(3)*ERF2(2)
      ERF3(2) = -F(1)*ERF2(3) + F(3)*ERF2(1)
       ERF3(3) = F(1) + ERF2(2) - F(2) + ERF2(1)
      CALL UVEC! ERF3.ERF3M }
C FIND THE X,Y,Z, COPPONENTS OF THE DIFFRACTED FIELD : .
      ED(1) = ED2*ERF2(1) + ED3*ERF3(1)
      ED(2) = ED2*ERF2(2) + ED3*ERF3(2)
      ED(3) = ED2*ERF2(3) + ED3*ERF3(3)
C RELATE THE PHASE OF THE DIFFRACTED FIELD TO THE SOURCE :
      DO 12 J = 1.3
   12 RD(J) = RP(J) - S(J)
      DELTAR = - DOT(F,RD)
      PHASE = CEXP( CMPLX( 0. . - TPI +DELTAR ) )
      DO 14 J = 1.3
   14 ED(J) = ED(J) + PHASE
      RETURN
      END
```

41

A. 1

9 Q d E D

Appendix

0

20

comple

11s

ct in

of

ē

'n

program

the Theory of 0 œ 1 1 Ψ, B rt Ð lating system

```
C GEOMETRICAL - OPTICS PROBLEM .
C SUBROUTINES REQUIRED & STREF. UVEC. REF. DOTA. MAGPH. PTPRT
      REAL PA(6.3).PB(6.3).S(3).F(3).AA(4).POL(3).ARR(4).PTN( 361 )
      COPMON / CONSTS / PI.TPI.PI2.PI4.RTD.DTR
      COMMEN / MAINI / ARR
      COPHON / STREFT / PA.PB.NR
      COMMON / SOURCE / S.POL
      COMMON / PIPRTI / IO.IM.ID.DBN
      COMPLEX ED.ER.ET.EREF(3)
      PI = 3.1415926
      TPI = 2. * PI
      DTR = PI / 189.
      RTD = 180. / PI
C LOCATE THE ENOPOINTS OF THE EDGE :
      w = 2.5
      NR<sub>5</sub> = 1
      PA(1.1) = -W
      PA(1.2) = 0.
      PA(1.3) = 0.
      P8(1.1) = W
      PB(1.2) = 0.
      P8(1.3) = 0.
      ICNT = 1
 2000 CONTINUE
      A = ARR( ICHT )
C LOCATE THE SCURCE :
      5(1) = 0.
      S(2) = A
      S(3) = 0.
      WRITE(6,100) { PA(1,1),1=1,3 },( P8(1,1),1=1,3 ),( S(1),1=1,3 )
  100 FORMAT( -1 -. -
                         *** GEOMETRICAL OPTICS PROBLEM ****
     1 ///. * ENDPOINTS OF THE EDGE : ..
     2/.20x.3ET5.7./.20x.3E15.7.
     3 //. * SOURCE POINT : 1.3E15.7 )
C SPECIFY THE REGIONS WHERE THE DIRECT FIELD IS SCREENED :
      PSIG = ATANE W / A )
      AL1 = PI - PSIO
C SET UP THE REFLECTED FIELD SUBROUTINE :
C
C CALCULATE THE PATTERN :
      D = CAl
 1000 CONTINUE
     PHI = IAD + DTR
C FIND THE DIRECT FIELD :
     ED = \{ -1..0. \}
      IF1 PHI .GT. ALL ) ED = ( 0..0. )
      F(1) = SIN( PHI )
     F(2) = COS( PHI )
     F(3) = 0.
C FIND THE REFLECTED FIELD :
     "CALL REF( F.EREF.1 )
      ER = EREF(3)
C FIND THE TOTAL FIELD :
     ET = ED + ER
```

TPI # TAR + 1

CALL MAGPHE ET. PTNE IPL ; . PSE } 5 + OA1 = OA1 IF(JAD -LT- 181) GO TO 1000 C WRITE THE PATTERN : 100 * 0 CALL PTPRT(PTN.IDG) ICNT = ICNT + 1 IF(ICNT .LE. 4) GO TO 2000 STOP END BLOCK DATA COMMON / PTPRT1 / 10.18.10.08N DATA 10-IM-10-DBN / 0-180-2-0- / COMMON / SOURCE / S.POL DIMENSION S(3) .POL(3) DATA POL / 0..0..1. / COMMON / MAIN1 / ARR REAL ARR(4) DATA ARR / .25..5..6..75 / END

```
*** TWO - DIMENSIONAL GOT PROGRAM ***
     COMPLEX ED.ER.ET.EDIFF1(3).EDIFF2(3).EDIF1.EDIF2 .EDIFF3(3).EDIF3
     COMPLEX EDIFF4(3).EDIF4.EREF(3)
      INTEGER !AMO(25). !AMM(25). [AMD(25)
     COMMON / MAIN2 / IAMO.JAMM, IAMO.INOYS
      REAL ARR(25).PA(6.3).PE(6.3).P1(6.3).P2(6.3).P3(6.3).N(6).NP.WA(6)
      REAL PT2( 361 ) . PS2( 361 )
     REAL PIN( 361 ).PS1(361).PT3(361).PS3(361).HARR(10)
     COMMON / MAIN1 / W.ARR.WA.PNORMM.IHIV.ILOM.ISRCEM.HARR.IHM
      INTEGER IHIM (25) . ILOM425)
      REAL F(3).D(8).S(3).ADEG(8).POL(3).PNORP#(25)
      COPMON / PTPRT1 / IANGE. IANGM. IANGD. DBN
      COPMON / STREFI / PA.PB.NR
     COMMON / STED4 / N.NE
      COMMON / STEDI / PI.P2.P3
     COMMON / SOURCE / S.POL
      COMMON / CONSTS / PI.TPI.PI2.PI4.RTD.DTR
      PI = 3.1415926
      TPI = 2. * PI
     P12 = P1 / 2.
      DTR = PJ / 18Q.
      RTO = 180. / PI
     P14 = P1 / 4.
     W = W / 2.
C LOCATE THE REFLECTING PLANE :
     PA(1.1) = 0.
      PA(1.2) = -W
      PA(1.3) = 0.
      PB(1.1) = 0.
      P8(1.2) * W
      PB(1.3) = 0.
      NR = 1
      H = HARR(1)
      INM = 1
      WRITE(6.100) (PA(1.J).J=1.2).(PB(1.J).J=1.2)
  100 FORMAT('1'. ***** THE FLAT PLATE ******
     1 ///.* ***LOCATION OF REFLECTING PLANE*.
     2/. * *START POINT : *.2E15.7./. * *END PCINT : *.2E15.7 }
C LOCATE THE DIFFRACTING EDGES :
      NE = 2
      H = H / 2.
      P1(1.1) = 0.
      P1(1,2) = -W
      P1(1,3) = -H
      P2(1,1) = 0.
      P2(1,2) = -W
      P2(1.3) = H
      P3(1,1) = 0.
      P3(1,2) = -w+1.
      P3(1,3) = -H
      P1(2.1) = 0.
      P1(2,2) = W
     P1(2,3) = H
      92(2.1) = 0.
      R2(2.2) = W
      P2(2.3) =-H
      P3(2.1) = 0.
```

P3(2.2) = W - 1.

P3(2.3) = H

```
00 201 1 = 1.NE
  201 N(1) = 2. -WA(1) / 180.
     WRITE(6.102)
  102 FORMAT(//. +++WEDGE DATA*)
     DG 200 I = 1.NE
  200 WRITE(6.105) [.WA(1).(P1([.J).J=1.3).(P2([.J).J=1.3).(P3([.J).J=1.
    131
  105 FORMAT( * *WEDGE # *, !! . 4x. *ANGLE : *. FS. 0. * DEGREES *. /. * **. 10x,
     1'START PCINT : '.3E15.7.
    1 /. *
                      END POINT : *.3E15.7.
    2 /. *
                      REF
                            POINT : '.3E15.7 )
     ISRCE # 1
 2000 S(1) = ARR( ISRCE )
C FIND THE REGIONS WHERE THE VARIOUS FIELDS ARE PRESENT :_
      A1 = ATAN( ( W - S(2) ) / S(1) )
      A2 = ATAN( ( W + S(2) ) / S(1) )
C DIRECT
     ADI = PI - AI
      AD2 = PI + A2
C REFLECTED
      ARI = AI
      AR2 = 2. + P1 - A2
C DIFFRACTED
      AD11 = P12
      AD12 = P12 + WA(1) +DTR
      AD21 = 3.* PI2 - WA(2)*DTR
      AD22 = 3.*P12
      WRITE(6.104) (S(J).J=1.3).(POL(J).J=1.3)
  104 FORMATI'S.
     1/// * SCURCE POINT # *.3E15.7.* WAVELENGTHS*.
     2/. * POLARIZATION : 1.3F5.0 )
      ADEG(1) = AD1 # RTD
      ADEG(2) = AD2 * RTD
      ADEG(3) = ARI # RTD
      ADEG(4) = AR2 * RTD
      ADEG(5) = AD11 * RTD
      ADEG(6) = AD12 * RTD
      ADEG(7) = AD21 # RTD
      ADEG(8) = AD22 * RTD
      #RITE(6.600) ( ADEG(J), J=1.8 )
  600 FORMAT(' './/. * LIMITING ANGLES : +
     2/. * DIRECT
                      : '.2E15.7.' DEGREES'.
     1/. * REFLECTION : ".ZE15.7. DEGREES".
     3/ * DIFFRACTION : 1,2E15.7./ DEGREES .
     4/. . .
                        : . . 2E15.7. DEGREES )
     CALL STREF
      CALL STEDG
      CALL STOFLO
     CALL FRESIN'
C ZERO THE PATTERN VECTORS :
     DO 190 J = 1.361
      PTN(J) = 0.
      PS1(J) = 0.
      PT2(J) = 0.
      PS2(J) = 0.
      PT3(J) = 0.
  190 PS3(J) = 0.
      IANGO = IAPO( INM )
```

IANGH = IAMM(INM)
IANGD = IAMD(INM)

IANG -= IANGO 1000 PHI = DTR + IANG # F(1) = COS(PHI) F(2) = SIN(PHI) F(3) = 0. C FIND THE DIRECT FIELD : ED = (-1..0.) IF(! PHI .GT. ADI) .AND. (PHI .LT. AD2)) ED = (0..0.)C FIND THE REFLECTED FIELD : CALL REF(F.EREF.1) ER = EREF(3) C FIND THE DIFFRACTED FIELD : EDIF1 = (0..0.) IF({ PHI .GT. AD11 } .AND. { PHI .LT. AD12 }) GO TO 1002 CALL DIFEDG(F.I.EDIFFI) EDIF1 = EDIFF1(3) 1002 CONTINUE EDIF2 = (0 .. 0 .) IF({ PHI .GT. AD21 } .AND. (PHI .LT. AD22 }) GO TO 1003 CALL DIFERG(F.2.EDIFF2) EDIF2 = EDIFF2(3) 1003 CONTINUE ET = ED + ER + EDIF1 + EDIF2 IPL = IANG + 1 CALL MAGPH(ET .PTN(IPL).PSI(IPL)) IANG = IANG + IANGD IF (IANG .LE. IANGM) GO TO 1000 DBN = 0. IF(INDYS .EQ. 0) GD TO 2010 PHORM & PHORMP(INM) IHI = THIM! INM) ILO = ILCM(INM) C FIND THE NORMALIZATION FACTOR : PPAX = PIN(ILO + 1) IPL = ILC + 1 + IANGD 3000 IF(PTN(IPL) .GT. PMAX) PMAX = PTN(IPL) IPL = IPL + IANGD IF(IPL .LE. IHI) GO TO 3000 C SPECIFY THE MAXIMUM VALUE OF THE DB PATTERN, : DBN = PNCRM - PMAX WRITE(6.110) PNORM.ILO. IHI. PMAX. DBN 110 FORMAT(////. ++++ NORMALIZATION DATA .. 1//." ** NORMED TO A MAXIMUM OF ".E15.7, " DB ". BETWEEN ', 13.' DEGREE'S AND ', 13.' DEGREES '. 4 //." * ACTUAL MAXIMUM ".E15.7." D8"2 5 //. * NORMALIZATION FACTOR DBN ".EIS.7." DB "} 2010 CONTINUE 100 = 0 1D1 = 1 WRITE(6.108) 108 FORMAT(//." * TOTAL FIELDS */) CALL PIPRI(PIN. 100) INM = INM + 1 ISRCE = ISRCE + 1 IF(ISRCÉ .LE. ISRCEM) GO TO 2000 8050 STAP , END

```
BLOCK DATA
      INTEGER' 10(25) . [M(25) . ID(25)
      COMMON _/ MAINS / IO.IM.ID.INOYS
      REAL ARR(25).WA(6).PNORMM(25).HARR(10)
      REAL S(3).POL(3)
      INTEGER IHIM(25).(LOM(25) .
      COMMON / MAINI / W.ARR.WA.PNORMM.IHIM.ILOM.ISRCEM.HARR.IMM
      REAL M.LAN.K
      COMMON / SOURCE / S.POL
C SPECIFY THE PLATE WIDTH :
      DATA W / 0.8 /
C SPECIFY THE SOURCE POINT :
      DATA ISRCEM / 3 /
      DATA ARR / .8.1.476.1.752 /
      DATA S / 0.,0.,0. /
C SPECIFY THE WEDGE ANGLES IN DEGREES :
      DATA WA / lestestes/
C SPECIFY THE SOURCE POLARIZATION :
      DATA PCL / 0..0..1. /
C SPECIFY THE PATTERN CALCULATION PARAMETERS :
      DATA 10 / 25+0 /
      DATA IN / 25*180 /
      DATA ID / 25+1 /
C IF INDYS = 0 . THEN THE COMPUTED PATTERNS ARE NOT NORMALIZED .
      DATA INDYS / 0 /
C SPECIFY THE PATTERN NORMALIZATION DATA :
      DATA PNORMM / -1.6 /
      DATA [LCM / 25+10 /
      DATA THIM / 25#20 /
      DATA THM / 1 /
      DATA HARR / 1.6 /
C SPECIFY GAUSSIAN CUADRATURE DATA FOR THE FRESHEL INTEGRAL EVALUATION
      DIMENSION B(6).Bw(e)
      COMMON / QUAD / RW.B.NG
      DATA NG / 6 /
      DATA 8# / .1713244923..3607615730..4679139345.
           -4679139345..3607615730..1713244923 /
      DATA B / ~.7324695142.~.6612093864.-.2366191860.
             .2386191860..6612093864..9324695142 /
C SPECIFY THE FRESNEL INTEGRAL CONSTANTS :
      COMPLEX FS(25)
      REAL 7(26)
      COMMON / FRESI / Z.FS
      DATA FS / (0..0.).
                                       ( .7798924E+00.
                                                           .4382589E+00),
                                                          $$75070E+001.
     C( .5288922E+00.
                         .7139727E+00).( .3210552F+00.
         .4865200F+00.
                                                           .4913917B+001.
                          .3434165E+00).( .64C8054E+00.
                                                           .50532094.001.
                          .6289401E+00).( .3803895E+00.
         .50f 6417E+00.
         .49561/6E+00p
                       3879700E+00).( .6057197E+00\
203628E+00).( .4042584E+00.
                                                           .49451268.001.
     C (
         .5031585E+00%
                                                          .5027465£+00).
     Cl . .4975837E+00.
                          .4083021E+00).( .5881257E+00.
                                                           .497856 #E+00).
     C1 .5019199E+00.
                          .5849428E+001.( .4179202E+00.
                                                           .5017356E+00).
         .4984219E+00.
                          .4205466E+001.1 .5771200E+00.
                                                           .4985603E+00).
     C (
         .5013230E+00.
                          .5749575E+001.( .4270349E+00.
                                                           .5012217E+001.
     Cl
         .49666BDE+00.
                          .4288787E+00).( .5694134E+00.
                                                            #989490E+00).
     C( .5009819E+00.
                          -5678215E+00).( -4336659E+00
                                                           .5009183E+00).
         .4991386E+00.
                          +4350601E+001 /
      DATA Z /
     C 0.0
                          .1000000E+01.
                                                           -1732051E+01.
                                          -1414213E-01.
         .2000000E+01.
                          .22360665+01.
                                          .2449490E+01.
                                                           .2645751E+01.
                                          .3162277E+01.
         .282P421F+01.
                          ,30000D0F+01.
                                                           ~3316625F+01+
                                          .3741657F+01.
                                                           .387298JE+01.
                          .30055576+01.
         . 34541021+01.
                                          .4242640E+01.
                                                           .4358899E+01.
       . .4000CO0E+01.
                          .4123106E+01.
         .4472136E+01.
                          .4582576E+01.
                                          -4690415E+G1.
                                                           -4795832E+01.
         .4998979E+01.
                          *200000E+01
      ENO
```

```
COMPLEX ED, ER, ET, EDIFF1(3), EDIFF2(3), EDIF1, EDIFF , EDIFF3(3), EDIF3
      COMPLEX EDIFF4(3), EDIF4, EREF(3)
      INTEGER [AMO(25), [AMM(25), [AMD(25)
      COMMON / MAINS / TAMO, TAMO, TAMO, TNOYS
      PEAL ARR(25).PA(6,3).PB(6,3).P1(6,3).P2(6,3).P3(6,3).N(6).NP.WA(6)
      REAL PT21 361 ) , PS21 361 )
      REAL PTN( 361 ).PS1(361).PT3(361).PS3(361).HARR(10)
      COPMON / MAIN! / W.ARR. HA, PNORFM, IHIF, ILOM, ISRCEM, HARR, IHM
      INTEGER [HIM(25), ILOM(25)
      REAL F(3), C(8), S(3), ACEG(8), POL(3), PNORMH(25)
      COPMON / PTPRT1 / LANGO, LANGM, LANGD, DBN
      COMMON / STREFL / PA,PB,NR
      COMMON / STED4 / N.NE
      COMMON / STED1 / P1.P2.P3
      COMMON / SOURCE / S.PCL
      COMMON / CONSTS / PI-TPI-PI2-PI4-RTO-DTR
      PI = 3.1415926
      TPI = 2. # PI
      PI2 = PI / 2.
      DTR 4 PI / 180.
      RTD = 180. / PE
      P14 = P1 / 4.
      W = W / 2.
C LOCATE THE REFLECTING PLANE :,
      PA(1:1) = 0.
      PA(1,2) = -W
      PA(1.3) = 0.
      PB(1,1) = 0.
      P8(1,2) = W
      P8(1.3) = 0.
      NR = 1
      H = HARR(1)
      INM = 1
   ₩RITE(6,100) (PA(1,1),J=1,2),(PB(1,1),J=1,2)
  100 FORMAT(*)*,* ***** THE FLAT PLATE *****,
     1 ///. ***LOCATION OF REFLECTING PLANE*,
     2/+" *START POINT " "+2E15.7+/+" *END POINT : "+2E15.Y )
C LOCATE THE DIFFRACTING EDGES :
      NF = 4
      H = H / 2.
      P1(1,1) = 0.
      P1(1,2) = -W
      P1(1,3) = -H
      P2(1,1) = 0.
      P2(1,2) = -k
      P2(1,3) = H
      P3(1,1) = 0.
      P3(1,2) = -W+1.
      P3(1,3) = -H
      P1(2,1) = 0.
      P1(2,21 = %
      P1{\{2,3\}} = H
      P2(2,1) = 0.
```

P2(2,2) = W

```
P2(2,3) =-H
      P3(2,1) = Q.
      P3(2,2) = W - 1.
      P3(2,3) * H
      P1(3,1) = 0.
      P1(3,2) = -W
      P1(3,3) = H
      P2(3,1) = 0.
      P2(3,2) = w
      P2(3,3) = H
      P3(3,1) = 0.
      P3(3,21 = -W
      P3(3,3) = -1. + H
      PX(4,1) = 0.
      P(14,2) = W
      P1(4,3) = -H
      P2(4,1) = 0.
      P2(4,2) = -W
      P2(4,3) = -H
      P3(4,1) = 0.
      P3(4,2) = W
      P3(4,3) = -H + 1.
      DO 201 I = 1.NE
  201 \text{ N(I)} = 2. - \text{WA(I)} / 180.
      WRITE(6,102)
  1C2 FORMAT(//, * ***WEDGE DATA*)
      DO 200 I = 1.NE
  200 WRITE(6,105) [,WA([],(P1([,J],J=1,3),(P2([,J],J=1,3),(P3([,J],J=1,
  105 FORMAT! *HEDGE # ', 11, 4x, 'ANGLE : ", F5.0, DEGREES', /, * *1,10x,
     A'START PCINT : 1,3E15.7,
     1 /, * *
                      END POINT : ',3E15.7,
     2 /,1 +
                       REF POINT : '.3E15.7 )
      ISRCE = 1
 2000 S(1) = ARR( ISRCE )
C FIND THE REGIONS THERE THE VARIOUS FIELDS ARE PRESENT 1
      A1 = ATAN( ( W - S(2) ) / S(1) )
      AZ = ATAN( ( 4/+ S(2) ) / S(1) )
      AD1 = PI - A1
      AD2 = P1 + AZ
C REFLECTED
      ARL = A1
      AR2 = 2. + PI - AZ
C DIFFRACTED
      AD11 = P12
      AD12' = PI2 + WAT11+DTR
      AD21 = 3.* PIZ - WA(2)*DTR
      AD22 = 3.*P[2
      WRITE(6,104) (S(J),J=1,3),(POL(J),J=1,3)
  104 FORMATI'O'.
     1///* * SOURCE ROINT : ",3E15.7," WAYELENGTHS".
     2/, * * POLARIZATION : ',365.0 )
      ADEG(1) = AD1 + RTD
```

A. 1

```
ADEG(2) = AD2 . RTD
      ADEG(3) = AR1- * RTD
      ADEG(4) = AR2 + RTD
      ADEG(5) = AD11 = RTD
      ADEG(6) = AD12 + RTD
      ACEG(7) = AD21 + RTD
      ADEG(8) = AD22 + RTD
      WRITE(6,600) ( ADEG(J),J=1,8 )
  GGO FORMATI' ",//," # LIMITING ANGLES : "
     2/. * DIRECT
                      : '.2E15.7.' DEGREES'.
     1/. * REFLECTION : ", ZE15.7. DEGREES".
     3/' * DIFFRACTION : 1,2815.7, * DEGREES',
    4/, *
                        :', 2615.7,' DEGREES')
      CALL STREF
      CALL STEDG .
      CALL STOFLO
      CALL FRESIN
C ZERO THE PATTERN VECTORS :
      DO 190 J = 1,361
      PIN(J) = 0.
      PS1(J) = 0.
      PT2(J) = 0.
      PSZ(J) = 0.
      PT3(J) = 0.
  190 PS3(J) -0.
      IANGO = IAPO( INM )
      IANGH = IAMM( INM )
      [ANGD = IAMD( INM )
      IANG . = IANGO
 ICCO PHI = DTR + TANG
      F(1) = COS(P+I)
      F(2) = SIN(PHI)
      Ff31 = 0.
C FIND THE DIRECT FIELD :'
      ED = \{ -1., 0. \}
      IF( ( PHI .GT. AD1 ) .AND. ( PHI .LT. AD2 ) ) ED = ( 0.,0. )
C FIND THE REFLECTED FIELD :
      CALL REF! F. EREF. 1 }
      ER = EREF( 3 )
C FIND THE DIFFRACTED FIELD :
      EDIF1 = ( 0..c. )
      IFI ( PHI .GT. ADI1 ) .AND. ( PHI .LT. ADI2 ) 1 GO TO 1002
      CALL DIFEDGE F,1.EDIFF1 1
    fEDIF1 = EDIFF1(3)
 1002 CONTINUE
      EDIF2 = ( 0..0. )
      IF( | PHI .GT. AD21 ) .AND. ( PHI .LT. AD22 ) ) GO TO 1003
      CALL DIFEOGI F.2.EDIFF2 ) -
      EDIF2 = EDIFF2(3)
 1CC3 CONTINUE
      ET = ED + ER + EDIF1 + EDIF2
      IPL = IANG + 1
      CALL MAGPH( ET .PTN(IPL).PS1(IPL) )
      IANG - IANG + IANGD
```

```
IF! TANG .LE. TANGE J GO TO 1000
      DBN = 0.
      IF( INOYS .EQ. 0 ) GO TO 2010
      PNORM = PNORMY ( INH )
      IHI = IHIM( IAM )
      ILO = ILOM( IAM )
C FIND THE NORMALIZATION FACTOR :
      PMAX = PTN( ILO + 1 )
      IPL = ILO + 1 + IANGD
 3000 IF( PTN( IPL ) .GT. PMAX ) PMAX = PTN( IPL )
      IPL = IPL + IANGD -
      IF( IPL .LE. IHI ) GO TO 3000
C SPECIFY THE MAXIMUM VALUE OF THE DB PATTERN :
      DBN = PNCRM - PMAX
      WRITE(6.110) PNORP, ILO, IHI, PMAX, DBN
  110 FORMAT(////, * **** NORMALIZATION DATA *.
     1//." ** NORMEC TO A MAXIMUM OF ".E15.7," DB ",
     2/. BETHEEN '.13. DEGREES AND '.13. DEGREES '.
     4 //. * ACTUAL MAXIMUM *. E15.7. D8.
     5 //+ * NORMALIZATION FACTOR DBN *,E15.7.* DB *)
 2010 CONTINUE
      100 = 0
      ID1 = 1
      WRITE(6,108)
  108 FORMAT(//, * TOTAL FIELDS */)
CALL PTPRT( PTN, IDO )
      INM = INF + 1
      ISRCE = ISRCE + 1
      IF( ISRCE .LE. ISRCEM ) GO TO 2000
8050 STOP
      END
```

```
*** 3-DIMENSIONAL GTD PROGRAM ***
      BLOCK DATA
      INTEGER 10(25), [M(25), [D(25)
      COMMON / MAINS / 10.19.10.1NOYS
      REAL ARR(251, WA(6), PNORMM(25), HARR(10)
      REAL S(3), PCL(3)
      INTEGER THIM(25). (LOP(25)
      COMMON '/ MAIN! / W.ARR.WA.PNORMM.IHIM.ILOM.ISRCEM.HARR.IHM
      REAL M, LAN, K
      COPMON / SCURCE / S.PGL.
C SPECIFY THE PLATE HEIGHT :
      DATA IHM / 1 /
C SPECIFY THE PLATE WIDTH :
C SPECIFY THE SOURCE POINT :
      DATA ISRCBM " 3 /
      DATA W / 0.8 /
      DATA HARR / 1.6 /
      DATA ARR / .8,1.476,1.752 /
      DATA S / 0.,0.,0. /
C SPECIFY THE WEDGE ANGLES IN DEGREES :
      DATA WA / 1.,1.,1.,1. /
C SPECIFY THE SOURCE POLARIZATION :
      DATA POL / 0..0..1. /
C SPECIFY THE PATTERY CALCULATION PARAMETERS :
     DATA 10 / 25*0 /
      DATA 1M / 25*180 /
      DATA ID / 25#1 /
C IF INOYS = 0 . THEN THE COMPUTED PATTERNS ARE NOT NORMALIZED .
      DATA INCYS / C /
C SPECIFY THE PATTERN NORMALIZATION DATA :
     DATA PNORMM / -1.6 /
      DATA ILC# / 25*10 /
      DATA IHIP 7 25+20 /
C SPECIFY GAUSSIAN CLADRATURE DATA FOR THE FRESNEL INTEGRAL EVALUATION
     DIMENSION B(8), BW(8)
      COMMON / QUAD / BW.B.NG
     DATA NG / 6 /
     DATA BW / $1713244923,.3607615730,.4679139345,
          .4679139345..3607615730..1713244923./
     DATA B / -.9324695142,-.6612093864,-.2386191860,
            .2386191860,.6612093864,.9324695142 /
C SPECIFY THE FRESNEL INTEGRAL CONSTANTS :
     COMPLEX FS(25)
      REAL Z(26)
      COMMON / FRESI / Z.FS
     DATA FS / {0..0.}.
                                      ( .7798924E+00,
                                                         .4382589E+001.
    C1 .5288922E+CO,
                         .7139727E+001,( .3210552E+00,
                                                         .5173070E+001,
     CI .4882509E+CO.
                         .3434165E+00).( .6408054E+00,
                                                         .4913917E+001 /
     C1 .5066417E+CO.
                         .6289401E+00),( .3803895E+00,
                                                         .5053209E+00),
   ~ C1 .4956176E+CO,
                         .3879700E+00),( .6057197E+00,
                                                         .4963126E+001.
    Ct .5031585E+CO.
                         .6003628E+00).( .4042584E+00.
                                                         .5027465E+001,
     CI
        .4975837E+CO,
                         .4083021E+00),( .5881257E+00,
                                                         .4978563E+001,
     CI
        .5019199E+00,
                         .5849428E+00),( .4179202E+00,
                                                          .5017356E+001,
        .4984219E+CQ.
                         .4205166E+00),( .5771200E+00.
                                                          .4985603E+001,
```

```
Ct .5013230E+CO.
                    .5749575E+001,1 .4270349E+00.
                                                     .5012217E+00).
   .4988680E+CQ.
                    .4288787E+00).( .5694134E+00.
                                                     .4989490E+001,
                    .5678215E+00),1 .4336659E+00.
   .5009819E+CO,
                                                     .5009183E+001.
   .4991386E+CO.
                    .4350601E+001 /
DATA Z /
                                    .1414213E+01.
C 0.0
                    .1C00000E+01.
                                                     .1732051E+01.
    .2000000E+01.
                    .2236068E+01.
                                     .2449490E+01.
                                                     .2645751E+01,
    .2828427E+C1,
                    .30000QQE+01,
                                     .3162277E+01.
                                                     .3316625E+01.
    .3464102E+C1,
                    .3605552E+01,
                                    .3741657E+01+
                                                     .3872983E+01,
    .4000000E+C1.
                    .4123106E+01,
                                     .4242640E+01.
                                                     .4358899E+01,
   .4472136E+01,
                   -.4582576E+01.
                                    .4690415E+01.
                                                     .4795832E+01,
    .4898979E+C1,
                    -5000000E+01
END
```

1. IS